



UNIWERSYTET ŚLĄSKI
INSTYTUT FIZYKI
IM. AUGUSTA CHEŁKOWSKIEGO

Uniwersytet Śląski w Katowicach
Wydział Nauk Ścisłych i Technicznych
Instytut Fizyki

PRACA DOKTORSKA

**Wpływ budowy molekularnej oraz warunków termodynamicznych
na strukturę supramolekularną alkoholi monohydroksylowych**

MGR JOANNA GRELSKA

Promotor: prof. dr hab. Sebastian Pawlus

Promotor pomocniczy: dr inż. Karolina Jurkiewicz



UNIWERSYTET ŚLĄSKI
W KATOWICACH

CHORZÓW 2024

Spis treści

Podziękowania	3
Streszczenie	4
I. Wstęp	5
A. Motywacja	5
B. Dokonania naukowe	7
C. Badane substancje	10
D. Metody eksperymentalne	12
E. Symulacje komputerowe	17
II. Wyniki i dyskusja	19
A. Wpływ budowy molekularnej na proces asocjacji	19
B. Agregacja związków z pierścieniem węglowym	20
C. Czas życia wiązań wodorowych w klastrach	23
D. Zmienne warunki termodynamiczne w układzie	24
E. Podsumowanie	26
III. Publikacje naukowe	28
A. P1. Supramolecular Structure of Phenyl Derivatives of Butanol Isomers	28
B. P2. Computer simulations as an effective way to distinguish supramolecular nanostructure in cyclic and phenyl alcohols	50
C. P3. Comment on “Universal features in the lifetime distribution of clusters in hydrogen-bonding liquids” by I. Jukić, M. Pożar, B. Lovrinčević and A. Perera, Phys. Chem. Chem. Phys., 2021, 23, 19537	62
D. P4. High-Pressure and Temperature Effects on the Clustering Ability of Monohydroxy Alcohols	67
E. Oświadczenia współautorów	85
Aktywność naukowa	91
Referencje	93

Podziękowania

Największe podziękowania składam Promotor Pomocniczej Dr inż. Karolinie Jurkiewicz za przekazywaną wiedzę oraz ogrom wspólnej pracy nad pomiarami, analizą danych, pisaniem wniosków i artykułów. Dziękuję także za wspólne zagraniczne wyjazdy pomiarowe do Francji i USA, a także na konferencje krajowe i międzynarodową konferencję w Japonii.

Bardzo dziękuję Promotorowi Prof. Sebastianowi Pawlusowi, za poświęcony czas i możliwość realizacji doktoratu w projekcie badawczym.

Prof. Kamilowi Kamińskiemu dziękuję za szansę na pierwszą współpracę i wprowadzenie do fizyki molekularnej.

Jestem wdzięczna za możliwość realizacji doktoratu w grupie badawczej Prof. Mariana Palucha.

Dziękuję Prof. Andrzejowi Burianowi za tutoring z teorii dyfrakcji rentgenowskiej układów nieuporządkowanych i Dr Kajetanowi Koperwasowi za tutoring z zakresu symulacji dynamiki molekularnej.

Składam podziękowania za możliwość odbycia zagranicznych staży i ich opiekunom, Dr Changyong Park z Argonne National Laboratory w USA za naukę pomiarów cieczy w kowadłach diamentowych na linii dyfrakcyjnej, Dr László Temleitner z Wigner Research Centre for Physics w Budapeszcie za współpracę przy symulacjach komputerowych oraz opracowaniu programu do analizy klastrów.

Dziękuję Współautorom artykułów naukowych, szczególnie Dr Andrzejowi Nowokowi za wyczerpujące dyskusje.

Serdeczne podziękowania składam znajomym Doktorantom Instytutu Fizyki Uniwersytetu Śląskiego, za mile wspólnie spędzony czas oraz rozważania naukowe i nie tylko.

Streszczenie

Nanostruktury supramolekularne są obserwowane w wielu fazach niekryształicznych, szklach i cieczech, gdzie molekuly oddziałują ze sobą poprzez słabe wiązania międzycząsteczkowe i asocjują w klastry o różnej wielkości i architekturze. Ze względu na zachodzenie procesu asocjacji molekuł w wielu biologicznie istotnych układach takich jak polisacharydy, polimery, białka tworzące DNA, jest to przedmiot szeroko prowadzonych badań. W ramach przygotowanej pracy doktorskiej badane były modelowe związki asocjujące poprzez wiązanie wodorowe – alkohole monohydroksylowe, różniące się długością łańcucha alkilowego, rodzajem pierścienia węglowego lub umiejscowieniem grupy hydroksylowej. Główną metodą badania struktury supramolekularnej tych układów w stanie ciekłym była dyfrakcja rentgenowska w szerokim zakresie kątów rozpraszania. Otrzymane dane dyfrakcyjne były analizowane w postaci czynnika struktury oraz funkcji rozkładu par atomów. Dodatkowo wykonano symulacje metodą dynamiki molekularnej w celu znalezienia modeli cieczy asocjujących. Wybór odpowiedniego pola siłowego umożliwił otrzymanie układów, dla których obliczone dane dyfrakcyjne wykazały bardzo dobrą zgodność z wynikami doświadczalnymi. Teoretyczne modele dostarczyły wielu informacji o strukturze badanych alkoholi, niemożliwych do otrzymania na podstawie danych eksperymentalnych, takich jak cząstkowe funkcje rozkładu par atomów, dystrybucje wielkości klastrów supramolekularnych czy czasy życia wiązań wodorowych. Pokazano, że stopień asocjacji i preferowany typ tworzonych klastrów w izomerach alkoholi jest ściśle związany z położeniem grupy hydroksylowej w molekule. W porównaniu z prostymi cząsteczkami alkoholi, w przypadku molekuł z pierścieniem węglowym zdolność do tworzenia klastrów związanych wodorowo jest ograniczona. Co więcej, wykazano, że aromatyczność pierścienia w molekule powoduje wystąpienie dodatkowych oddziaływań międzycząsteczkowych i wzrost heterogeniczności struktury. Ważnym punktem było opracowanie charakterystyki procesu asocjacji molekuł w różnych warunkach termodynamicznych. W celu eksperymentalnego zbadania struktury cieczy pod wysokim ciśnieniem wykonano synchrotronowe badania dyfrakcyjne w kowadłach diamentowych. Uzyskano unikalne dane dyfrakcyjne, które zinterpretowane wraz z wynikami symulacji ujawniły propagację agregacji poprzez wiązania wodorowe pod wysokim ciśnieniem. Ponadto, ich zestawienie z wynikami efektu zmian temperatury pokazało odmienny wpływ energii kinetycznej molekuł oraz globalnej gęstości na proces asocjacji. Wyniki omawianych badań zawarte zostały w czterech publikacjach naukowych będących podstawą pracy doktorskiej. Prezentowane badania są istotnym krokiem w celu lepszego zrozumienia powszechnego w przyrodzie procesu agregacji molekuł poprzez wiązania wodorowe.

I. Wstęp

A. Motywacja

Ciecze asocjujące to substancje, których molekuly na skutek wzajemnych słabych oddziaływań elektrostatycznych agregują tworząc większe struktury zwane klastrami. Istnieje wiele różnych asocjujących układów molekularnych w przyrodzie, będących ważnymi budulcami natury oraz człowieka. Przykładami są białka tworzące łańcuch DNA, cząsteczki cukrów czy woda [1–6]. Do celów dokładnych badań procesu asocjacji pożądanym jest układ modelowy, gdzie molekuly nie są złożone z wielu atomów (jak białka), ale posiadający dużo możliwości wariacji położenia grupy hydroksylowej odpowiedzialnej za oddziaływania wodorowe (co nie jest możliwe np. w przypadku wody). Ważne jest również, aby w molekule nie występowały wiązania wewnątrzcząsteczkowe, które mogłyby utrudniać interpretację struktur tworzonych przez oddziaływania międzycząsteczkowe. Modelowym układem do badania procesu asocjacji są alkohole monohydroksylowe.

Alkohole monohydroksylowe posiadają pojedynczą grupę hydroksylową w molekule. Grupa hydroksylowa jest źródłem silnego międzycząsteczkowego wiązania wodorowego łączącego molekuly w większe agregaty supramolekularne [7–10]. Molekuła najprostszycy alkoholi składa się oprócz tego z atomów węgla i wodoru, jednak może mieć różne rozmiary, kształty i pozycje atomów w cząsteczce. Alkohole monohydroksylowe można porównywać między innymi ze względu na długość łańcucha węglowego, obecność i rozmieszczenie grup funkcyjnych (np. pierścienia aromatycznego), oraz rozmieszczenie grupy hydroksylowej. Tak szeroki wybór prostych układów, które jednocześnie posiadają możliwość różnych modyfikacji czyni alkohole monohydroksylowe idealnymi kandydatami do poznania wpływu struktury molekularnej na właściwości asocjacji i spajających je wiązań wodorowych.

Szczególnie istotne jest poznanie zachowania asocjacji supramolekularnej w różnych warunkach termodynamicznych. Przede wszystkim brakuje wiedzy na temat struktury cieczy asocjujących w warunkach wysokiego ciśnienia. Zaletą badania alkoholi jest to, że w wielu przypadkach pozostają cieczami – ze względu na tendencję do przechłodzenia do stanu szklistego – w szerokim zakresie temperatur oraz ciśnień, co pozwala na obserwacje ewolucji procesu asocjacji w fazie ciekłej. Badania izotermiczne w funkcji ciśnienia są bardzo cenne, ponieważ dostarczają informacji zależnych jedynie od zmian gęstości układu, podczas gdy energia kinetyczna molekuł pozostaje

niezmieniona – inaczej niż w przypadku izobarycznych badań temperaturowych. Dyfrakcyjne badania ciśnieniowe są jednak niezwykle wymagające w przypadku alkoholi, które jako organiczne ciecze słabo rozpraszają promieniowanie rentgenowskie. Dlatego, obecnie takie eksperymenty mogą być prowadzone jedynie w ośrodkach synchrotronowych, gdzie stosuje się intensywną wiązkę promieniowania X [11–13].

Obecna wiedza na temat procesu asocjacji alkoholi opiera się głównie na wynikach otrzymanych metodami spektroskopowymi. Badania spektroskopii dielektrycznej dostarczyły informacji na temat relaksacji strukturalnej związanej z ruchem molekuly, oraz relaksacji Debye'a, która związana jest z ruchem supramolekularnych struktur łańcuchowych połączonych poprzez wiązania wodorowe [14,15]. Metoda spektroskopii w podczerwieni pozwoliła na uzyskanie wielu informacji na temat stopnia asocjacji molekuł w układzie, a także siły wiązań wodorowych [16,17]. Dotychczasowe badania, w niewielkim jednak stopniu scharakteryzowały architekturę oraz dystrybucję zasocjowanych molekuł. W tym kontekście, ze względu na szczególnie, mały rozmiar zakresu korelacji strukturalnych i klastrów supramolekularnych, wynoszący około 1 – 5 nm, dyfrakcja rentgenowska w zakresie szerokokątowym jest techniką, będącą w stanie przybliżyć strukturę tego typu układów. Dopelnieniem charakterystyki są symulacje dynamiki molekularnej dostarczające bezpośrednich informacji na temat układu molekuł. Połączenie wyników z symulacji zweryfikowane przez eksperyment pozwala na poprawne opisanie modeli asocjacji molekuł.

Dotychczas pokazano, że proces Debye'a przyjmuje różne natężenia dla układów, w zależności od pozycji grupy hydroksylowej w cząsteczce [18]. Sugeruje to występowanie różnych, dominujących typów klastrów w układzie. Badania alkoholi z pierścieniem węglowym pokazują przekrywanie się procesów strukturalnego i Debye'a co ogranicza wyciąganie wniosków lub może nawet prowadzić do błędnych wniosków na temat agregacji w tych układach [19,20]. Z kolei w przypadku obserwacji widm podczerwonych, w alkoholach fenylowych widoczne jest dodatkowe pasmo od niezasocjowanych wodorowo molekuł [14], co jednak nie daje informacji na temat tego czy w układzie tworzy się inna konkurencyjna agregacja. Badania spektroskopii dielektrycznej pod ciśnieniem wykazały wyraźne zmiany natężenia procesu Debye'a w układach prostych alkoholi [21,22]. Sugeruje to zachodzenie zmian dynamiki klastrów molekuł, będących efektem

reorganizacji struktury. Jednak szczegółowy opis tego procesu wymaga dalszych badań opierających się na poznaniu struktury układów asocjujących.

B. Dokonania naukowe

W pracy doktorskiej poruszyłam następujące problemy badawcze:

- jaki wpływ ma struktura cząsteczki: długość łańcucha alkilowego, lokalizacja grupy hydroksylowej, zawada steryczna w postaci pierścienia węglowego, aromatyczność pierścienia, na proces asocjacji molekuł wybranych etanoli, butanoli i heksanoli, i morfologię klastrów supramolekularnych, a także czas życia wiązań wodorowych;
- jakie są różnice w uporządkowaniu supramolekularnym oraz występowaniu w układzie asocjacji związanych wiązaniami wodorowymi a tworzonym przy udziale innych oddziaływań międzycząsteczkowych;
- jaki wpływ mają warunki termodynamiczne (temperatura, ciśnienie) na morfologię, architekturę, stopień uporządkowania, ilość i stabilność asocjacji molekularnych;
- jaki wpływ ma wysokie ciśnienie na konformacje molekuł badanych układów i, w rezultacie, na strukturę klastrów supramolekularnych.

Wyniki przedstawione w rozprawie zostały opublikowane w następujących artykułach z listy filadelfijskiej:

- P1. **Grelska, J.**, Jurkiewicz, K., Burian, A., & Pawlus, S. (2022). Supramolecular Structure of Phenyl Derivatives of Butanol Isomers. *The Journal of Physical Chemistry B*, 126(19), 3563
- P2. **Grelska, J.**, Jurkiewicz, K., Nowok, A., & Pawlus, S. (2023). Computer simulations as an effective way to distinguish supramolecular nanostructure in cyclic and phenyl alcohols. *Physical Review E*, 108(2), 024603
- P3. **Grelska, J.** (2024). Comment on “Universal features in the lifetime distribution of clusters in hydrogen-bonding liquids” by I. Jukić, M. Pożar, B. Lovrinčević and A. Perera, *Phys. Chem. Chem. Phys.*, 2021, 23, 19537. *Physical Chemistry Chemical Physics*, 26(6), 5713

P4. **Grelska, J.**, Temleitner, L., Park, C., Jurkiewicz, K., & Pawlus, S. (2024). High-Pressure and Temperature Effects on the Clustering Ability of Monohydroxy Alcohols. *The Journal of Physical Chemistry Letters*, 15, 3118

Ponadto, jestem współautorką publikacji powiązanych z tematyką pracy doktorskiej, gdzie stosowano kombinację różnych metod eksperymentalnych – spektroskopii dielektrycznej, spektroskopii podczerwonej, dyfrakcji rentgenowskiej oraz metod komputerowych – symulacji dynamiki molekularnej oraz modelowania teorią funkcjonału gęstości, w celu poznania struktury oraz dynamiki procesu asocjacji związków alkoholi i ich pochodnych. W tych artykułach mój wkład polegał na wykonaniu pomiarów dyfrakcji rentgenowskiej w warunkach pokojowych, temperaturowych, a także synchrotronowych badań pod ciśnieniem oraz przeprowadzeniu symulacji dynamiki molekularnej:

R1. Hachula, B., **Grelska, J.**, Soszka, N., Jurkiewicz, K., Nowok, A., Szeremeta, A. Z., Pawlus, S., Paluch, M., & Kaminski, K. (2022). Systematic studies on the dynamics, intermolecular interactions and local structure in the alkyl and phenyl substituted butanol isomers. *Journal of Molecular Liquids*, 346, 117098

R2. Nowok, A., Dulski, M., **Grelska, J.**, Szeremeta, A. Z., Jurkiewicz, K., Grzybowska, K., Musial, M., & Pawlus, S. (2021). Phenyl Ring: A Steric Hindrance or a Source of Different Hydrogen Bonding Patterns in Self-Organizing Systems? *The Journal of Physical Chemistry Letters*, 12(8), 2142

R3. Hachula, B., Włodarczyk, P., Jurkiewicz, K., **Grelska, J.**, Scelta, D., Fanetti, S., Paluch, M., Pawlus, S., & Kamiński, K. (2023). Pressure-Induced Aggregation of Associating Liquids as a Driving Force Enhancing Hydrogen Bond Cooperativity. *The Journal of Physical Chemistry Letters*, 15(1), 127

R4. Łucak, K., Szeremeta, A., Wrzalik, R., **Grelska, J.**, Jurkiewicz, K., Soszka, N., Hachula, B., Kramarczyk, D., Grzybowska, K., Yao, B., Kaminski, K., & Pawlus, S. (2023). Experimental and Computational Approach to Studying Supramolecular Structures in Propanol and Its Halogen Derivatives. *The Journal of Physical Chemistry B*, 127(42), 9102

R5. Soszka, N., Hachula, B., Tarnacka, M., **Grelska, J.**, Jurkiewicz, K., Geppert-Rybczyńska, M., Wrzalik, R., Grzybowska, K., Pawlus, S., Paluch, M., & Kaminski, K. (2022). Aromaticity Effect

on Supramolecular Aggregation. Aromatic vs. Cyclic Monohydroxy Alcohols. *Spectrochimica Acta Part A: Molecular and Biomolecular Spectroscopy*, 276, 121235

R6. Nowok, A., Dulski, M., Jurkiewicz, K., **Grelska, J.**, Szeremeta, A. Z., Grzybowska, K., & Pawlus, S. (2021). Molecular stiffness and aromatic ring position– Crucial structural factors in the self-assembly processes of phenyl alcohols. *Journal of Molecular Liquids*, 335, 116426

R7. Soszka, N., Hachula, B., Tarnacka, M., Kaminska, E., **Grelska, J.**, Jurkiewicz, K., Geppert-Rybczynska, M., Wrzalik, R., Grzybowska, K., Pawlus, S., Paluch, M., & Kaminski, K. (2021). The impact of the length of alkyl chain on the behavior of benzyl alcohol homologues – the interplay between dispersive and hydrogen bond interactions. *Physical Chemistry Chemical Physics*, 23(41), 23796

R8. Jurkiewicz, K., Kolodziej, S., Hachula, B., Grzybowska, K., Musial, M., **Grelska, J.**, Bielas, R., Talik, A., Pawlus, S., Kaminski, K., & Paluch, M. (2020). Interplay between structural static and dynamical parameters as a key factor to understand peculiar behaviour of associated liquids. *Journal of Molecular Liquids*, 319, 114084

R9. Nowok, A., Jurkiewicz, K., Dulski, M., Hellwig, H., Malecki, J. G., Grzybowska, K., **Grelska, J.**, & Pawlus, S. (2021). Influence of molecular geometry on the formation, architecture and dynamics of H-bonded supramolecular associates in 1-phenyl alcohols. *Journal of Molecular Liquids*, 326, 115349

Rezultaty moich badań zaprezentowałam na międzynarodowych konferencjach naukowych:

- *Opportunities for Advancement for Studies of Matter at Extreme Condition*, Lemont, USA (07-09/11/2023), prezentacja plakatu: Molecular clustering in alcohols under high-pressure and temperature conditions
- *9th International Discussion Meeting on Relaxations in Complex Systems (IDMRCS)*, Chiba, Japonia (12-18/08/2023), wystąpienie ustne na zaproszenie: Comprehensive studies on molecular self-aggregation in alcohols
- *15th International School and Symposium on Synchrotron Radiation in Natural Science (ISSRNS)*, Przegorzaly, Polska (22-25/08/2022), wystąpienie ustne: Structure of alcohols under high pressure

- *The European Physical Society (EPS) Forum*, Paryż, Francja (02-04/06/2022), prezentacja plakatu: Predicting properties of self-associating liquids under high-pressure
- *Young Multis – Multiscale Phenomena in Condensed Matter Conference for young researchers*, online (05-07/07/2021), wystąpienie ustne: The supramolecular structure of associating alcohols

Badania, których wyniki zawarte są w pracy doktorskiej były finansowane w ramach projektu Narodowego Centrum Nauki OPUS *Wysokociśnieniowe badania spektroskopowe i dyfrakcyjne jako klucz do zrozumienia osobliwego zachowania asocjujących cieczy z wiązaniami wodorowymi i oddziaływaniami van der Waalsa* (no. UMO-2019/35/B/ST3/02670). Badania synchrotronowe były przeprowadzane w ośrodkach badawczych: Europejskim Centrum Synchrotronowym (ESRF) we Francji oraz Advanced Photon Source (APS), Argonne National Laboratory, w USA. W ramach prowadzenia badań do pracy odbyłam staże naukowe w grupach badawczych: High Pressure Collaborative Access Team (HPCAT) w Argonne National Laboratory, USA, oraz Liquid Structure Research Group w Wigner Research Centre for Physics, Węgry.

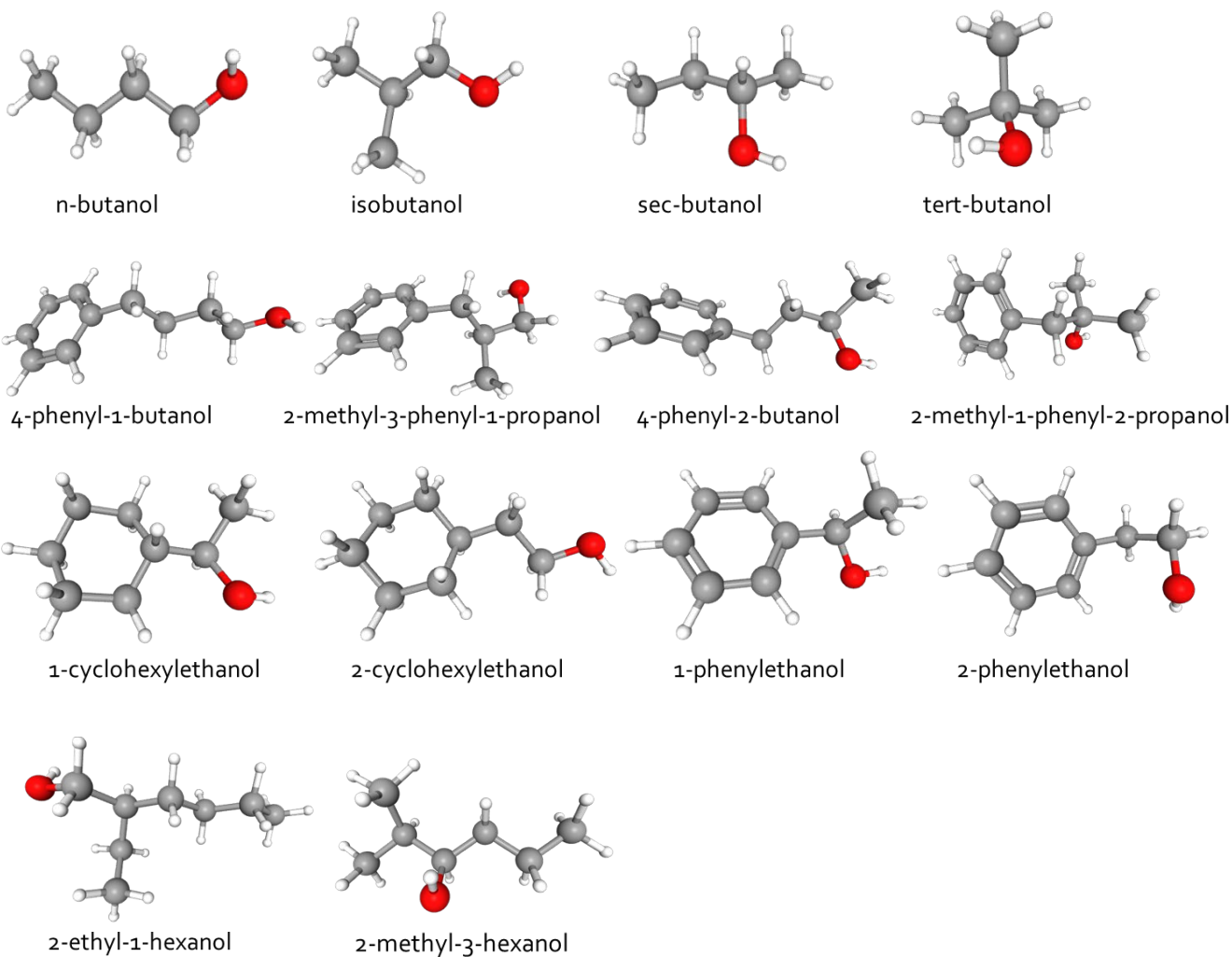
C. Badane substancje

Badane substancje to alkohole monohydroksylowe, posiadające pojedynczą grupę hydroksylową w molekułe, różniące się jej położeniem w łańcuchu węglowym, a także innymi różnicami w budowie cząsteczki. W pracy skupiono się na następujących grupach alkoholi:

- izomerach butanoli (n-butanol, isobutanol, sec-butanol, tert-butanol), czyli molekuł o tym samym składzie chemicznym, ale różnym przestrzennym rozmieszczeniu atomów,
- fenyłowych pochodnych butanoli, izomerach (4-phenyl-1-butanol, 2-methyl-3-phenyl-1-propanol, 4-phenyl-2-butanol, 2-methyl-1-phenyl-2-propanol) posiadających w budowie aromatyczny pierścień fenyłowy,
- fenyłowych pochodnych etanolu, izomerach (1-phenylethanol, 2-phenylethanol) różniących się pozycją grupy hydroksylowej – blisko pierścienia i na końcu łańcucha węglowego,
- cyklicznych odpowiednikach pochodnych etanolu, izomerach (1-cyclohexylethanol, 2-cyclohexylethanol) posiadających w budowie alifatyczny pierścień cykliczny,

- heksanolach (2-ethyl-1-hexanol, 2-methyl-3-hexanol) posiadających dłuższe łańcuchy węglowe, różniących się pozycją grupy hydroksylowej – w środku molekuly i na końcu łańcucha węglowego.

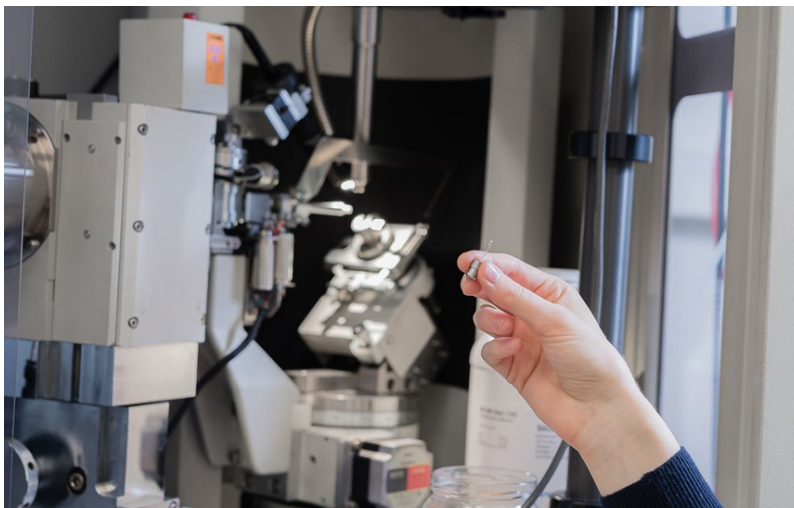
Struktury cząsteczek wszystkich badanych alkoholi zostały przedstawione na Rys. 1. Nazwy związków alkoholi są podane w języku angielskim, tak jak w publikacjach naukowych.



Rys. 1. Modele cząsteczek badanych alkoholi monohydroksylowych.

D. Metody eksperymentalne

Główną metodą eksperymentalną zastosowaną do badania struktury substancji na poziomie atomowym była szerokokątowa dyfrakcja rentgenowska. Do pomiarów wykorzystano laboratoryjny dyfraktometr rentgenowski wyposażony w srebrną rotującą anodę oraz dwuwymiarowy detektor, przedstawiony na Rys. 2. Długość monochromatyzowanego promieniowania padającego na próbkę wynosiła 0.5608 \AA , co w połączeniu z zastosowaną geometrią, pozwoliło na zebranie danych w szerokim zakresie wektorów rozpraszania, około $0.2 - 20 \text{ \AA}^{-1}$. Zakres niskich kątów rozpraszania dostarczał ważnych informacji o obecności i cechach maksimum dyfrakcyjnych związanych z występowaniem w strukturze badanych alkoholi uporządkowania średniego zasięgu. Natomiast zakres szerokich kątów rozpraszania był istotny do otrzymania funkcji rozkładu par atomów o dobrej rozdzielczości. Pomiarów próbek wykonywano w szklanych kapilarach. Przystawka temperaturowa dawała możliwość pomiarów w zakresie $-100 - 200^\circ\text{C}$. Przykład zebranego obrazu dyfrakcyjnego jest pokazany na Rys. 3. Dane z postaci dwuwymiarowego dyfraktogramu były następnie całkowane do postaci jednowymiarowej funkcji natężenia, oraz, po korekcy i normalizacji, przekształcane do postaci czynnika struktury w przestrzeni odwrotnej oraz funkcji rozkładu par w przestrzeni rzeczywistej za pomocą poniżej zaprezentowanych równań.



Rys. 2. Dyfraktometr Rigaku-Denki D/MAX RAPID II-R (Instytut Fizyki, Uniwersytet Śląski w Katowicach) wraz z prezentacją próbki mierzonej w kapilarze.



Rys. 3. Dwuwymiarowy obraz dyfrakcyjny (isobutanol) otrzymany za pomocą laboratoryjnego dyfraktometru.

Teoria rozpraszania promieniowania X na periodycznym układzie atomów opiera się na prawie Bragga:

$$d = \frac{\lambda}{2\sin\theta}, \quad (1)$$

gdzie odległość międzypłaszczyznową d można obliczyć znając połowę kąta rozpraszania θ , przy którym obserwuje się maksimum dyfrakcyjne, oraz długość fali promieniowania padającego λ . Do przedstawienia danych dyfrakcyjnych stosuje się skalę wektora rozpraszania Q niezależnego od długości fali używanej w eksperymencie:

$$Q = \frac{4\pi\sin\theta}{\lambda}. \quad (2)$$

Rozwiązując strukturę cieczy i szkieł należy mieć na uwadze, że nie posiadają periodycznej struktury kryształu. Natężenie promieniowania rozproszonego $I(Q)$ przez dowolny izotropowy układ N atomów opisuje równanie Debye'a [23]:

$$I(Q) = \sum_{i=1}^N \sum_{j=1}^N f_i f_j \frac{\sin(Qr_{ij})}{Qr_{ij}}, \quad (3)$$

gdzie f_i, f_j to atomowe współczynniki rozpraszania atomów, które znajdują się w odległości r_{ij} . W celu unormowania natężenia przypadającego na jeden atom, zakładając koncentrację rodzaju atomu x_α i liczbę wszystkich rodzajów atomów w układzie m , definiuje się czynnik struktury $S(Q)$:

$$S(Q) = \frac{I(Q) - \sum_{\alpha=1}^m x_\alpha f_\alpha^2(Q)}{(\sum_{\alpha=1}^m x_\alpha f_\alpha(Q))^2}. \quad (4)$$

Z drugiej strony, można zdefiniować parcjalaną funkcję rozkładu par atomów $g_{\alpha\beta}(r)$, która jest określana na podstawie stosunku gęstości atomów różnych rodzajów $\rho_{\alpha\beta}(r)$ w odległości r od dowolnie wybranego układu odniesienia, do średniej gęstości atomowej substancji ρ_0 :

$$g_{\alpha\beta}(r) = \frac{\rho_{\alpha\beta}(r)}{\rho_0}. \quad (5)$$

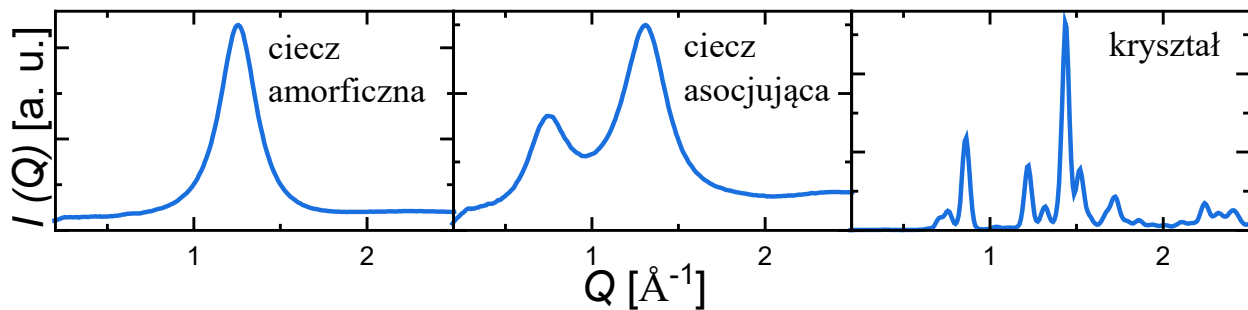
Wtedy, parcjalny czynnik struktury $S_{\alpha\beta}(Q)$ można zdefiniować jako sinusową transformatę Fouriera funkcji rozkładu par:

$$S_{\alpha\beta}(Q) = \frac{4\pi\rho_0}{Q} \int_0^{r_{max}} r(g_{\alpha\beta}(r) - 1) \sin(Qr) dr. \quad (6)$$

Całkowity czynnik struktury to kombinacja liniowa czynników parcjalnych:

$$S(Q) = \sum_{\alpha=1}^m \sum_{\beta=1}^m \frac{x_{\alpha}x_{\beta}f_{\alpha}(Q)f_{\beta}(Q)S_{\alpha\beta}(Q)}{(\sum_{\alpha=1}^m x_{\alpha}f_{\alpha}(Q))^2}. \quad (7)$$

Zmierzone w eksperymencie natężenie $I(Q)$ może być więc przeliczone do postaci czynnika struktury za pomocą równania (4) przy uwzględnieniu poprawek na absorpcję, polaryzację oraz efekt Comptona. Obrazy dyfrakcyjne cieczy asocjujących, do których należą badane alkohole monohydroksylowe mają cechy, które kwalifikują tego typu związki jako posiadające strukturę pomiędzy nieuporządkowaną (amorficzną) a uporządkowaną (krystaliczną), Rys. 4.

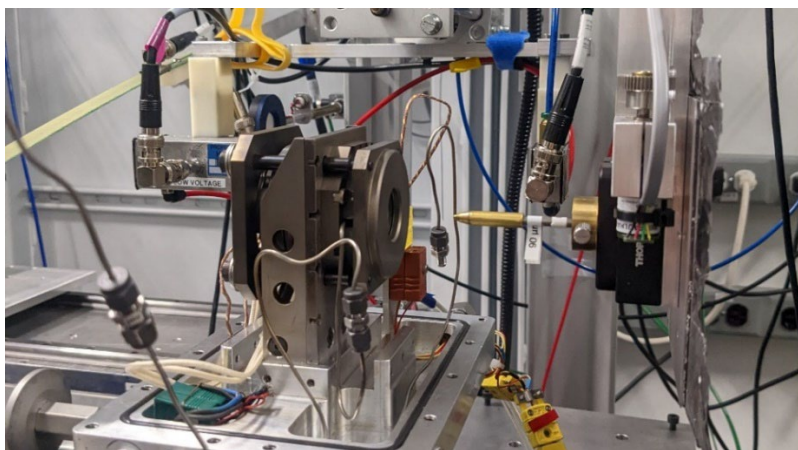


Rys. 4. Dyfraktogramy rentgenowskie (eksperymentalne natężenia) substancji o różnym typie struktury atomowej: ciecz amorficzna (cyclohexane, 293 K), ciecz asocjująca (tert-butanol 293 K), kryształ (tert-butanol, 143 K).

Dyfraktogram kryształu wykazuje wąskie piki braggowskie, które reprezentują promieniowanie rozproszone na rodzinach płaszczyzn krystalograficznych. Dyfraktogram cieczy amorficznej charakteryzuje się jednym szerokim „halo”, które pojawia się w wyniku korelacji strukturalnych

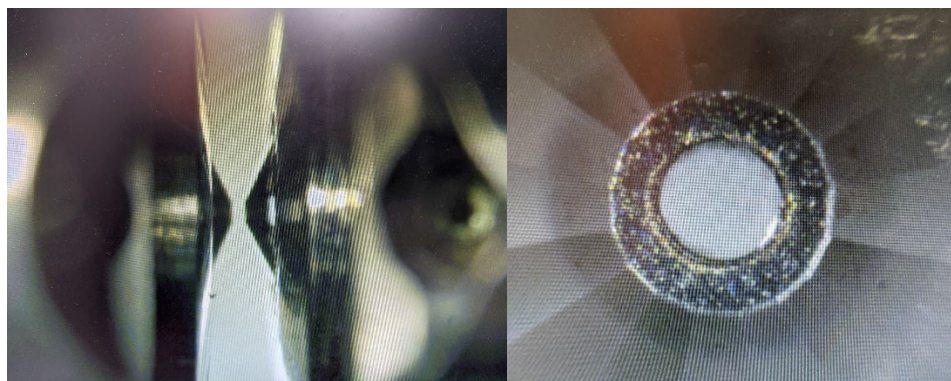
w zakresie bliskiego zasięgu i jego położenie odzwierciedla średnie najbliższe odległości między cząsteczkami. Natomiast typowy dyfraktogram alkoholu monohydroksylowego charakteryzuje się występowaniem dodatkowego maksimum dyfrakcyjnego w zakresie mniejszych wektorów rozpraszania niż główne halo. Z tego względu określa się go mianem „prepiku” (ang. „prepeak”). Jego położenie odzwierciedla periodyczności korelacji strukturalnych w zakresie średniego zasięgu. Korzystając z równań (1) i (2) otrzymujemy zależność $d = 2\pi/Q$, która określa relację między pozycjami maksimum Q w przestrzeni odwrotnej a rzeczywistymi periodycznościami d w układzie. W badanych alkoholach pozycja prepiku około $0.5 - 0.9 \text{ \AA}^{-1}$ oznacza występowanie powtarzających się odległości w przestrzeni rzeczywistej wynoszących około $7 - 13 \text{ \AA}$ przepisywanym średnim odległościom pomiędzy klastrami molekuł związanych wiązaniami wodorowymi.

Większość badanych alkoholi podczas przechłodzenia nie krystalizuje, a przechodzi do fazy szklistej znacznie poniżej temperatury zamarzania wody. W pracy doktorskiej badano substancje w szerokim zakresie temperatur – pomiędzy temperaturami przejścia szklistego a wrzenia. Badania dyfrakcyjne w warunkach wysokiego ciśnienia (do około 3 GPa), sięgającego ciśnienia zeszklenia, nie były możliwe do wykonania na laboratoryjnym dyfraktometrze. Pomiarów te wykonano w ośrodku synchrotronowym, który dysponuje znacznie wyższym natężeniem promieniowania X (Rys. 5.), a także możliwością zamontowania układu kowadeł diamentowych służących do wytworzenia wysokiego ciśnienia na próbce (Rys. 6.).

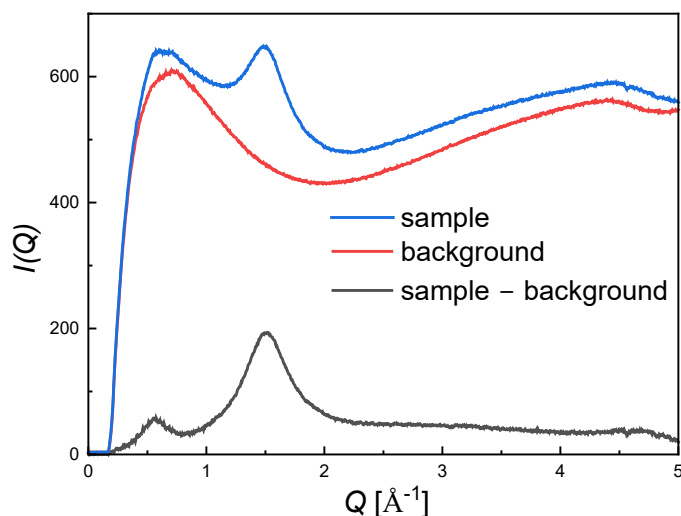


Rys. 5. Linia pomiarowa 16-BM-D w Argonne National Laboratory, USA.

Eksperymenty wysokociśnieniowe wymagały precyzyjnego umieszczenia ciekłej substancji pomiędzy diamentowymi kowadłami, a także dobrania odpowiedniej energii promieniowania, tak aby nie wywołać zniszczenia radiacyjnego próbki, a przy tym mierzony zakres kątów rozpraszania był dostatecznie szeroki. Wymagająca była również redukcja i korekcja otrzymanych dyfraktogramów, które zawierały znaczący wkład tła wynikającego z silnego rozpraszania promieniowania przez kowadła diamentowe (Rys. 7.). Po korekcji tła dane dyfrakcyjne zostały unormowane do postaci czynnika struktury za pomocą oprogramowania Amorpheus [24].



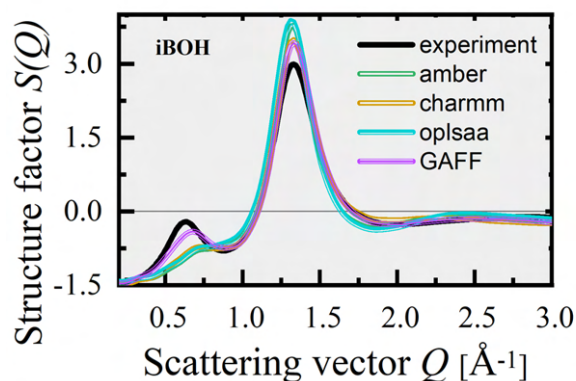
Rys. 6. Układ diamentowych kowadeł widziany równoległe (po lewej), i prostopadle (po prawej) do padającej wiązki promieniowania. Próbką nakładana jest na środek powierzchni diamentu (rysunek po prawej).



Rys. 7. Porównanie dyfraktogramów alkoholu (2-ethyl-1-hexanol, 1 GPa, 293 K) zmierzonego w kowadłach diamentowych i zawierającego wkład od tła (sample), tła czyli pustych kowadeł diamentowych (background), oraz alkoholu po odjęciu tła (sample – background).

E. Symulacje komputerowe

Modele struktury otrzymane w wyniku przeprowadzenia symulacji komputerowych mogą dostarczyć wielu informacji o budowie w skali atomowej, trudnych lub niemożliwych do pozyskania z wyników eksperymentów dyfrakcyjnych. W ramach niniejszej pracy przeprowadzono symulacje badanych alkoholi metodą dynamiki molekularnej w pakiecie GROMACS [25–27]. Istotnym elementem optymalizacji otrzymywanych modeli struktury był wybór pola siłowego, które najlepiej opisuje oddziaływania międzycząsteczkowe, i w efekcie rozmieszczenie cząsteczek. Testowane były różne pola siłowe, a obliczony na podstawie uzyskanego modelu struktury całkowity czynnik struktury porównywany był z wynikiem eksperymentalnym (Rys. 8.). Najlepszą zgodność dało pole siłowe GAFF [28], zaprojektowane do opisu prostych związków organicznych, także zawierających pierścienie aromatyczne.



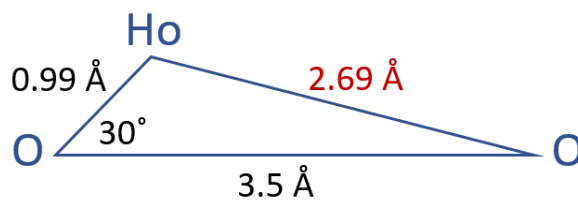
Rys. 8. Porównanie czynnika struktury otrzymanego na podstawie danych z eksperymentu dyfrakcyjnego (experiment) dla isobutanolu, oraz czynników struktury otrzymanych na bazie danych z symulacji dla różnych pól siłowych (amber, charmm, oplsa, GAFF).

Dodatkowo, testowane były różne czasy symulacji oraz wielkości układu (liczby cząsteczek). Zadowalające wyniki uśrednionej struktury otrzymano dla układów składających się z 2000 molekuł i czasu symulacji 2 ns dla warunków pokojowych. W przypadku symulacji przeprowadzonych w różnych warunkach termodynamicznych, czas symulacji był wydłużony. W zakresie temperatur 293 – 413 K czas symulacji wynosił 10 ns, w temperaturach 213 – 273 K oraz dla ciśnień w zakresie 0.1 – 3 GPa wynosił 50 ns ze względu na wolniejszą relaksację molekuł. Do analizy wykorzystywano około 100 trajektorii położenia atomów w układzie. W przypadku symulacji układów, dla których wyznaczane były czasy życia wiązań wodorowych,

wykorzystano wcześniej zoptymalizowane modele struktury i czas symulacji wynosił 0.3 ns z gęstym zapisem danych co 0.002 ps. Krok czasowy wszystkich symulacji wynosił 0.001 ps.

Do analizy wyników z symulacji zastosowano program TRAVIS [29–31], służący do obliczenia parcjalnych funkcji rozkładu par atomów, parcjalnych czynników struktury oraz całkowitych czynników struktury zgodnie z równaniami (5-7). Program posłużył także do otrzymania dystrybucji wektorów molekuł. Podprogramy pakietu GROMACS zostały wykorzystane do obliczenia dystrybucji klastrów (*gmx clustsize*), liczby i czasu życia wiązań wodorowych (*gmx hbond*) oraz dystrybucji kątów walencyjnych w molekułach (*gmx angle*). Dodatkowo, w ramach współpracy opracowano program do obliczenia dystrybucji i wizualizacji różnych typów klastrów supramolekularnych [32].

W celu określenia układu związanych molekuł (klastra) zastosowano różne definicje wiązania wodorowego przez grupy hydroksylowe, które były konsekwentnie stosowane dla badanych grup alkoholi w publikacjach. Warunek na odległość atomów tlenu dwóch molekuł biorących udział w wiązaniu ($O-O < 3.5 \text{ \AA}$) był przyjęty jako minimum funkcji rozkładu par atomów i stosowany bez dodatkowej restrykcji na kąt wiązania. Warunek na odległość tlenu i wodoru kowalencyjnie związanego z tlenem z drugiej molekuły ($O-H_O < 2.69 \text{ \AA}$), otrzymany na podstawie najbliższej odległości między atomami wodoru i tlenu w funkcji rozkładu par atomów 0.99 \AA , spełniał jednocześnie warunek na maksymalny kąt wiązania 30° , Rys. 9. W przypadku symulacji w różnych warunkach termodynamicznych, gdzie długość wiązania wodorowego się zmienia, zastosowano warunek na odległości ($O-O < 4 \text{ \AA}$, $O-H_O < 2.7 \text{ \AA}$) oraz kąt wiązania ($OH_O-O < 40^\circ$).



Rys. 9. Schematyczne przedstawienie przyjętych warunków geometrycznych na tworzenie się wiązania wodorowego pomiędzy cząsteczkami badanych alkoholi.

II. Wyniki i dyskusja

A. Wpływ budowy molekularnej na proces asocjacji

W pierwszej publikacji [P1] badano wpływ pozycji grupy hydroksylowej w molekułe na proces asocjacji w izomerach butanolu, oraz ich odpowiednikach fenyłowych. Czynniki struktury obliczone na bazie eksperymentu oraz symulacji w szerokim zakresie kątów rozpraszania wykazały bardzo dobrą zgodność, obliczone współczynniki rozbieżności wynosiły tylko ok. 10% (Fig. 2 [P1]). Wyznaczone czynniki struktury (Fig. 2 [P1]) pokazują, że charakterystyczny prepik jest bardziej wyraźny w serii butanolu, w porównaniu do ich fenyłowych odpowiedników. Co więcej, wśród grupy izomerów butanolu, prepik ma różne natężenia i pozycje. W celu wyjaśnienia opisanych różnic, na podstawie danych z symulacji obliczono cząstkowe czynniki struktury, które sumują się do całkowitego czynnika struktury. Z ich przebiegu (Fig. 3 [P1]) można zauważyć, że za główny wkład do prepiku odpowiadają korelacje OO oraz CO. W przypadku alkoholi fenyłowych, korelacje CO są ujemne, i razem z dodatnimi, ale o niewielkim natężeniu korelacjami OO, znoszą się dając natężenie prepiku bliskie zeru w całkowitym czynniku struktury. Natomiast w przypadku izomerów butanolu, natężenia korelacji OO są większe niż dla ich odpowiedników fenyłowych i razem z dodatnimi korelacjami CO sumują się do intensywniejszych prepików w całkowitych czynnikach struktury. Korelacje funkcji OO są utożsamiane z porządkiem uformowanym przez klastry cząsteczek związanych wodorowo. Każda molekula posiada jeden atom tlenu w grupie hydroksylowej uczestniczącej w wiązaniu wodorowym, dlatego są to korelacje czysto międzycząsteczkowe, wynikające z układu cząsteczek asocjujących przez wiązania wodorowe. Na podstawie modeli z symulacji policzono dystrybucje klastrów związanych wodorowo (Fig. 5 [P1]) oraz zwizualizowano wycinki modeli struktur (Fig. 6 [P1]). Z histogramów (Fig. 5 [P1]) można zauważyć odmienny sposób agregacji alkoholi butylowych w porównaniu do ich fenyłowych odpowiedników. Cząsteczki izomerów butanolu są w dużym stopniu (ok. 97%) zasocjowane w klastry związane wodorowo, natomiast cząsteczki alkoholi fenyłowych w mniejszym stopniu (ok. 80-90%). W dalszej części publikacji przedstawiono obliczone rozkłady wybranych kątów walencyjnych cząsteczek, które pozwalały na określenie ich konformacji. Celem analizy konformacji było poznanie związków między różnorodnością konformacyjną a rodzajem tworzonych klastrów supramolekularnych. Na podstawie przedstawionych rozkładów (Fig. SI5 Supporting Information for [P1]) widać, że przed przeprowadzeniem symulacji i optymalizacji geometrii wszystkie molekuly przyjmowały jedną

konformację. Jest to związane ze sposobem tworzenia pudełka symulacyjnego, gdzie na początku jeden model cząsteczki jest powielany w układzie. Następnie, po zadanym czasie symulacji obserwuje się szerokie rozkłady kątów walencyjnych. W przypadku sześciu alkoholi posiadających giętkie łańcuchy węglowe, trzech izomerów butanolu i ich trzech fenylowych odpowiedników, widoczne są wyróżniające się dwa maksima w rozkładach kątów walencyjnych, co odpowiada pojawieniu się dwóch konformacji molekuł w układzie. Alkohole fenyłowe mają niemal identyczne rozkłady kątów jak odpowiadające im proste butanole. Z kolei w przypadku tert-butanolu (i jego fenyłowego odpowiednika), widoczna jest tylko jedna konformacja, co jest związane ze sferycznym kształtem tych cząsteczek i krótszym łańcuchem węglowym. Taka budowa może determinować bardziej ograniczony sposób asocjacji cząsteczek tego izomeru. Natomiast molekuly pozostałych izomerów zdolnych do tworzenia różnych konformacji mogą w większym stopniu dopasowywać ułożenie grup hydroksylowych w celu lub jako skutek tworzenia wiązań wodorowych. Na wycinkach modeli (Fig. 6 [P1]) zobrazowana jest różnica w klastrach tworzonych przez izomery butanolu, gdzie alkohol z grupą hydroksylową na końcu molekuly (n-butanol) tworzy klastry o średniej wielkości 16 molekuł i kształcie długich łańcuchów, a tert-butanol o sferycznej budowie cząsteczki tworzy klastry o kształcie kolistym i preferowanej liczbie 4 molekuł w klastrze. Na wycinkach modeli alkoholi fenyłowych (Fig. 6 [P1]) można zauważyć dodatkowy typ organizacji cząsteczek poprzez pierścienie fenyłowe, znany w literaturze jako agregacja π - π . Dodatkowa agregacja wyjaśnia fakt występowania mniejszej ilości zasocjowanych wodorowo molekuł w związkach fenyłowych w porównaniu z prostymi butanolami.

B. Agregacja związków z pierścieniem węglowym

Agregacja cząsteczek alkoholi poprzez pierścienie stała się tematem kolejnej publikacji. W artykule [P2] badano alkohole cykliczne posiadające cykliczny, alifatyczny pierścień węglowy, charakteryzujący się giętkością i łatwością tworzenia różnych konformacji, oraz ich fenyłowe odpowiedniki, których aromatyczny, sztywny pierścień może być źródłem oddziaływań π - π , a także oddziaływań OH- π pomiędzy grupą hydroksylową a pierścieniem aromatycznym. Badane izomery cykliczne oraz fenyłowe dodatkowo różniły się pozycją grupy OH – blisko pierścienia i na końcu molekuly. Zmierzone oraz obliczone z danych symulacyjnych czynniki struktury (Fig. 1 [P2]) charakteryzują się widocznymi różnicami pomiędzy grupą alkoholi fenyłowych i cyklicznych. Alkohole cykliczne wykazują bardziej intensywny prepik oraz główne halo

dyfrakcyjne o mniejszej szerokości połówkowej. W odpowiednikach fenylowych prepik jest mniej widoczny, a halo ma niższe natężenie i jest bardziej rozmyte. Takie zachowanie świadczy o większej dystrybucji bliskich odległości między molekułami w alkoholach fenylowych niż w cyklicznych. Podobnie jak w poprzedniej pracy, pochodzenie prepiku zostało wyjaśnione na podstawie parcjalnych czynników struktury (Fig. S11 Supplementary Information for [P2]), gdzie można zauważyć wyższe natężenie funkcji korelacji OO dla alkoholi cyklicznych, ale też wyższe natężenie funkcji CO dla alkoholi z grupą OH bliżej pierścienia (cyklicznego oraz fenyłowego) niż na końcu łańcucha węglowego. Wyższe natężenie korelacji CO w regionie prepiku może być związane z architekturą klastrów o wysokim porządku, np. jednorodnych klastrów kołowych. W celu charakterystyki struktury supramolekularnej badanych alkoholi zdefiniowane były trzy typy klastrów (Fig. 3 [P2]). Pierwszy typ klastrów dotyczył grup cząsteczek połączonych wiązaniami wodorowymi, gdzie średni rozmiar klastrów był większy w przypadku alkoholi cyklicznych, a liczba niezasocjowanych molekuł była trzy razy niższa (3% wszystkich cząsteczek w układzie) niż w alkoholach fenylowych (ok. 10% układu). W celu definicji klastrów drugiego typu – układów pierścieni węglowych, odzwierciedlających agregację typu π - π , w obu grupach związków wybrano najprostszy warunek uwzględniający odległości pomiędzy pierścieniami węglowymi. Dla alkoholi fenylowych odległość ta wyniosła 4 Å, dla alkoholi cyklicznych ze względu na mniejszą gęstość maksymalna odległość wynosiła 4.14 Å. Większą agregację poprzez pierścienie węglowe obserwuje się w alkoholach fenylowych, gdzie dotyczy ona 60% cząsteczek w całym układzie i objawia się występowaniem agregatów składających się najczęściej z dwóch, trzech cząsteczek, ale zdarzają się też większe agregaty. Tymczasem w alkoholach cyklicznych agregaty pierścieni stanowią 40% wszystkich cząsteczek i są wynikiem raczej przypadkowego ułożenia dwóch sąsiednich molekuł. Ostatnim typem wykrytych klastrów były struktury odpowiadające agregatom tworzonym poprzez wiązanie OH- π . Taki typ klastrowania został znaleziony tylko w alkoholach fenylowych, gdzie dotyczy ok. 20% cząsteczek w modelu, z czego można wywnioskować że jest najmniej preferowany spośród rozważanych trzech typów układów supramolekularnych. Potwierdzenie tego wniosku zostało znalezione w wynikach eksperymentalnych spektroskopii w podczerwieni (Fig. S12 Supplementary Information for [P2]), które pokazały, że oprócz pasma pochodzącego od grup związanych wodorowo, obecnego dla wszystkich alkoholi, widoczne jest pasmo pochodzące od wiązań typu OH- π obecne tylko dla alkoholi fenylowych. Wycinki modeli (Fig. 4 [P2]) dobrze obrazują różne sposoby i wielkości

tworzących się agregatów w badanych alkoholach. Molekuły alkoholi cyklicznych łączą się w długie łańcuchy związane wodorowo, a w przypadku alkoholu cyklicznego z grupą hydroksylową położoną bliżej pierścienia, klastry mają też kształt kolisty. W porównaniu z odpowiednikami cyklicznymi, alkohole fenyłowe tworzą mniejsze klastry związane wodorowo. W alkoholach cyklicznych brak jest widocznej konkurencji w tworzeniu agregatów związanych wodorowo. Natomiast, dla alkoholi fenyłowych wyraźnie widoczna jest agregacja typu π - π (poprzez pierścienie aromatyczne) i typu OH- π , sprawiając, że w efekcie możliwych różnych typów oddziaływań międzycząsteczkowych tworzy się zróżnicowana, heterogeniczna struktura układu. Dla zobrazowania sposobu uporządkowania sąsiednich molekuł, zdefiniowano wektor imitujący moment dipolowy molekuły i policzono dystrybucje wektorów w układzie (Fig. 4 [P2]). Na wykresach widać większe natężenia dystrybucji ułożeń molekuł dla alkoholi cyklicznych, w porównaniu z fenyłowymi, co oznacza więcej sąsiednio uporządkowanych cząsteczek w układzie. Kolejną ciekawą obserwacją było zauważenie podobieństw w organizacji cząsteczek alkoholi o tej samej pozycji grupy OH. Niezależnie, czy był to alkohol cykliczny czy fenyłowy, obserwowano równoległe ułożenie wektorów (maksimum natężenia dla około 180°) dla alkoholi z grupą hydroksylową ułożoną na końcu molekuły oraz prostopadłe ułożenie (maksimum natężenia około 120°) dla alkoholi z grupą OH położoną bliżej pierścienia. Potwierdza to bardziej kołowy sposób ułożenia cząsteczek w klastrach w przypadku drugiej wspomnianej grupy związków. Warto nadmienić, że wyniki symulacji korelują z wynikami uzyskanymi za pomocą spektroskopii dielektrycznej, a konkretnie – współczynnikiem Kirkwooda (Fig. SI3 Supplementary Information for [P2]). Wysoka wartość współczynnika Kirkwooda jest obserwowana dla układów, gdzie cząsteczki alkoholi układają się równoległe wzdłuż łańcuchów wiązań wodorowych i gdzie ilość takich ułożeń jest duża. Najwyższą wartość czynnika Kirkwooda dla badanych alkoholi, w temperaturze pokojowej, odnotowano dla 2-cyclohexylethanolu, co koreluje z silnym równoległym uporządkowaniem wektorów molekuł. Następnie, niższą wartość współczynnika Kirkwooda obserwuje się dla 1-cyclohexylethanolu o prostopadłym ułożeniu molekuł, ale silnie zasocjowanych i tworzących duże klastry, oraz dla dwóch fenyłowych alkoholi, gdzie występują mniejsze klastry o większym nieporządku ułożeń wektorów cząsteczek. W artykule pokazano, że struktura supramolekularna alkoholi fenyłowych, w porównaniu do alkoholi cyklicznych, mimo podobnej budowy molekuły, wykazuje większą heterogeniczność, której źródłem jest dodatkowa agregacja wynikająca z aromatyczności pierścienia.

C. Czas życia wiązań wodorowych w klastrach

W kolejnej pracy [P3] za pomocą symulacji dynamiki molekularnej zbadano czas życia wiązań wodorowych alkoholi. Motywacją do przeprowadzenia tych badań była chęć weryfikacji tezy na temat uniwersalnego rozkładu czasu życia wiązań wodorowych przedstawionej w artykule [33]. Autorzy tej publikacji pokazali, że rozkłady czasów życia prostych alkoholi monohydroksylowych posiadają trzy charakterystyczne maksima, przy założeniu warunku na odległość wiązania wodorowego 2.5 – 3.5 Å. Pierwsze maksimum nazwali „dimer peak” i jego pochodzenie przypisali wiązaniu w układach dwóch molekuł (dimerów). Drugie i trzecie maksima o nazwie „cluster peak” i „topology peak” autorzy przypisali kolejno wiązaniom wodorowym w większych klastrach molekuł oraz topologii tych klastrów. Co ciekawe, dwa ostatnie maksima, w przeciwieństwie do pierwszego, którego pozycja przesuwiała się w stronę dłuższych czasów życia wraz ze zwiększaniem warunku na odległość, miały stałe pozycje, wynoszące ok. 0.02 ps i 0.05 ps. Autorzy twierdzili, że taka dystrybucja maksimów czasów życia wiązań wodorowych jest cechą uniwersalną różnych alkoholi tworzących struktury związane wodorowo. Wykorzystując metodykę zaproponowaną w opisanym artykule, wyznaczono dystrybucje czasów życia wiązań wodorowych alkoholi i uzyskano podobne ich przebiegi (Fig. 2 [P3]). W celu zbadania zależności czasów życia od topologii klastrów, analizie poddano dwie pary związków – tworzący w większości liniowe klastry n-butanol i jego izomer tert-butanol tworzący w większości klastry kołowe, oraz parę heksanoli o podobnych preferencjach klastrowania. Na uzyskanych dystrybucjach (Fig. 3 [P3]) nie zauważono zmian w pozycji trzeciego maksimum, powiązanego z topologią klastrów. Z kolei widoczna była zmiana położenia pierwszego maksimum – było one przesunięte w kierunku dłuższych czasów życia dla związków tworzących klastry kołowe w porównaniu do związków tworzących klastry liniowe. W rezultacie pokazano, że charakterystyczna topologia klastrów związanych wodorowo jest odzwierciedlona w pierwszym maksimum dystrybucji czasów życia. Dodatkowo, z wyznaczonych dystrybucji można wywnioskować, że wiązania wodorowe w układach klastrów kołowych charakteryzują się dłuższymi czasami życia niż w klastrach liniowych. Zaprezentowane badania pokazały różną stabilność wiązań wodorowych w zależności od typów klastrów alkoholi, co może znaleźć szersze zastosowanie w innych układach związanych wodorowo.

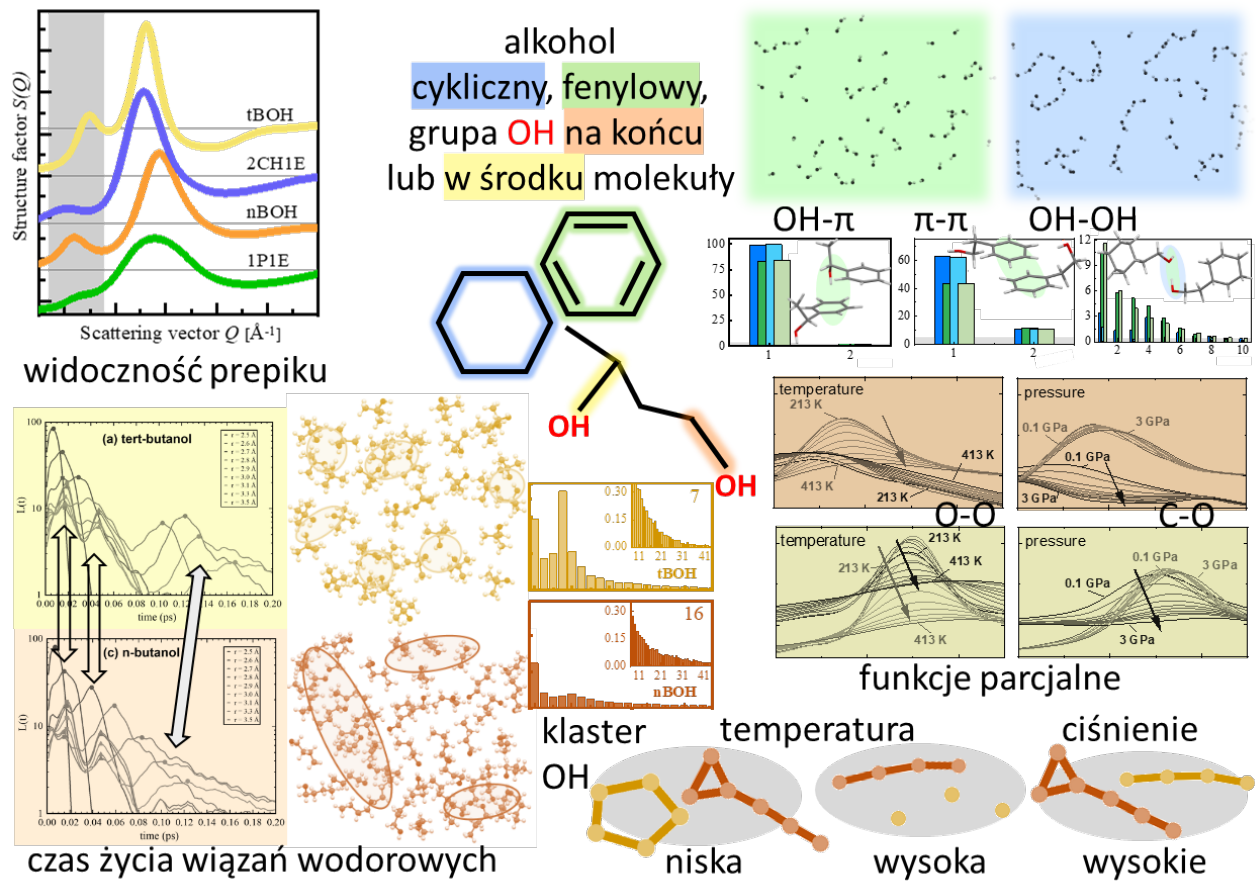
D. Zmienne warunki termodynamiczne w układzie

Zachowanie procesu asocjacji w różnych warunkach termodynamicznych jest kluczem do poznania jakie czynniki mają decydujący wpływ na tworzenie się struktur supramolekularnych. W pracy [P4] zbadano dwa związki alkoholi, heksanole, różniące się pozycją grupy hydroksylowej i tym samym tendencją do tworzenia różnych typów architektury klastrów supramolekularnych. Alkohol 2-ethyl-1-hexanol z grupą OH na końcu łańcucha węglowego ma tendencję do tworzenia klastrów liniowych, natomiast 2-methyl-3-hexanol z grupą OH ulokowaną w środkowej części molekuly ma preferencje do tworzenia klastrów kołowych. Wyniki wysokociśnieniowych pomiarów dyfrakcyjnych wykonanych w ośrodku synchrotronowym zostały zestawione z wynikami eksperymentalnymi w niskiej i wysokiej (w porównaniu do pokojowej) temperaturze oraz sprzęgnięte z wynikami symulacji komputerowych. Opublikowane zestawienia (Fig. 2 [P4]) pokazują zachowanie dwóch głównych pików dyfrakcyjnych w różnych warunkach termodynamicznych. Widoczne są efekty zmiany gęstości układu – zmieniające się odległości sąsiednich molekuł w przestrzeni rzeczywistej, co w przestrzeni odwrotnej przekłada się na zmianę pozycji głównego halo na dyfraktogramach. Co ciekawe, pozycja prepiku pozostaje niemal stała, jednak zmienia się jego natężenie – wraz ze wzrostem ciśnienia spada, a ze wzrostem temperatury również spada i wyraźnie się poszerza. Parcjalne funkcje czynników struktury (Fig. 3 [P4]) wskazały, że spadek intensywności prepiku wraz z podwyższeniem temperatury związany jest głównie ze spadkiem korelacji OO, co wskazuje na redukcję liczby molekuł związanych wodorowo w klastry. Z kolei, wraz ze wzrostem ciśnienia korelacje OO utrzymują się na podobnym poziomie, a zmniejsza się natężenie korelacji CO, co związane jest z reorganizacją architektury klastrów. Takie obserwacje pokazują odmienny wpływ dwóch podstawowych parametrów termodynamicznych – temperatury i ciśnienia – na agregację molekuł. Dalsza analiza struktury alkoholi w różnych warunkach termodynamicznych miała na celu pogłębioną charakterystykę architektury tworzących się klastrów. W tym celu, zdefiniowano różne typy klastrów określające sposób łączenia się cząsteczek przez wiązania wodorowe (liniowy, kołowy, rozgałęziony). Wyznaczono także liczby molekuł niezwiązanych wodorowo i policzono dystrybucje liczby cząsteczek związanych w różnych typach klastrów w zależności od temperatury i ciśnienia w układach alkoholi. Z zaprezentowanych dystrybucji (Fig. 4 [P4]) można zauważyć jak liczba niezwiązanych molekuł (monomerów) rośnie wraz ze wzrostem temperatury, a z wysokim ciśnieniem spada prawie do 0%. Klastry liniowe stanowią większość w obu układach

alkoholi, w temperaturze pokojowej i wyższej. W najniższej badanej temperaturze, większość układu 2-ethyl-1-hexanolu stanowią klastry rozgałęzione, natomiast 2-methyl-3-hexanolu – klastry kołowe. Wysokie ciśnienie, podobnie jak niska temperatura, powoduje powstawanie większej liczby rozgałęzionych klastrów w pierwszym związku. Drugi związek, z grupą OH ulokowaną w środku molekuly, prawie w ogóle nie tworzy klastrów o typie rozgałęzionym. Ważną obserwacją jest spadek liczby klastrów kołowych w obu układach wraz ze zwiększaniem ciśnienia, na rzecz tworzenia się innych typów – rozgałęzionych lub liniowych. Obszary wspólnych wartości gęstości, które można uzyskać poprzez zmiany temperatury w ciśnieniu 1 bar lub zmiany ciśnienia w temperaturze 293 K, zostały otrzymane na podstawie danych eksperymentalnych oraz z symulacji (Fig. SI2 Supporting Information for [P4]). Interesującym odkryciem było, że stany o zbliżonej gęstości, ale osiągnięte w różnych warunkach termodynamicznych wykazują różne architektury klastrów (Fig. 4 [P4]). Wizualizacja modeli (Fig. 5 [P4]) w różnych warunkach termodynamicznych wraz z dystrybucjami wielkości klastrów pozwala na jakościowe oraz ilościowe zobrazowanie struktury supramolekularnej badanych alkoholi. W temperaturze 213 K w 2-ethyl-1-hexanolu widoczne są klastry liniowe o dużych rozmiarach, nawet kilkuset molekuł. Natomiast klastry kołowe w 2-methyl-3-hexanolu przyjmują rozmiary maksymalnie kilku molekuł, co może wynikać z ograniczeń energetycznych tworzenia większych tego typu agregatów. W warunkach pokojowych rośnie liczba niezwiązanych molekuł, a średnia wielkość klastra spada. Z kolei w najwyższej temperaturze 413 K klastry mają rozmiar maksymalnie kilkunastu molekuł i dużą część układu stanowią monomery. Wycinki modeli obrazujące strukturę w warunkach najwyższego ciśnienia 3GPa, wykazują podobieństwo do obrazów agregacji w niskiej temperaturze 213 K. Jednak w tych pierwszych, klastry są mniejsze i więcej jest klastrów rozgałęzionych (w przypadku 2-ethyl-1-hexanolu) oraz mniej klastrów kołowych (w przypadku 2-methyl-3-hexanolu). Podsumowując, w pracy pokazano różny wpływ zadanych zmiennych warunków termodynamicznych na odpowiedź agregacji molekuł alkoholi monohydroksylowych. Najważniejszym wnioskiem płynącym z przeprowadzonych badań jest to, że przeciwnie niż wysoka temperatura, która ma destrukcyjny wpływ na wiązania wodorowe, wysokie ciśnienie promuje asocjacje molekuł, ale jednocześnie zmienia architekturę klastrów supramolekularnych.

E. Podsumowanie

W pracy pokazano wpływ budowy molekuly i warunków termodynamicznych na proces asocjacji wybranych alkoholi monohydroksylowych. Badania struktury bazujące na metodzie dyfrakcji rentgenowskiej zostały zinterpretowane w oparciu o wyniki symulacji dynamiki molekularnej. Najważniejsze wyniki badań zebrano na grafice – Rys. 10. Dyfraktogramy badanych alkoholi monohydroksylowych charakteryzowały się występowaniem prepików, których natężenie oraz położenie różniło się w zależności od budowy molekuly determinującej budowę supramolekularną. Szczegółowych informacji na temat struktury i typów tworzonych w układzie klastrów dostarczyły symulacje dynamiki molekularnej. Pokazano, że związki, w których grupa hydroksylowa ulokowana jest na końcu łańcucha węglowego molekuly tworzą długie łańcuchy związane wodorowo – klastry o kształcie liniowym. Alkohole, gdzie grupa OH umieszczona jest w środku molekuly lub blisko pierścienia, mają tendencję do tworzenia klastrów kołowych. Ponadto, pokazano że czasy życia wiązań wodorowych w klastrach kołowych są dłuższe niż w klastrach liniowych. Badania alkoholi z pierścieniem węglowym wykazały ciekawą prawidłowość, alkohole cykliczne mimo zawady sterycznej w postaci pierścienia agregują się w duże klastry związane wodorowo. Tymczasem, w bardzo podobnych do nich w budowie wewnątrzcząsteczkowej alkoholach fenylowych, pierścień aromatyczny jest źródłem konkurencyjnych oddziaływań w układzie, co wpływa na mniejszy rozmiar tworzonych klastrów związanych wodorowo. Badania w różnych warunkach termodynamicznych dały możliwość zweryfikowania, co dzieje się z klastrami związanymi wodorowo pod wpływem zmiany zewnętrznych warunków. Pokazano, że wysoka temperatura skutkuje zmniejszeniem liczby związanych wodorowo molekuł w układzie. Wraz z obniżaniem temperatury uzyskano stany gęstości o wartościach równych tym podczas kompresowania układu. Jednak wykazano, że architektura supramolekularna klastrów otrzymana po tych dwóch ścieżkach termodynamicznych nie była taka sama. Istotnym osiągnięciem było zademonstrowanie, że wysokie ciśnienie wzmacnia asocjację poprzez wiązania wodorowe w prostych alkoholach monohydroksylowych. Prezentowane badania poruszają fundamentalny temat oddziaływań międzycząsteczkowych i pokazują oryginalne wyniki w tej dziedzinie. Wyniki zostały zaprezentowane w czterech publikacjach naukowych w wysoko punktowanych czasopismach z listy filadelfijskiej. Wynikające z nich wnioski mogą zostać w przyszłości zastosowane jako podstawa dalszych badań na temat asocjacji bardziej skomplikowanych układów molekularnych.



Rys. 10. Grafika podsumowująca wyniki pracy, zawierająca figury z publikacji [P1 – P4].

III. Publikacje naukowe

A. P1. Supramolecular Structure of Phenyl Derivatives of Butanol Isomers

Grelska, J., Jurkiewicz, K., Burian, A., & Pawlus, S. (2022). *The Journal of Physical Chemistry B*, 126(19), 3563-3571. DOI:10.1021/acs.jpcc.2c01269

Punkty MNiSW (2024): 140

Impact Factor (2023): 3.3

Mój wkład w publikację polegał na wykonaniu pomiarów dyfrakcji rentgenowskiej, wykonaniu symulacji dynamiki molekularnej, analizie wyników i ich dyskusji oraz przygotowaniu artykułu.

Supramolecular Structure of Phenyl Derivatives of Butanol Isomers

Joanna Grelska,* Karolina Jurkiewicz,* Andrzej Burian, and Sebastian Pawlus



Cite This: *J. Phys. Chem. B* 2022, 126, 3563–3571



Read Online

ACCESS |



Metrics & More

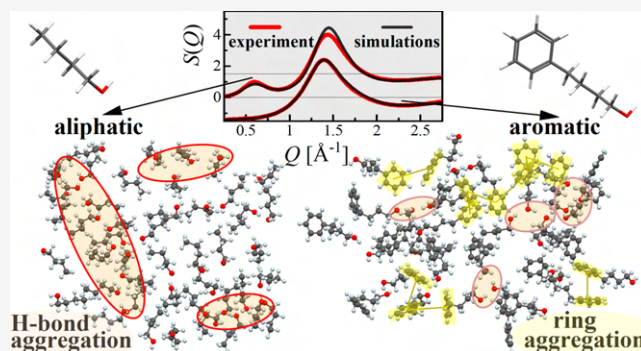


Article Recommendations



Supporting Information

ABSTRACT: Wide-angle X-ray scattering patterns were recorded for a series of aliphatic butanol isomers (*n*-, *iso*-, *sec*-, *tert*-butanol) and their phenyl derivatives (4-phenyl-1-butanol, 2-methyl-3-phenyl-1-propanol, 4-phenyl-2-butanol, and 2-methyl-1-phenyl-2-propanol, respectively) to determine their atomic-scale structure with particular emphasis on the formation of supramolecular clusters. In addition, molecular dynamics simulations were carried out and yielded good agreement with experimental data. The combination of experimental and theoretical results allowed clarification of the origin of the pre-peak appearing at low scattering angles for the aliphatic butanols and its absence for their phenyl counterparts. It was demonstrated that the location of the hydroxyl group in the molecule of alkyl butanol, its geometry, and rigidity determine the morphology of the supramolecular clusters, while the addition of the aromatic moiety causes more disordered organization of molecules. The phenyl group significantly decreases the number of hydrogen bonds and size of the supramolecular clusters formed via the O–H...O scheme. The lower association ability of phenyl alcohols via H-bonds is additionally attenuated by the appearance of competing π – π configurations evidenced by the structural models.



1. INTRODUCTION

In ordinary “nonassociating” liquids, the intermolecular structure is isotropic and the structural correlations between molecules are usually lost beyond the second-neighbor shell. However, in many liquids, specific interactions, which include, e.g., hydrogen bonding, hydrophobic relations, π – π stacking, van der Waals, or dipole–dipole forces, can induce spontaneous self-assembly of molecules into aggregates without any external trigger. One example is monohydroxy alcohols, which form supramolecular clusters through hydrogen bonds (HBs) and exhibit a much longer correlation length than ordinary liquids. Despite the growing number of studies for alcohols in binary mixtures, at various interfaces, or in nanoconfinement,^{1–4} there is still a lack of thorough understanding of their association ability in neat bulk forms. One class of alcohols that is largely unexamined in this regard is phenyl alcohols.

Recent years have seen a huge development in molecular dynamics (MD) as a technique to simulate the dynamics and structure of alcohols. Several studies were conducted comparing with a good agreement experimental and simulated total scattering (diffraction) data, e.g., for water–ethanol mixtures,⁵ *n*-pentanol and pentanal mixtures,⁶ and neat linear alcohols.^{7,8} To the best of our knowledge, there are no such studies for phenyl alcohols such as phenyl derivatives of butanols. In contrast, the structure of aliphatic butanols has been widely reported in the literature. It was shown experimentally or/and using molecular dynamics simulations

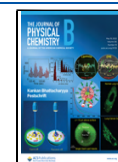
that *n*- and *sec*-butanols create chainlike H-bonded clusters,^{9–11} while *tert*-butanol has a tendency to create cyclic structures.^{9,10,12,13} It was also postulated that the steric effect of *tert*-butanol’s globular shape is an obstacle for creating larger supramolecular clusters.¹⁴

In fact, the discussions on the steric hindrance effect of molecular shape, the impact of the alkyl chain length, and the position of the OH group on the supramolecular structure in various alcohols are abundant in the literature.^{15–19} However, the information on the associating phenomena of alcohols with the steric hindrance in the form of the attached phenyl group is based practically only on the dielectric and infrared spectroscopy studies and many contradictions have arisen on this topic.^{20–28} First, Kalinovskaya et al.²⁷ and Johari et al.²⁸ postulated that the phenyl group in 1-phenyl-1-propanol reduces the extent of intermolecular H-bonding as the Debye-type relaxation process vanishes. Subsequently, Böhmer et al.²⁶ concluded that the aromatic ring only affects the supramolecular architecture of phenyl-propanols, while the structure formation through HBs is not generally suppressed by the increased steric hindrance. Thus, the two above

Received: February 22, 2022

Revised: April 26, 2022

Published: May 6, 2022



hypotheses were mutually exclusive. Our recent results based on the combination of calorimetric, dielectric, infrared, and diffraction studies suggested that HBs are effectively formed in phenyl alcohols, irrespectively of the steric effect of the aromatic ring. The major factors deciding their degree of association and morphology are the intramolecular architecture and the location of the OH group in relation to the carbon skeleton.^{20,22} In turn, in another paper,²⁴ we demonstrated that the phenyl ring exerts a strong effect on the self-organization of 1-phenyl alcohols' molecules, leading to a significant decline in the size and concentration of H-bonded clusters. Furthermore, it was postulated that besides playing the role of steric hindrance, the bulky aromatic ring acts as a source of additional $\pi\cdots\pi/\text{OH}\cdots\pi$ interactions affecting the supra-molecular organization. However, this hypothesis needs a strong verification.

With regard to the gap in understanding of the supra-molecular assembly and structure of phenyl alcohols, in the current study, we focus on a series of structural alkyl butanol isomers and their phenyl counterparts. To get a deeper insight into the influence of the molecular geometry, location of the hydroxyl group, and, most of all, the presence of the steric hindrance posed by the phenyl moiety on the association of molecules, molecular dynamics simulations were employed. The optimized models of the studied alcohols show very good compliance with the experimental total X-ray diffraction data in real and reciprocal spaces and, therefore, they can be used to interpret the characteristic features of their supra-molecular structure.

2. EXPERIMENTAL SECTION

2.1. Materials. Aliphatic butanols with the chemical formula $\text{C}_4\text{H}_{10}\text{O}$: *n*-butanol (nBOH), isobutanol (iBOH), *sec*-butanol (sBOH), and *tert*-butanol (tBOH), and their phenyl derivatives with the chemical formula $\text{C}_{10}\text{H}_{14}\text{O}$: 4-phenyl-1-butanol (4Ph1BOH), 2-methyl-3-phenyl-1-propanol (2M3Ph1POH), 4-phenyl-2-butanol (4Ph2BOH), and 2-methyl-1-phenyl-2-propanol (2M1Ph2POH) with purity of at least 97% were purchased from Sigma-Aldrich. For simplicity, we will refer to these phenyl derivatives of butanols as phenyl butanols later in the text. The models of the chemical structure of all studied alcohols are presented in Figure 1.

2.2. X-ray Diffraction Measurements. Wide-angle X-ray diffraction (XRD) measurements were carried out on a Rigaku-Dezki D/MAX RAPID II-R diffractometer equipped with a rotating Ag anode, an incident beam (002) graphite monochromator, and a two-dimensional image plate detector, operating in the Debye–Sherrer geometry. Samples were measured in capillaries at around 293 K, except for 2-methyl-1-phenyl-2-propanol, which, due to crystallization, was measured at a higher temperature around 297 K. The two-dimensional XRD patterns were transformed to the one-dimensional functions of the scattering intensity versus the scattering vector $Q = 4\pi \sin \theta/\lambda$, where 2θ is the scattering angle and $\lambda = 0.5608 \text{ \AA}$ is the wavelength. The maximum value of Q in the experiment, Q_{max} , was 20 \AA^{-1} . In the next step, the total coherently scattered intensity $I(Q)$, corrected by background, absorption, polarization, and Compton effects and normalized to electron units by the high-angle method²⁹ using in-house software, was converted to the scattering factor $S(Q)$ using the following formula

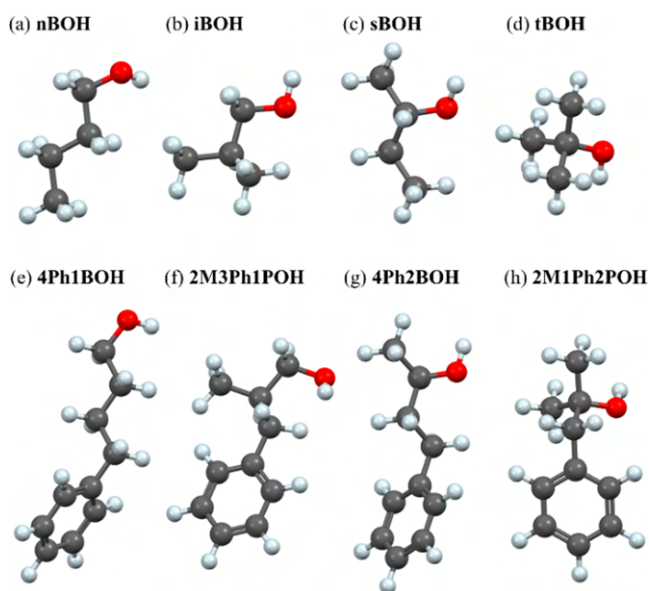


Figure 1. Models of molecules of the investigated alcohols: *n*-butanol (a), isobutanol (b), *sec*-butanol (c), *tert*-butanol (d), 4-phenyl-1-butanol (e), 2-methyl-3-phenyl-1-propanol (f), 4-phenyl-2-butanol (g), and 2-methyl-1-phenyl-2-propanol (h). The abbreviated names used in the article are given above the molecules. Carbon atoms are marked in dark gray, oxygen in red, and hydrogen in light gray.

$$S(Q) = \frac{I(Q) - \sum_{i=1}^N x_i f_i^2(Q)}{\left(\sum_{i=1}^N x_i f_i(Q)\right)^2} \quad (1)$$

where x_i is the fraction and $f_i(Q)$ is the atomic scattering factor of the i -th atomic species, respectively, and N is the number of atomic species in the sample.

2.3. Computational Section. Molecular dynamics simulations were carried out using GROMACS package (version 2020).^{30–32} The calculations were performed at the NVT ensemble (constant volume and temperature), at temperature 297 K for 2-methyl-1-phenyl-2-propanol and at 293 K for the rest of the compounds to represent the laboratory conditions. Each starting simulation box contained 2000 randomly distributed molecules. The size of the cubic box was estimated based on the density of a compound at the given temperature and molar masses of molecules. The values of these parameters in Table S11 as well as details of the simulations are presented in the Supporting Information. The topology files were created in the Antechamber module (AmberTool21)³³ with interactions described by the general AMBER force field (GAFF).³⁴ The trajectories of the final 100 configurations were collected for further analysis of the systems. Longer simulation time and larger box size were also tested and gave similar results, see Supporting Information, Figures SI6–SI10.

The `gmx_rdf`, `gmx_hbond`, `gmx_clustsize`, and `gmx_angle` programs in the GROMACS package were used to calculate the partial radial distribution functions of atoms and the radial distribution functions of the center of molecules as well as to analyze the properties of supra-molecular clusters, hydrogen bonds, and intramolecular structure. TRAVIS software^{35–37} was used to calculate the partial $S_{ij}(Q)$ and total $S(Q)$ structure factors from the partial radial distribution functions $g_{ij}(r)$ as follows

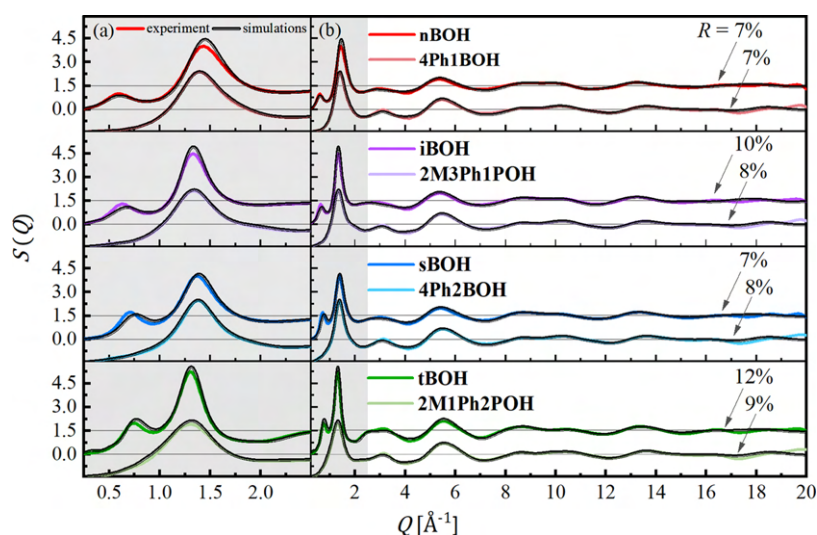


Figure 2. Experimental (colored lines) and simulated (black lines) total structure factors $S(Q)$ of investigated butanols in the pre-peak and main-peak region (a) and in the whole measured range of the scattering vector Q (b). The curves for alkyl butanols are upshifted with the value of 1.5 with respect to their phenyl counterparts. The values of discrepancy factors R are given on the right part of the graph.

$$S_{ij}(Q) = \frac{4\pi\rho_0}{Q} \int_0^{r_{\max}} r(g_{ij}(r) - 1)\sin(Qr) dr \quad (2)$$

where the indices i and j run over N different atom types, ρ_0 is the number density, r is the interatomic distance, and r_{\max} is the maximum sampled distance in the radial distribution function (equal to the box length). Partial structure factors obtained from simulations were multiplied by the weighting factors to get the weighted partial structure factors $S'_{ij}(Q)$

$$S'_{ij}(Q) = (2 - \delta_{ij}) \frac{x_i x_j f_i(Q) f_j(Q) S_{ij}(Q)}{(\sum_{i=1}^N x_i f_i(Q))^2} \quad (3)$$

where δ_{ij} is the Kronecker delta, which sums to the total structure factor $S(Q)$

$$S(Q) = \sum_{i \leq j}^N S'_{ij}(Q) \quad (4)$$

and can be directly compared with the experimental $S(Q)$.

3. RESULTS AND DISCUSSION

3.1. Total Structure Factors and Pair Distribution Functions from Experiment and Simulations. The experimental structure factors of the different alcohols are compared in Figure 2. In the case of a low- Q range (Figure 2a), a dominant main peak (MP) around $Q_{\text{MP}} \approx 1.3\text{--}1.4 \text{ \AA}^{-1}$ as well as a pre-peak (PP) around $Q_{\text{PP}} \approx 0.6\text{--}0.7 \text{ \AA}^{-1}$ are observed for each ordinary butanol. However, the positions of both peaks systematically vary for the different isomers. The MP shifts to a higher Q value and decreases in intensity with decreasing branching of the molecule, from globular tBOH, through less branched iBOH and sBOH, to linear nBOH. The position of a diffraction peak in reciprocal space can be interpreted in real space through the relation $d = 2\pi/Q$. For dense liquids, the Q_{MP} position fingerprints an average particle–particle distance.⁸ The fact that the butanol isomers exhibit different Q_{MP} simply reflects the different sizes and geometry of the molecules and their packing ability. $d_{\text{MP}} \approx \frac{2\pi}{1.3 \text{ \AA}^{-1}} \approx 4.8 \text{ \AA}$ for tBOH, while $d_{\text{MP}} \approx \frac{2\pi}{1.43 \text{ \AA}^{-1}} \approx 4.4 \text{ \AA}$

for nBOH. Thus, nBOH molecules are more densely packed than tBOH molecules at the same thermodynamic conditions applied, i.e., room temperature and ambient pressure. One may observe similar behavior for phenyl derivatives, i.e., the position of the MP shifts toward a higher Q with decreasing branching of the molecules. However, the MPs of phenyl counterparts are visibly wider and have a lower intensity than those of ordinary butanols.

The principal difference in the structure factors between the aliphatic butanols and their aromatic counterparts is the presence of the scattering PP in the low- Q region for the former group and its absence for the latter class of alcohols. The origin of the PP in the structure factor of alcohols has been generally attributed to the self-assembly of molecules in aggregates via HBs.^{38–40} It was shown that PP in the total structure factor of neat alcohols becomes the major peak in the partial structure factors involving H-bonding sites, i.e., O–O, H–H, and O–H.¹² The PP's position is related to the repeating distance between the hydroxyl head groups in the aggregates and, therefore, to the size of the H-bonded clusters. However, the architecture of the aggregates strongly influences both the PP's position and amplitude.³⁹ In fact, the total PP's amplitude depends on how different partial atom–atom contributions sum up or cancel out. Therefore, based on solely experimental total $S(Q)$, it is not possible to assign unambiguously the observed diffraction peaks to specific interatomic correlations. From our previous studies using infrared and dielectric spectroscopy, it was established that the phenyl moiety affects only slightly the degree of association and does not influence the strength of HBs in the phenyl butanols compared to their alkyl counterparts.²⁰ Moreover, phenyl butanols were characterized by similar values of the Kirkwood factor, which measures the long-distance correlations between the dipole moments of molecules, to those determined for their aliphatic analogues. In this context, to explain the lack of the PPs in the structure factors of the studied phenyl butanols, in the further part of the paper, the partial atomic contributions $S'_{ij}(Q)$ to the total $S(Q)$ were examined based on the optimized models.

A look at the comparison of the experimental and model-based structure factors in Figure 2 allows noticing that the data derived from the MD simulations behave similarly to the experimental ones. The simulation results reproduce the presence of the PP for alkyl butanols and its lack for their phenyl derivatives. Since the low- Q region is assigned mainly to the medium-range intermolecular correlations, the good agreement between the model-based and the experimental data in this region is essential for the appropriate characterization of the supramolecular structure and quantifying the effect of the phenyl group on the molecular assembly. The positions, widths, and amplitudes of the PP and MP in the simulated $S(Q)$ fit well the data derived from the XRD experiment for each alcohol. Also, the oscillations arising mainly due to the intramolecular correlations, observed for higher Q values in Figure 2b, are well reproduced by the functions derived from the MD computations. The agreement between the total model-based, $S_M(Q)$, and experimental, $S_{EX}(Q)$, structure factors was quantified using the discrepancy factor,

$$R = \sqrt{\frac{\sum_{k=1}^{Q_{\max}} [S_{EX}(Q_k) - S_M(Q_k)]^2}{\sum_{k=1}^Z S_{EX}(Q_k)^2}} \cdot 100\%, \text{ where index } k \text{ runs over}$$

the whole Q range with a step of 0.01 \AA^{-1} . The values of R , given in Figure 2, are below 10% for almost all alcohols. Thus, the obtained MD models provide a reasonable description of the entire molecular organization of the studied systems at different length scales.

The intermolecular correlations can be also probed by the oscillations of the total pair distribution functions, which are presented in Figure S11 in the Supporting Information. The functions show that the aliphatic butanols are characterized by longer-range correlations, extending up to around 30 \AA . In turn, for phenyl butanols, there are no oscillations beyond around 20 \AA . It indicates suppression of the intermolecular order due to the presence of an aromatic ring. In an attempt to understand these observations more deeply, as a trace of the supramolecular aggregation, the data derived from the MD models were further analyzed.

3.2. Model-Based Structural Correlations. The calculated partial scattering contributions $S'_{ij}(Q)$ to the total scattering of the modeled systems, according to eq 4, are depicted in Figure 3. The analysis of their positive and negative parts reveals the origin of the pre-peak in the total $S(Q)$ functions for aliphatic butanols and its lack for phenyl derivatives of the butanols. The strongest positive contribution to the PP region comes from $S'_{OO}(Q)$ correlations, which are the fingerprint of the H-bonding organization. The positive first peak in $S'_{OO}(Q)$ is observed for both aliphatic and phenyl butanols, indicating the existence of a periodicity in the arrangement of oxygen atoms for all alcohols. However, for phenyl derivatives of butanols, the intensity of this peak is significantly lower and its position is shifted toward lower Q values compared to the aliphatic counterparts. There is a greater disorder in the organization of oxygen sites and the O–O correlation length is greater for phenyl alcohols. For instance, the correlation length $l_{OO} \approx \frac{2\pi}{0.64 \text{ \AA}^{-1}} \approx 9.8 \text{ \AA}$ for nBOH while $l_{OO} \approx \frac{2\pi}{0.55 \text{ \AA}^{-1}} \approx 11.4 \text{ \AA}$ for 4Ph1BOH, which is understandable given the different sizes of the molecules. $S'_{OH}(Q)$, also associated largely with structural correlations of HBs, reveals as well a positive bump in the low- Q region around $0.5\text{--}0.7 \text{ \AA}^{-1}$. Interestingly, $S'_{CO}(Q)$ is strongly negative in that region for all phenyl butanols. As a result, positive and

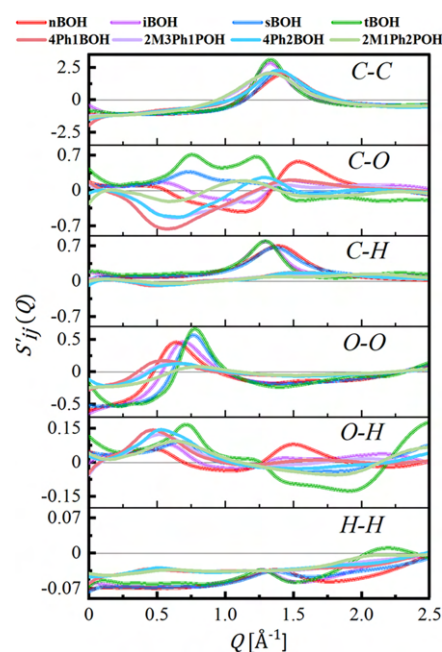


Figure 3. Partial structure factors $S'_{ij}(Q)$ calculated based on the optimized molecular dynamics models of the investigated butanols.

negative partial contributions to the total scattering cancel out and no pre-peak is observed.

In turn, for aliphatic nBOH, iBOH, sBOH, and tBOH, the higher intensity of the $S'_{CO}(Q)$ as well as strong $S'_{OO}(Q)$ correlations in this range leads, in consequence, to clear PP feature in total $S(Q)$ around $0.6\text{--}0.7 \text{ \AA}^{-1}$ for aliphatic butanols. It is also worth indicating that there are considerable differences in the partial contributions to total $S(Q)$ between the different butanol isomers that explain the various amplitude of the PP. Tertiary tBOH alcohol shows the strongest positive $S'_{OO}(Q)$, $S'_{OH}(Q)$, and $S'_{CO}(Q)$ correlations, while for primary nBOH, $S'_{CO}(Q)$ gives negative correlations in the PP region. Consequently, one may observe that the PP in the experimental functions has the highest intensity for tBOH and the lowest intensity for nBOH. Such a characteristic suggests that the cluster structure of the latter system is less pronounced than that of the former. It is also interesting to note that $S'_{CC}(Q)$ contributes mostly to the main peak of the total $S(Q)$ for all studied butanols.

In Figure 4, the selected site–site pair distribution functions for all butanols were compared to complement the information given by the structure factors. Figure 4a shows the correlations between mass centers of molecules $g_{cm}(r)$. The first peaks in the $g_{cm}(r)$ function comprise the short-range behavior due to interactions between neighboring molecules. The first distinguishing features of $g_{cm}(r)$ are two pronounced peaks for tBOH, at around 4.6 and 6 \AA . They indicate the spatial heterogeneity of the local structure of this alcohol in the near-neighbor range. The first maximum may be identified as a distance between two neighboring molecules aggregated within a cluster, while the second maximum is the distance between the center of masses for the nearest molecules involved in separate clusters. These distances were marked on the structural model presented further in Figure 6c. Similar two-component behavior of the nearest-neighbor distances, but with considerably lower intensity, can be observed for secondary sBOH. For the primary butanols, nBOH and

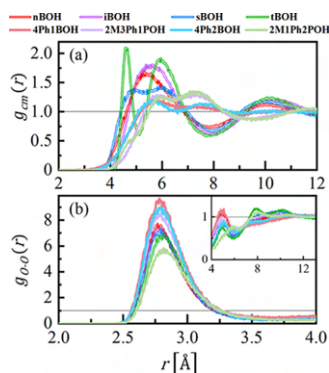


Figure 4. Center of mass $g_{cm}(r)$ (a) and oxygen–oxygen $g_{OO}(r)$ (b) radial distribution functions obtained from the optimized structural models. The inset shows the $g_{OO}(r)$ correlations for longer distances.

iBOH, the nearest-neighbor intermolecular structure is much more homogeneous with one maximum at around 5.5 Å. For phenyl derivatives of butanols, the correlations between molecules in the nearest-neighbor region are significantly weaker and shifted toward greater distances, as expected, due to the increase in the size of the molecules after attaching the phenyl group. The addition of the phenyl moiety leads also to the heterogeneity in the short-range organization of molecules that can be observed as the appearance of two maxima in $g_{cm}(r)$, at around 5.5 and 7.5 Å. All $g_{cm}(r)$ functions for the different phenyl butanols behave this way and have a related shape that indicates their short-range intermolecular structure is similar.

Figure 4b shows correlations involving oxygen sites $g_{OO}(r)$. Since each of the investigated butanols contains only one oxygen atom involved in the H-bonding per one molecule, the $g_{OO}(r)$ function provides information on the structure of HBs. All other partial $g_{ij}(r)$ functions are shown in Figure S12 in the Supporting Information. The strong first peak in the $g_{OO}(r)$ distribution appears at a distance of around 2.8 Å, which is the generally accepted length for the O–H...O bond,⁴¹ and witnesses the strong association of oxygen atoms in clusters. The position of the first maxima does not differ significantly between the different butanols; however, it can be noted that in each pair of aliphatic–aromatic butanol, the maximum is shifted slightly toward greater distances for phenyl alcohol. It means that the strength of the HBs is somewhat lowered after the addition of the phenyl group to the molecule. The strongest O–O correlations in the nearest-neighbor range show nBOH, while the weakest show 2M1Ph2POH, which is the most sterically hindered system. The first maxima in the $g_{OO}(r)$ are followed by depleted correlations due to a lower number of the O–O neighbors. It is interesting that all $g_{OO}(r)$ functions show oscillations up to distances around 12 Å (Figure 4b, inset). This observation denotes that the formation of the medium-range order between molecules in the studied butanols takes place with the participation of the O–O correlations resulting from the O–H...O bonds.

3.3. H-bonding and Supramolecular Clusters. In the previous section, it was demonstrated that the formation of the medium-range order in the studied butanol alcohols and their phenyl derivatives is due to the intermolecular H-bonding. The molecules form supramolecular clusters via HBs. In general, the analysis of the H-bonding, described in the Supporting Information, indicated that aliphatic butanols form more HBs than their phenyl derivatives, while in the latter group, there

are more unbounded molecules. Regardless of the angular conditions imposed on the atoms participating in the H-bonding, the number of all HBs in aliphatic butanol is much higher than in its phenyl analogue, for all isomers (see Figure S13 in the Supporting Information). The HB distance and angle distributions as well as their average values are shown in Figure S14 in the Supporting Information. The average HB length is very similar for all alcohols, lying within the limits of 2.81 Å for nBOH and 2.85 Å for 2M1Ph2POH. The average HB angle values are also very close to each other for all systems, around 10°. Moreover, the HB distance and angle distributions for all systems are also similar. It suggests that the H-bonding pattern for all of the studied alcohols is not very different, despite the revealed differences in the number of identified HBs.

Going back to the degree of association of molecules via H-bonds, it is worth mentioning the infrared (IR) spectroscopy results reported in our previous paper.²⁰ The IR spectra indicated that at room temperature, aliphatic butanols do not exhibit a signal from unbounded OH moieties while phenyl butanols exhibit a very weak peak associated with vibrations of free OH groups. The numbers of HBs determined here based on the optimized MD models with the broadest angle restriction (H–O–O angle $\leq 90^\circ$, see the Supporting Information) best correspond to the results of the previous IR studies. One can see that for this restriction, aliphatic butanols are well associated; however, some molecules are still unbounded. An extension of the angular range for the definition of HB or the complete omission of this restriction could result in a further increase in the degree of association, which would even better match the IR results. Moreover, Gereben & Pusztai⁵ tested different criteria on HBs and stated that sensibly chosen solely distance criteria is sufficient to obtain quantitative results. These findings encouraged us to impose the criterion only on the O–O distance for the analysis of the supramolecular clusters. Thus, the definition ‘cluster’ was used to describe assemblies of H-bonded molecules, which are so close to each other that the distances between intermolecular oxygen atoms do not exceed 3.5 Å and no angle restriction is taken. The term ‘cluster size’ corresponds to the number of molecules in the clusters.

The calculated histograms of the number of clusters versus the total number of molecules in the clusters are depicted in Figure 5. The first column of these diagrams concerns unassociated molecules. The insets in Figure 5 show the comparison of the histograms for a wider range of cluster sizes. Analyzing the histograms, the following observations can be made:

- (1) The number of unassociated molecules increases from around 1.5 to 3% going from primary nBOH, branched primary iBOH, secondary sBOH, and tertiary tBOH. It means that increasing the steric hindrance due to the location of OH group relative to the carbon skeleton and the transformation of the geometry of molecules from linear to globular suppress the clustering ability of these butanols.
- (2) For phenyl butanols, this tendency is generally maintained. However, the number of unassociated molecules is much higher (11–24%) for phenyl alcohols compared to their aliphatic counterparts. Thus, it can be argued that the phenyl group is the severe steric hindrance prior to supramolecular clustering.

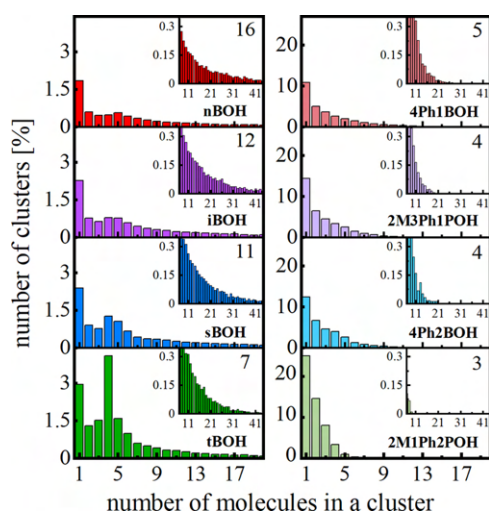


Figure 5. Histograms of the number of clusters as a function of the number of molecules in a cluster. The insets show the distributions in a wider range of cluster sizes. The average number of molecules in the cluster is displayed in the right top corner of each panel.

- (3) The width of the cluster size distribution decreases from primary to tertiary alcohols, both for aliphatic and phenyl types. However, for phenyl alcohols, the distributions are much more limited for larger sizes. The narrowest distribution is observed for the most sterically hindered 2M1Ph2POH.
- (4) For aliphatic butanols, one can notice a preferential number of molecules in the cluster (local maximum in the distribution): five for nBOH, four to five for iBOH and sBOH, and very pronounced four for tBOH. For phenyl butanols, the number of molecules in the clusters

systematically decreases with increasing cluster size and there is no privileged cluster size.

3.4. Spatial Models of the Molecular Structure. The supramolecular organization evidenced by the cluster analysis may be illustrated based on the optimized structural models. To clearly visualize the clustering of the molecules, two-dimensional planes cut from the three-dimensional models were presented for selected butanols and their phenyl derivatives in Figure 6, which summarizes the findings that we intended to report in this paper. The selected model fragments representing compounds from two series, aliphatic and aromatic, illustrate their tendency to associate with molecules. From this picture, one can see that nBOH molecules group in big, longitudinal aggregates where HBs arrange in the chainlike structures (Figure 6a). In comparison, the clusters in tBOH are smaller with rather cyclic geometry (Figure 6c). These findings are consistent with the previous predictions of the architecture of H-bonded clusters for butanol isomers. For example, based on the calculated cluster size distributions, the average number of molecules contained in the aggregates was around 13, 11, 11, and 4 for *n*-, *sec*-, *iso*-, and *tert*-butanol, respectively.¹⁵ In other computational works,^{7,8} the probability of finding monomers and pentamers in *n*-butanol was the highest. In the case of *tert*-butanol, it was predicted to form either cyclic tetramers¹³ or hexamers.⁴² On the other hand, Figure 6b,d shows the structures of phenyl derivatives of nBOH and tBOH—4Ph1BOH and 2M1Ph2POH, respectively. One may notice a striking difference in the organization of molecules between these two classes of alcohols. For phenyl alcohols, only small supramolecular clusters are formed with a rather chaotic chainlike organization of HBs. It results in a higher degree of spatial disorder than in aliphatic alcohols where more extended

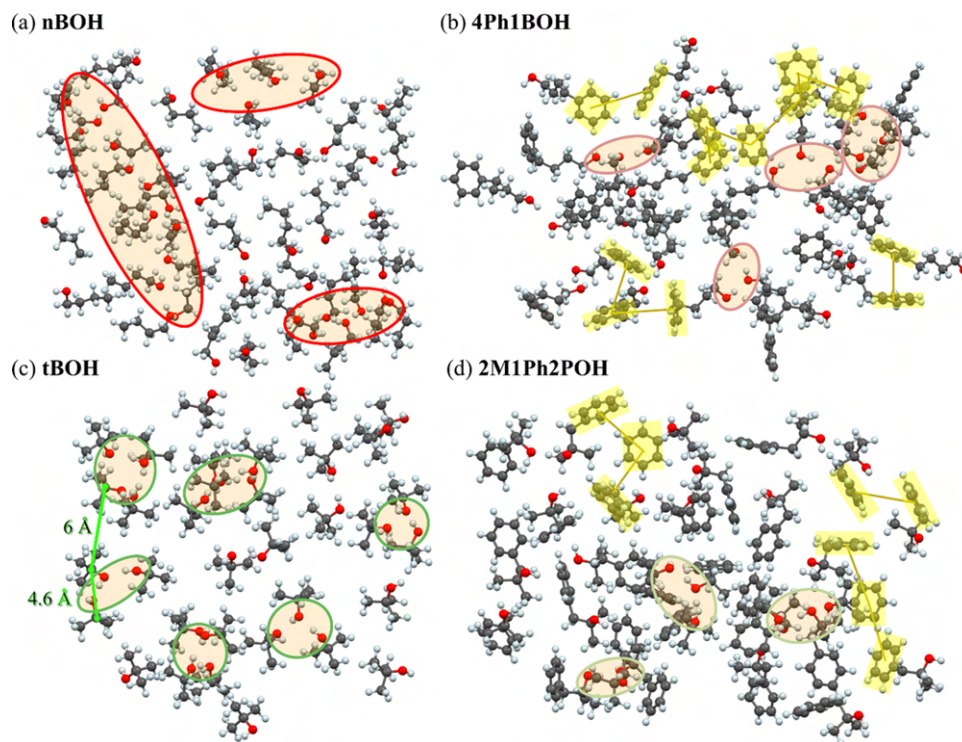


Figure 6. Two-dimensional planes cut from the optimized structural models of nBOH (a), 4Ph1BOH (b), tBOH (c), and 2M1Ph2POH (d). The loops show clusters of H-bonds. The highlighted yellow areas show π - π structural motifs.

networks of HBs direct the arrangement of molecules in the space.

The models shown in Figure 6 verify also the hypothesis of the $\pi\cdots\pi/\text{OH}\cdots\pi$ interactions in the phenyl alcohols. In archetypal aromatic benzyl alcohol, several $\pi\cdots\pi$ structural motifs for dimers were reported, such as parallel or offset-parallel stacked and perpendicular Y- or T-shaped.⁴³ For liquid benzene, the distribution of the nearest-neighbor distances between phenyl ring centers was predicted in the range of 4–7 Å, depending on the offset and angle between the aromatic planes. Taking these values as references for the $\pi\cdots\pi$ interactions, it was possible to identify arrangements of molecules in the studied phenyl alcohols meeting these criteria. Such structural motifs were highlighted in the models of phenyl butanols in Figure 6b,d. The $\pi\cdots\pi$ configurations were found to occur locally as dimeric or trimeric forms as well as more extended aggregates of several molecules like the one in the right top corner of Figure 6b. In most of these configurations, the aromatic rings are not stacked in parallel face to face but occur in offset and distorted Y- and T-shaped arrangements. Concerning the predicted $\text{OH}\cdots\pi$ bonds, only very sporadic such structural motifs were identified in the models of phenyl butanols. The whole optimized three-dimensional models of all of the studied alcohols are included in the Supporting Information as .pdb files. It should be emphasized that the models do not directly prove the presence of $\pi\cdots\pi$ -type interactions but demonstrate the possible configurations of phenyl rings where such interactions would be feasible. Usually, the interactions between aromatic rings or between a functional group and an aromatic ring are not described by general force fields implemented in the classical molecular dynamics simulations. However, here, the GAFF force field was used, which was developed for organic compounds containing phenyl moieties, such as pharmaceuticals, proteins, and nucleic acids.³⁴ Therefore, the aromatic ring was distinguishable when calculating the molecular dynamics with the GAFF force field—not at the atomic level but by a different van der Waals bond strength.

It is also worth noting that different molecular conformations were observed in the optimized three-dimensional models of the studied alcohols. The analysis of the molecular conformations, based on the distributions of chosen angles between three atoms in the molecule of each alcohol, is presented in Figure S15 in the Supporting Information. It was revealed that these distributions for primary and secondary butanols as well as their phenyl derivatives are bimodal. The two components of these distributions correspond to the conformers with bent and linear geometries of molecular skeleton, whereas tertiary butanol and its phenyl derivative occur in only one conformation. That is reasonable taking into account the geometry of these molecules and their rigidity. As predicted, the broadest distributions of molecular conformations are observed for nBOH and its phenyl counterpart, which are very elastic due to the flexible long alkyl tail and the location of OH moiety at its end. Such a molecular structure favors folding of the chain. The flexibility of the molecules and the variability of their conformations facilitate the formation of numerous HBs and big supramolecular clusters, as revealed in the previous section.

4. CONCLUSIONS

Based on the experimental diffraction studies and molecular dynamics simulations, the supramolecular structure of a series

of isomeric butanols and their phenyl derivatives was characterized in detail. The main novel contribution on the topic of the supramolecular clustering of alcohols via H-bonding is the quantitative analysis of the influence of phenyl group attaching to molecules of the butanols on their association ability, the H-bonding pattern, and the structure of the supramolecular clusters. The results allow us to dispel the doubts about whether the steric hindrance in the form of phenyl moiety affects the ability of molecules to link through H-bonds. It was demonstrated that the presence of the phenyl group significantly decreases the number of H-bonds and the size of the supramolecular clusters (the number of molecules aggregated in the clusters), regardless of the location of the OH group in the molecules. The detailed analysis of the atom–atom structure factor contributions exhibited that the presence of the pre-peak in the total structure factor of aliphatic butanols is related to the medium-range order correlations between the OH groups, while the lack of the pre-peak for phenyl butanols is related to weaker O–O correlations as well as the negative contribution coming from the partial C–O correlations, which cancel out.

Furthermore, the analysis of the molecular clustering showed that the distribution of the cluster size changes from broader to narrower while the average number of molecules linked in clusters decreases coming from primary to tertiary butanols. The preference for a specific number of molecules organized in the clusters was displayed, the most prominent for tBOH (4 molecules). In the case of phenyl butanols, clusters were on average 3 times smaller (5–3 molecules) than in aliphatic counterparts (7–16 molecules), with no preferable number of molecules in the cluster size distribution. However, the trend in the H-bonding and clustering properties for phenyl butanols was similar to the series of aliphatic butanols.

Moreover, it was demonstrated that for primary and secondary butanols and their phenyl counterparts, the distribution of the molecular conformations is broad and bimodal. The two components of these distributions correspond to the conformers with bent and linear geometry of molecular skeleton. Thus, the MD simulations showed that the primary and secondary butanols are characterized by higher flexibility of molecular skeletons compared to rigid tertiary butanol. This factor, together with the location of the OH group in the molecule and the presence of the phenyl ring strongly affect the association ability of molecules through H-bonds.

Finally, analysis of the structural models for phenyl butanols allowed us to identify arrangements of molecules where $\pi\cdots\pi$ interactions may occur. Such structural motifs may prevent the organization of molecules via H-bonds and enhance the structural disorder. We believe the optimized structural models of the studied butanols and their phenyl derivatives will be helpful for the interpretation of their physical properties. Particularly valuable will be a confrontation of these models with the results of dielectric studies, which so far have yielded many conflicting conclusions about the influence of the phenyl group on the supramolecular association of alcohols and molecular relaxation processes.

■ ASSOCIATED CONTENT

SI Supporting Information

The Supporting Information is available free of charge at <https://pubs.acs.org/doi/10.1021/acs.jpcb.2c01269>.

Details of the molecular dynamics simulations and their additional analyses (hydrogen bonds, molecular conformations, results for a longer simulation time and a bigger box size) and the atomic pair distribution function analysis (PDF)

nBOH (PDB)

iBOH (PDB)

sBOH (PDB)

tBOH (PDB)

4Ph1BOH (PDB)

2M3Ph1POH (PDB)

4Ph2BOH (PDB)

2M1Ph2POH (PDB)

AUTHOR INFORMATION

Corresponding Authors

Joanna Grelska – A. Chełkowski Institute of Physics, University of Silesia in Katowice, 41-500 Chorzów, Poland; Silesian Center for Education and Interdisciplinary Research, 41-500 Chorzów, Poland; orcid.org/0000-0002-7001-4083; Email: joanna.grelska@us.edu.pl

Karolina Jurkiewicz – A. Chełkowski Institute of Physics, University of Silesia in Katowice, 41-500 Chorzów, Poland; Silesian Center for Education and Interdisciplinary Research, 41-500 Chorzów, Poland; orcid.org/0000-0002-4289-7827; Email: karolina.jurkiewicz@us.edu.pl

Authors

Andrzej Burian – A. Chełkowski Institute of Physics, University of Silesia in Katowice, 41-500 Chorzów, Poland; Silesian Center for Education and Interdisciplinary Research, 41-500 Chorzów, Poland

Sebastian Pawlus – A. Chełkowski Institute of Physics, University of Silesia in Katowice, 41-500 Chorzów, Poland; Silesian Center for Education and Interdisciplinary Research, 41-500 Chorzów, Poland; orcid.org/0000-0001-9209-4056

Complete contact information is available at:
<https://pubs.acs.org/10.1021/acs.jpcc.2c01269>

Notes

The authors declare no competing financial interest.

ACKNOWLEDGMENTS

J.G., K.J., and S.P. are thankful for the financial support from the Polish National Science Centre within the OPUS project (no. UMO-2019/35/B/ST3/02670). The authors thank Dr. Kajetan Koperwas for guidance and discussion on computer simulation methodology in GROMACS package.

REFERENCES

- (1) Foster, W.; Miyazawa, K.; Fukuma, T.; Kusumaatmaja, H.; Voitchovsky, K. Self-Assembly of Small Molecules at Hydrophobic Interfaces Using Group Effect. *Nanoscale* **2020**, *12*, 5452.
- (2) Zangi, R. Self-Assembly of Alcohols Adsorbed on Graphene. *J. Phys. Chem. C* **2019**, *123*, 16902.
- (3) Bampoulis, P.; Witteveen, J. P.; Kooij, E. S.; Lohse, D.; Poelsema, B.; Zandvliet, H. J. W. Structure and Dynamics of Confined Alcohol–Water Mixtures. *ACS Nano* **2016**, *10*, 6762.
- (4) Voitchovsky, K.; Giofrè, D.; José Segura, J.; Stellacci, F.; Ceriotti, M. Thermally-Nucleated Self-Assembly of Water and Alcohol into Stable Structures at Hydrophobic Interfaces. *Nat. Commun.* **2016**, *7*, No. 13064.

(5) Gereben, O.; Pusztai, L. Hydrogen Bond Connectivities in Water–Ethanol Mixtures: On the Influence of the H-Bond Definition. *J. Mol. Liq.* **2016**, *220*, 836.

(6) Pethes, L.; Temleitner, L.; Tomšič, M.; Jamnik, A.; Pusztai, L. Unexpected Composition Dependence of the First Sharp Diffraction Peak in an Alcohol-Aldehyde Liquid Mixture: N -Pentanol and Pentanal. *Phys. Status Solidi B* **2018**, *255*, No. 1800130.

(7) Mariani, A.; Ballirano, P.; Angiolari, F.; Caminiti, R.; Gontrani, L. Does High Pressure Induce Structural Reorganization in Linear Alcohols? A Computational Answer. *ChemPhysChem* **2016**, *17*, 3023.

(8) Požar, M.; Bolle, J.; Sternemann, C.; Perera, A. On the X-Ray Scattering Pre-Peak of Linear Mono-Ols and the Related Microstructure from Computer Simulations. *J. Phys. Chem. B* **2020**, *124*, 8358.

(9) Jadzyn, J.; Świergiel, J. Mesoscopic Clustering in Butanol Isomers. *J. Mol. Liq.* **2020**, *314*, No. 113652.

(10) Durov, V. A.; Shilov, I. Yu.; Tereshin, O. G. Modeling of Supramolecular Structure and Dielectric Properties of Butanols from Melting Point to Supercritical State. *J. Phys. Chem. B* **2008**, *112*, 8076.

(11) Lehtola, J.; Hakala, M.; Hämäläinen, K. Structure of Liquid Linear Alcohols. *J. Phys. Chem. B* **2010**, *114*, 6426.

(12) Zoranić, L.; Sokolić, F.; Perera, A. Microstructure of Neat Alcohols: A Molecular Dynamics Study. *J. Chem. Phys.* **2007**, *127*, No. 024502.

(13) Yonker, C. R.; Wallen, S. L.; Palmer, B. J.; Garrett, B. C. Effects of Pressure and Temperature on the Dynamics of Liquid Tert -Butyl Alcohol. *J. Phys. Chem. A* **1997**, *101*, 9564.

(14) Andanson, J.-M.; Soetens, J.-C.; Tassaing, T.; Besnard, M. Hydrogen Bonding in Supercritical Tert-Butanol Assessed by Vibrational Spectroscopies and Molecular-Dynamics Simulations. *J. Chem. Phys.* **2005**, *122*, No. 174512.

(15) Choi, S.; Parameswaran, S.; Choi, J.-H. Effects of Molecular Shape on Alcohol Aggregation and Water Hydrogen Bond Network Behavior in Butanol Isomer Solutions. *Phys. Chem. Chem. Phys.* **2021**, *23*, 12976.

(16) Bierwirth, S. P.; Büning, T.; Gainaru, C.; Sternemann, C.; Tolan, M.; Böhmer, R. Supramolecular X-Ray Signature of Susceptibility Amplification in Hydrogen-Bonded Liquids. *Phys. Rev. E* **2014**, *90*, No. 052807.

(17) Požar, M.; Perera, A. On the Existence of a Scattering Pre-Peak in the Mono-Ols and Diols. *Chem. Phys. Lett.* **2017**, *671*, 37.

(18) Pothoczki, S.; Pusztai, L.; Bakó, I. Variations of the Hydrogen Bonding and Hydrogen-Bonded Network in Ethanol–Water Mixtures on Cooling. *J. Phys. Chem. B* **2018**, *122*, 6790.

(19) Jurkiewicz, K.; Kołodziej, S.; Hachula, B.; Grzybowska, K.; Musiał, M.; Grelska, J.; Bielas, R.; Talik, A.; Pawlus, S.; Kamiński, K.; Paluch, M. Interplay between Structural Static and Dynamical Parameters as a Key Factor to Understand Peculiar Behaviour of Associated Liquids. *J. Mol. Liq.* **2020**, *319*, No. 114084.

(20) Hachula, B.; Grelska, J.; Soszka, N.; Jurkiewicz, K.; Nowok, A.; Szeremeta, A. Z.; Pawlus, S.; Paluch, M.; Kaminski, K. Systematic Studies on the Dynamics, Intermolecular Interactions and Local Structure in the Alkyl and Phenyl Substituted Butanol Isomers. *J. Mol. Liq.* **2022**, *346*, No. 117098.

(21) Gabriel, J. P.; Thoms, E.; Richert, R. High Electric Fields Elucidate the Hydrogen-Bonded Structures in 1-Phenyl-1-Propanol. *J. Mol. Liq.* **2021**, *330*, No. 115626.

(22) Nowok, A.; Jurkiewicz, K.; Dulski, M.; Hellwig, H.; Małcki, J. G.; Grzybowska, K.; Grelska, J.; Pawlus, S. Influence of Molecular Geometry on the Formation, Architecture and Dynamics of H-Bonded Supramolecular Associates in 1-Phenyl Alcohols. *J. Mol. Liq.* **2021**, *326*, No. 115349.

(23) Nowok, A.; Dulski, M.; Jurkiewicz, K.; Grelska, J.; Szeremeta, A. Z.; Grzybowska, K.; Pawlus, S. Molecular Stiffness and Aromatic Ring Position – Crucial Structural Factors in the Self-Assembly Processes of Phenyl Alcohols. *J. Mol. Liq.* **2021**, *335*, No. 116426.

(24) Nowok, A.; Dulski, M.; Grelska, J.; Szeremeta, A. Z.; Jurkiewicz, K.; Grzybowska, K.; Musiał, M.; Pawlus, S. Phenyl Ring: A Steric

Hindrance or a Source of Different Hydrogen Bonding Patterns in Self-Organizing Systems? *J. Phys. Chem. Lett.* **2021**, *12*, 2142.

(25) Kołodziej, S.; Knapik-Kowalczyk, J.; Grzybowska, K.; Nowok, A.; Pawlus, S. Essential Meaning of High Pressure Measurements in Discerning the Properties of Monohydroxy Alcohols with a Single Phenyl Group. *J. Mol. Liq.* **2020**, *305*, No. 112863.

(26) Böhmer, T.; Gabriel, J. P.; Richter, T.; Pabst, F.; Blochowicz, T. Influence of Molecular Architecture on the Dynamics of H-Bonded Supramolecular Structures in Phenyl-Propanols. *J. Phys. Chem. B* **2019**, *123*, 10959.

(27) Kalinovskaya, O. E.; Vij, J. K.; Johari, G. P. Mechanism of the Major Orientation Polarization in Alcohols, and the Effects of Steric Hindrance-, and Dilution-Induced Decrease on H-Bonding. *J. Phys. Chem. A* **2001**, *105*, 5061.

(28) Johari, G. P.; Kalinovskaya, O. E.; Vij, J. K. Effects of Induced Steric Hindrance on the Dielectric Behavior and H Bonding in the Supercooled Liquid and Vitreous Alcohol. *J. Chem. Phys.* **2001**, *114*, 4634.

(29) Charpentier, T.; Menziani, M. C.; Pedone, A. Computational Simulations of Solid State NMR Spectra: A New Era in Structure Determination of Oxide Glasses. *RSC Adv.* **2013**, *3*, 10550.

(30) Abraham, M. J.; Murtola, T.; Schulz, R.; Páll, S.; Smith, J. C.; Hess, B.; Lindahl, E. GROMACS: High Performance Molecular Simulations through Multi-Level Parallelism from Laptops to Supercomputers. *SoftwareX* **2015**, *1–2*, 19.

(31) Páll, S.; Abraham, M. J.; Kutzner, C.; Hess, B.; Lindahl, E. *Tackling Exascale Software Challenges in Molecular Dynamics Simulations with GROMACS, in Solving Software Challenges for Exascale*, edited by, Markidis, S.; Laure, E., Eds.; Springer International Publishing: Cham, 2015; Vol. 8759, pp 3–27.

(32) Pronk, S.; Páll, S.; Schulz, R.; Larsson, P.; Bjelkmar, P.; Apostolov, R.; Shirts, M. R.; Smith, J. C.; Kasson, P. M.; van der Spoel, D.; Hess, B.; Lindahl, E. GROMACS 4.5: A High-Throughput and Highly Parallel Open Source Molecular Simulation Toolkit. *Bioinformatics* **2013**, *29*, 845.

(33) Case, D. A.; Aktulga, H. M.; Belfon, K.; Ben-Shalom, I. Y.; Brozell, S. R.; Cerutti, D. S.; Cheatham, T. E., III; Cisneros, G. A.; Cruzeiro, V. W. D.; Darden, T. A.; Duke, R. E.; Giambasu, G.; Gilson, M. K.; Gohlke, H.; Goetz, A. W.; Harris, R.; Izadi, S.; Izmailov, S. A.; Jin, C.; Kasavajhala, K.; Kaymak, M. C.; King, E.; Kovalenko, A.; Kurtzman, T.; Lee, T. S.; LeGrand, S.; Li, P.; Lin, C.; Liu, J.; Luchko, T.; Luo, R.; Machado, M.; Man, V.; Manathunga, M.; Merz, K. M.; Miao, Y.; Mikhailovskii, O.; Monard, G.; Nguyen, H.; O'Hearn, K. A.; Onufriev, A.; Pan, F.; Pantano, S.; Qi, R.; Rahnamoun, A.; Roe, D. R.; Roitberg, A.; Sagui, C.; Schott-Verdugo, S.; Shen, J.; Simmerling, C. L.; Skrynnikov, N. R.; Smith, J.; Swails, J.; Walker, R. C.; Wang, J.; Wei, H.; Wolf, R. M.; Wu, X.; Xue, Y.; York, D. M.; Zhao, S.; Kollman, P. A. *Amber 2021*, AmberTools21; University of California: San Francisco, 2021.

(34) Wang, J.; Wolf, R. M.; Caldwell, J. W.; Kollman, P. A.; Case, D. A. Development and Testing of a General Amber Force Field. *J. Comput. Chem.* **2004**, *25*, 1157.

(35) Brehm, M.; Thomas, M.; Gehrke, S.; Kirchner, B. TRAVIS—A Free Analyzer for Trajectories from Molecular Simulation. *J. Chem. Phys.* **2020**, *152*, No. 164105.

(36) Hollóczy, O.; Macchiagodena, M.; Weber, H.; Thomas, M.; Brehm, M.; Stark, A.; Russina, O.; Triolo, A.; Kirchner, B. Triphilic Ionic-Liquid Mixtures: Fluorinated and Non-Fluorinated Aprotic Ionic-Liquid Mixtures. *ChemPhysChem* **2015**, *16*, 3325.

(37) Brehm, M.; Kirchner, B. TRAVIS - A Free Analyzer and Visualizer for Monte Carlo and Molecular Dynamics Trajectories. *J. Chem. Inf. Model.* **2011**, *51*, 2007.

(38) Ghoufi, A. Molecular Origin of the Prepeak in the Structure Factor of Alcohols. *J. Phys. Chem. B* **2020**, *124*, 11501.

(39) Almásy, L.; Kuklin, A. I.; Požar, M.; Baptista, A.; Perera, A. Microscopic Origin of the Scattering Pre-Peak in Aqueous Propylamine Mixtures: X-Ray and Neutron Experiments versus Simulations. *Phys. Chem. Chem. Phys.* **2019**, *21*, 9317.

(40) Požar, M.; Lovrinčević, B.; Zoranić, L.; Primorać, T.; Sokolić, F.; Perera, A. Micro-Heterogeneity versus Clustering in Binary Mixtures of Ethanol with Water or Alkanes. *Phys. Chem. Chem. Phys.* **2016**, *18*, 23971.

(41) Herschlag, D.; Pinney, M. M. Hydrogen Bonds: Simple after All? *Biochemistry* **2018**, *57*, 3338.

(42) Nath, P. P.; Sarkar, S.; Krishna, P. S. R.; Joarder, R. N. Intermolecular Structure of Liquid D- Tert -Butanol by Neutron-Diffraction Data. *Appl. Phys. A: Solids Surf.* **2002**, *74*, s348.

(43) Headen, T. F. Temperature Dependent Structural Changes in Liquid Benzene Studied Using Neutron Diffraction. *Mol. Phys.* **2019**, *117*, 3329.

Supporting Information for

Supramolecular structure of phenyl derivatives of butanol isomers

Joanna Grelska^{1,2,*}, *Karolina Jurkiewicz*^{1,2,*}, *Andrzej Burian*^{1,2}, *Sebastian Pawlus*^{1,2}

¹ A. Chełkowski Institute of Physics, University of Silesia in Katowice, ul. 75 Pułku Piechoty
1, 41-500 Chorzów, Poland

² Silesian Center for Education and Interdisciplinary Research, ul. 75 Pułku Piechoty 1A, 41-
500 Chorzów, Poland

*Correspondence e-mails: joanna.grelska@us.edu.pl, karolina.jurkiewicz@us.edu.pl

1. Calculation of the pair distribution function

The total atomic pair distribution function is defined as follows:

$$G(r) = 4\pi r [\rho(r) - \rho_0] = 4\pi r \rho_0 [g(r) - 1]. \quad [\text{SI1}]$$

The physical meaning of $\rho(r)$ is that $4\pi r^2 \rho(r) dr$ determines the number of atoms within the spherical shell of the radius r and the thickness dr , and ρ_0 is the number density. $g(r) = \frac{\rho(r)}{\rho_0}$ gives the actual number density surrounding the reference atom and defines the structural features at the atomic scale. $G(r)$ was determined and calculated using the sine Fourier transform of total $S(Q)$:

$$G(r) = \frac{2}{\pi} \int_0^{Q_{max}} S(Q) \sin(Qr) \frac{\sin(\pi Q/Q_{max})}{\pi Q/Q_{max}} dQ, \quad [\text{SI2}]$$

where the last fraction denotes the Lorch modification function reducing effects arising from the finite value of the upper Q limit.

2. Details of the molecular dynamics simulations

Table S11. Densities and molar masses of the investigated compounds as well as the lengths of the cubic boxes containing 2000 molecules that were taken for the molecular dynamics simulations.

compound name	density [g/cm ³]	molar mass [g/mol]	box length [Å]
nBOH	0.81	74.123	67.233
4Ph1BOH	0.984	150.22	79.739
iBOH	0.802	74.123	67.456
2M3Ph1POH	0.9841	150.22	79.736
sBOH	0.806	74.123	67.344
4Ph2BOH	0.98	150.22	79.847
tBOH	0.781	74.123	68.055
2M1Ph2POH	0.974	150.22	80.010

It must be stressed out that other force fields, CHARMM27, OPLS-AA, AMBERGS, were also tested with topology files generated by LigParGen server, but the models did not give satisfying agreement with experimental diffraction data. The total charge of studied molecules was equal to zero. The smoothed particle-mesh Ewald (SPME) method treated Coulomb and Van der Waals interactions with cutoff at 20 Å. The intramolecular bond lengths and angles were kept flexible. The time step in simulations was 1 fs. At first, the energy minimization was performed by the steepest descent algorithm for $2 \cdot 10^6$ steps. Then, equations of motion were integrated for 2 ns using a velocity Verlet algorithm. The temperature was maintained by the Nose-Hoover thermostat, the time constant for coupling was 0.1 ps.

3. The comparison of the experimental and theoretical total atomic pair distribution functions

Apart from the structure factors, the intramolecular and short-range intermolecular correlations can be also probed by the first few peaks of the atomic pair distribution functions presented in Figure SI1a, while longer-range correlations are shown in Figure SI1b. The positions and amplitudes of $G(r)$ peaks derived from simulations are in very good agreement with experimental data in the whole range of r . The model-based functions reconstruct also the differences in the damping of the $G(r)$ peaks for long r between the aliphatic and phenyl butanols. It is clear from Figure SI1b that the former butanols are characterized by longer range intermolecular correlations, extending up to around 30 Å. In turn, for phenyl butanols there are no oscillations beyond around 20 Å. It indicates suppression of the longer-range intermolecular order by the presence of an aromatic ring. In an attempt to understand these observations more deeply, as a trace of the supramolecular aggregation, the data derived from the MD models are further analyzed.

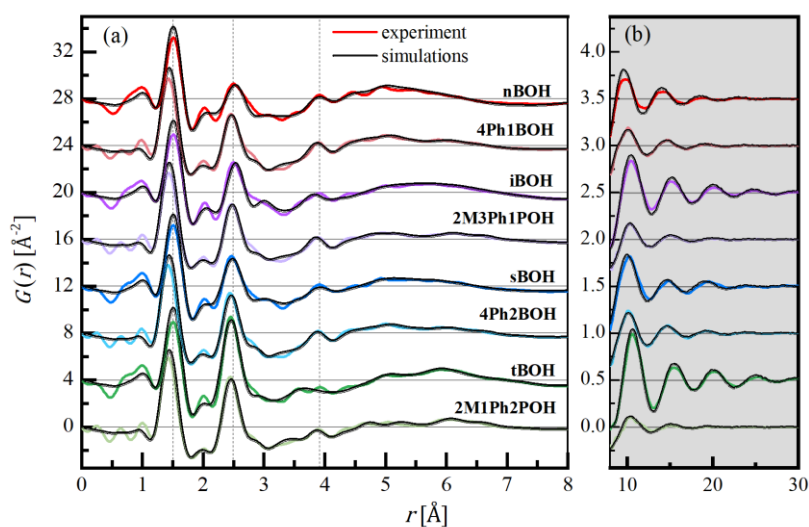
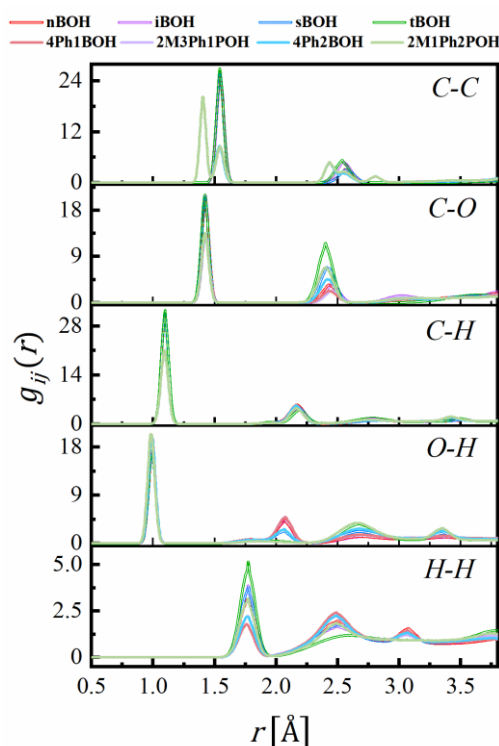


Figure SI1. Experimental (colored lines) and simulated (black lines) total pair distribution functions $G(r)$ of investigated butanols in the region of short (a) and longer (b) distances r . The curves are shifted by 4, starting with 2M1Ph2POH in panel (a). In panel (b), the curves are shifted by 0.5, beginning with 2M1Ph2POH.

4. Partial radial distribution functions

The partial radial distribution functions $g_{ij}(r)$ determined between pairs of atomic species in the system, where the indices i and j run over N different atom types, are shown in Figure SI2. The $g_{OO}(r)$ function is presented in the article in Figure 4.



SI2. Partial radial distribution functions $g_{ij}(r)$ obtained from the optimized structural models of butanol isomers and their phenyl derivatives.

5. The analysis of hydrogen bonds and supramolecular clusters

The definition of supramolecular cluster depends crucially on the criteria qualifying how two molecules are linked to each other. Here, H-bonding links are considered. In the case of the studied alcohols, the HBs occur between the electronegative oxygen atom O in one molecule and the positive hydrogen atom H' attached to the oxygen O' from neighbouring molecule. This way the linked molecules may form supramolecular clusters of diverse architectures. The

number and size of the clusters depend strongly on the connectivity geometrical restrictions concerning the distance and angle between the atoms forming the O'–H'...O connections, so on the number and geometry of HBs. The maximal distance between O' and O atoms participating in H-bonding is usually taken as a value of the first minimum in the $g_{OO}(r)$ function^{1–3}. In many papers the value of 3.5 Å is set^{1,4,5} while for the H'–O'–O angle criteria the upper value of 30° or no angle restrictions are the most often applied^{1,3,6,7}. In Supporting Information in order to test how the angular criteria are sensitive for estimation of the HBs number, three ranges for H'–O'–O angle were considered: 1) $\leq 30^\circ$, 2) $\leq 60^\circ$ and 3) $\leq 90^\circ$. Simultaneously, the upper limit for HB distance was set as the first $g_{OO}(r)$ minimum of 3.5 Å for all butanols (as shown in Figure 3b). The results of the total number of HBs existing in the models and numbers of lone molecules, assuming the above conditions, are presented in Figure. Taking the same conditions, the average HB angles and the HB distances were calculated and are depicted in Figure SI4.

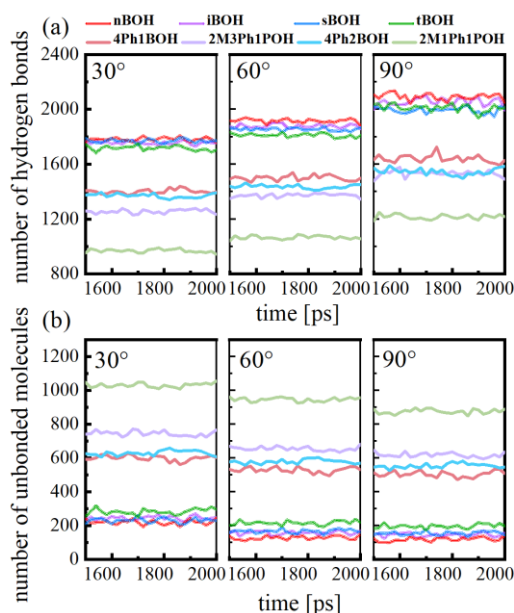


Figure SI3. Fluctuations of the number of all hydrogen bonds (a) and unbounded molecules (b) for last 500 steps of molecular dynamics simulations of the investigated systems calculated for three H'–O'–O angle restrictions: $\leq 30^\circ$, $\leq 60^\circ$, $\leq 90^\circ$, and O'–O distance restriction ≤ 3.5 Å.

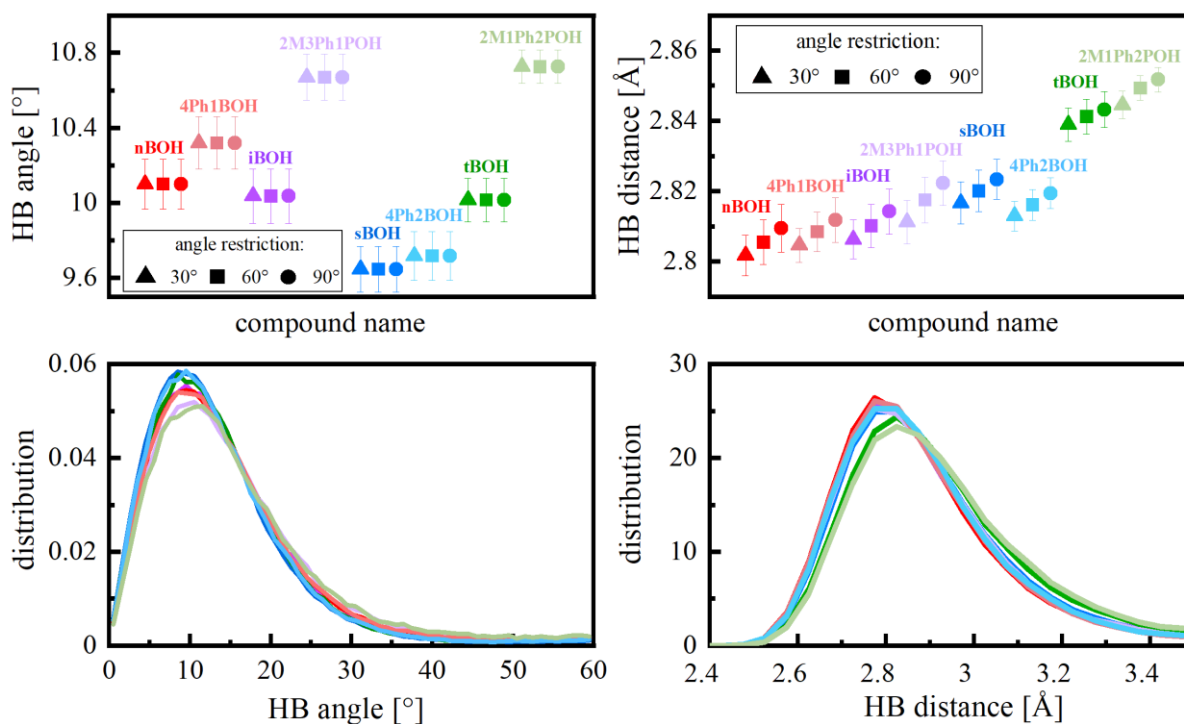


Figure SI4. Average values (top panel) of the distributions (bottom panel) of hydrogen bond (HB) distance and angle, for three H'–O'–O angle restrictions: 1) $\leq 30^\circ$, 2) $\leq 60^\circ$, and 3) $\leq 90^\circ$, and O'–O distance restriction ≤ 3.5 Å. The average values were obtained as central positions of the distributions fitted with Gauss function.

6. Molecular conformations

In the optimized 3-dimensional models of the studied alcohols, different molecular conformations were observed. In order to analyze them, we chose the angle between three atoms in the molecule of each alcohol, which strongly depends on the molecular conformation. Figure SI5 depicts the distributions of these angles for all simulating systems composed of 2000 molecules. In Figure SI5 also the angles corresponding to the maxima of these angular distributions for aliphatic butanols were graphically marked by orange lines on the models of molecular conformers. For phenyl butanols the same angles were defined as for their aliphatic counterparts. These angles refer to the same atoms in aliphatic alcohols and their corresponding

phenyl counterparts, independently of the phenyl ring, while the phenyl ring is a rigid part of the molecule. The presented distributions disclose that the molecules used for MD simulations resided in one molecular conformation since the simulation box was created as a set of 2000 molecules having the same geometry. After the simulations, in turn, two characteristic types on molecular conformations appeared for primary and secondary butanols as well as their phenyl derivatives. Whereas, tertiary butanol and its phenyl derivative occurred in only one, starting conformation. That is reasonable taking into account the geometry of these molecules and their rigidity. The distributions of the selected intramolecular angles after simulations are much broader than the starting ones as the MD causes fluctuations of the atomic positions. The broadest distributions with two maxima at around 100° and 130° are observed for nBOH and its phenyl counterpart, which are the stretchiest due to the flexible long alkyl tail and the location of OH moiety at its end. Such a molecular structure favors folding of the chain. The area under the peak with the maximum for the smaller angle is bigger, suggesting that there are more nBOH molecules with bent geometry of the alkyl tail than with more linear skeleton. Such finding is consistent with previous conformational studies of nBOH by the vibrational spectroscopy and ab initio calculations, which suggested that in the liquid nBOH molecules take diverse conformations⁸. In turn, for iBOH and sBOH, as well for their phenyl counterparts, two distinct conformations appear with a majority of molecules with the smaller angle that refer to starting atom positions. The flexibility of the molecules and the variability of their conformations facilitate the formation of HBs and bigger supramolecular clusters, as revealed in the previous section.

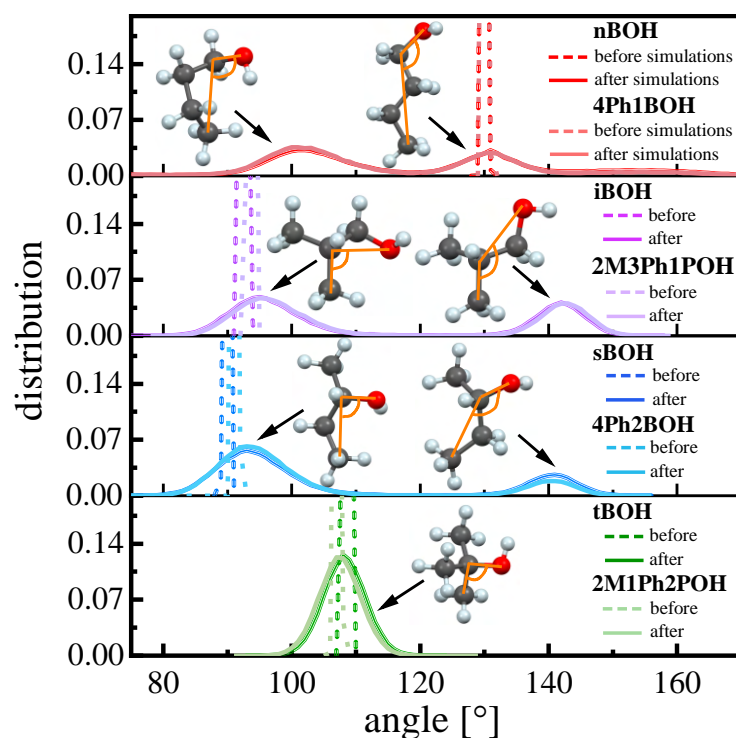


Figure SI5. Distributions of selected intramolecular angles in the studied alcohols before and after MD simulations. The distributions are normalized to 1, but the range of the vertical axis is limited to 0.2 to emphasize the results after MD optimization. The insets show the characteristic molecular conformations for aliphatic butanols with the preferred angles, marked with orange lines, which correspond to the maxima in the distributions.

7. The results of simulations with a longer time and a bigger box size

In order to test the correctness of the chosen simulation time and box size, we performed simulations for the same box size of 2000 molecules but with a longer time of 10 ns as well as for a time of 2 ns but with a bigger box size of 16000 molecules for one of the studied alcohols - isobutanol. The obtained results in the form of: the structure factors, histograms of the number of clusters as a function of the number of molecules, oscillations of the average number of molecules in the clusters with time, distributions of the molecular conformations based on the selected intramolecular angle and oscillations of the angle with the simulation time are presented in Figure SI6-10, respectively. The obtained results demonstrate that the simulation

time of 2 ns and the box size of 2000 molecules are enough to obtain stable and statistically-averaged structural properties.

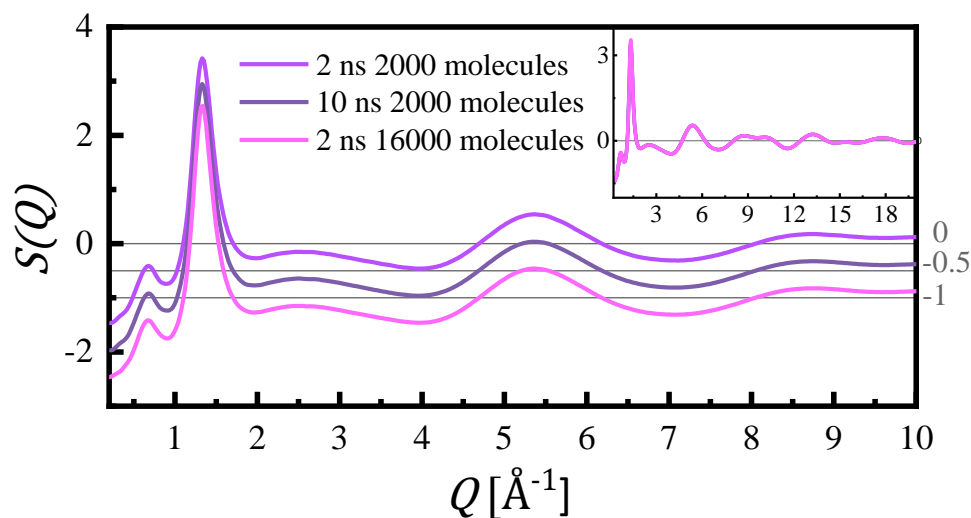


Figure SI6. The comparison of the total structure factors calculated for three models of isobutanol with different parameters: 1) simulation time of 2 ns and box size of 2000 molecules; 2) simulation time of 10 ns and box size of 2000 molecules; 3) simulation time of 2 ns and box size of 16000 molecules. The inset shows that these three structure factors overlap each other.

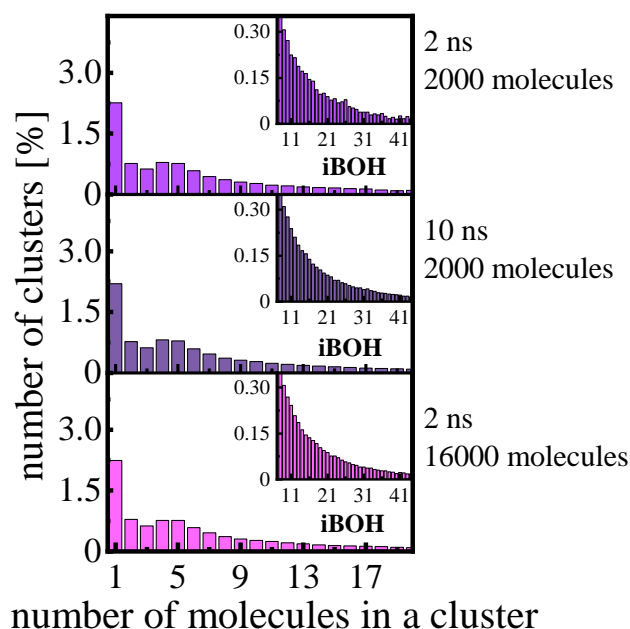


Figure SI7. Histograms of the number of clusters as a function of the number of molecules in the clusters for isobutanol. The results obtained based on three optimized models with: 1) simulation time of 2 ns and box size of 2000 molecules; 2) simulation time of 10 ns and box size of 2000 molecules; 3) simulation time of 2 ns and box size of 16000 molecules.

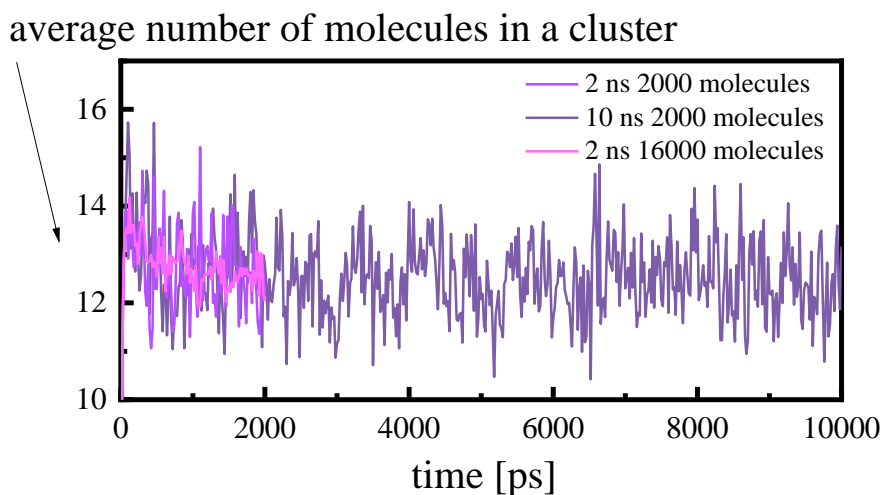


Figure SI8. The oscillations of the average number of molecules in the clusters of isobutanol in time for three models: 1) simulation time of 2 ns and box size of 2000 molecules; 2) simulation time of 10 ns and box size of 2000 molecules; 3) simulation time of 2 ns and box size of 16000 molecules.

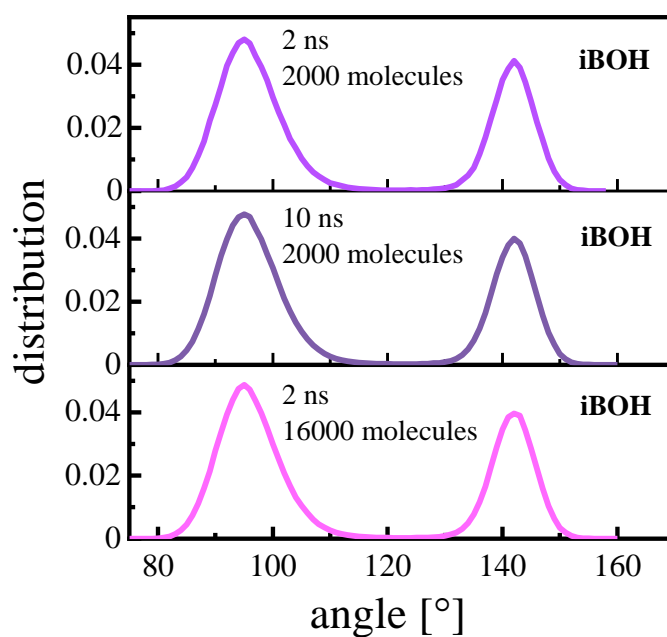


Figure SI9. The comparison of the conformations of isobutanol molecules calculated for three models: 1) simulation time of 2 ns and box size of 2000 molecules; 2) simulation time of 10 ns and box size of 2000 molecules; 3) simulation time of 2 ns and box size of 16000 molecules.

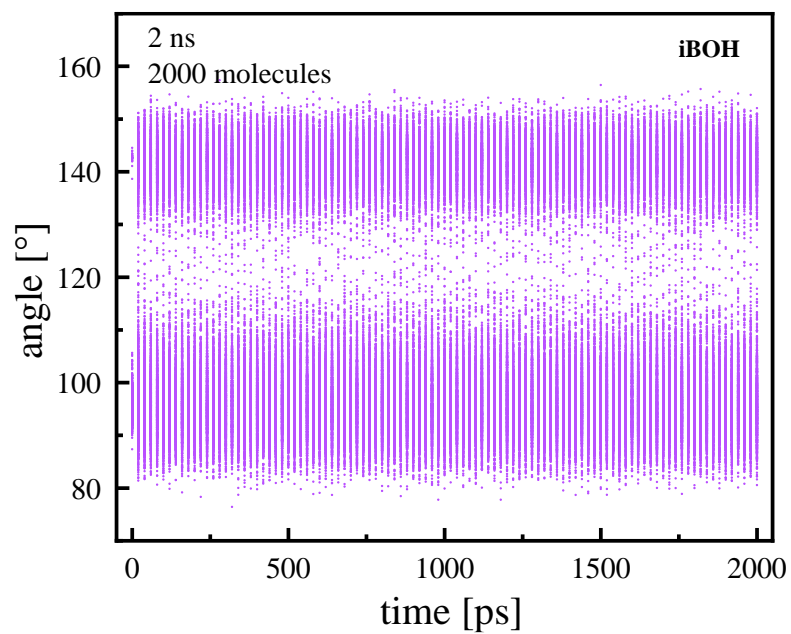


Figure SI10. The distribution of the selected intramolecular angle of isobutanol (indicated in Figure SI5) with the time of the simulations.

References

1. Gereben, O. & Pusztai, L. Hydrogen bond connectivities in water–ethanol mixtures: On the influence of the H-bond definition. *Journal of Molecular Liquids* **220**, 836–841 (2016).
2. Choi, S., Parameswaran, S. & Choi, J.-H. Effects of molecular shape on alcohol aggregation and water hydrogen bond network behavior in butanol isomer solutions. *Phys. Chem. Chem. Phys.* **23**, 12976–12987 (2021).
3. Požar, M. *et al.* Micro-heterogeneity versus clustering in binary mixtures of ethanol with water or alkanes. *Phys. Chem. Chem. Phys.* **18**, 23971–23979 (2016).
4. Geiger, A. & Stanley, H. E. Low-Density ‘Patches’ in the Hydrogen-Bond Network of Liquid Water: Evidence from Molecular-Dynamics Computer Simulations. *Phys. Rev. Lett.* **49**, 1749–1752 (1982).
5. Oleinikova, A., Brovchenko, I., Geiger, A. & Guillot, B. Percolation of water in aqueous solution and liquid–liquid immiscibility. *The Journal of Chemical Physics* **117**, 3296–3304 (2002).
6. Gómez-Álvarez, P., Romaní, L. & González-Salgado, D. Association effects in pure methanol via Monte Carlo simulations. I. Structure. *The Journal of Chemical Physics* **138**, 044509 (2013).
7. Bolle, J. *et al.* Isomeric effects in structure formation and dielectric dynamics of different octanols. *Phys. Chem. Chem. Phys.* **23**, 24211–24221 (2021).
8. Ohno, K., Yoshida, H., Watanabe, H., Fujita, T. & Matsuura, H. Conformational Study of 1-Butanol by the Combined Use of Vibrational Spectroscopy and ab Initio Molecular Orbital Calculations. *J. Phys. Chem.* **98**, 6924–6930 (1994).

B. P2. Computer simulations as an effective way to distinguish supramolecular nanostructure in cyclic and phenyl alcohols





Grelska, J., Jurkiewicz, K., Nowok, A., & Pawlus, S. (2023). *Physical Review E*, 108(2), 024603-1-7. DOI:10.1103/PhysRevE.108.024603

Punkty MNiSW (2024): 140

Impact Factor (2023): 2.4

Mój wkład w publikację polegał na wykonaniu pomiarów dyfrakcji rentgenowskiej, wykonaniu symulacji dynamiki molekularnej, analizie wyników i ich dyskusji oraz przygotowaniu artykułu.

Computer simulations as an effective way to distinguish supramolecular nanostructure in cyclic and phenyl alcohols

Joanna Grelska ^{1,*} Karolina Jurkiewicz ^{1,†} Andrzej Nowok ^{2,3} and Sebastian Pawlus ¹

¹*A. Chelkowski Institute of Physics, University of Silesia in Katowice, 75 Pułku Piechoty 1, 41–500 Chorzów, Poland*

²*Department of Experimental Physics, Wrocław University of Science and Technology,
Wybrzeże Stanisława Wyspiańskiego 27, 50–370 Wrocław, Poland*

³*Laboratoire National des Champs Magnétiques Intenses, UPR 3228, CNRS-UGA-UPS-INSA, Grenoble and Toulouse, France*



(Received 16 September 2022; accepted 2 July 2023; published 4 August 2023)

Molecular dynamics simulations supported by x-ray-diffraction experimental data were utilized to demonstrate how replacing the cyclic ring with the phenyl one in molecules of alcohols significantly differentiates their nanostructure by reducing the number of H-bonded clusters. Besides, molecules in the phenyl alcohols associate themselves in clusters via phenyl ring organization which likely is the result of $\text{OH} \cdots \pi$ and $\pi \cdots \pi$ interactions. Thus, at room temperature, the supramolecular structure of phenyl alcohols is more heterogeneous and governed by the formation of various clusters arising due to three types of interactions, while in cyclic alcohols, the H bonding controls the association of molecules. We believe that our methodology could be applied to better understand the fundamental process of association via H bonding and the competitive aggregation caused by phenyl rings.

DOI: [10.1103/PhysRevE.108.024603](https://doi.org/10.1103/PhysRevE.108.024603)

I. INTRODUCTION

The process of supramolecular aggregation on the nanoscale is the subject of extensive studies as it plays an important role in the properties and reactions of building blocks of living organisms such as proteins, polysaccharides, nucleotides in DNA chain, and other large biomolecules [1–7]. One of the most important driving forces for the supramolecular nanostructuring in biological systems are hydrogen bonds and $\pi \cdots \pi$ interactions of aromatic groups. These forces are considered while designing supramolecular solid-state architectures of self-assembled drug-delivery systems [8,9]. Therefore, knowledge of the organization of molecules in systems where hydrogen bonds and aromatic ring interactions cooperate is important for both fundamental science and technical applications. However, while the characterization of the structure of macromolecular complex systems is very demanding, more impact needs to be placed on simple model systems. Such a group is alcohols that create supramolecular clusters, in the size of a few nanometers, via hydrogen bonds formed by hydroxyl groups of molecules. Furthermore, the chemical structure of alcohols can be easily altered by attaching various functional groups. Especially, the hydrogen bond network can be suppressed when a steric hindrance, e.g., a carbon ring, is introduced in the neighborhood of the OH group [10,11]. However, up to now, there have been many misconceptions about how the association changes when the aromaticity of the functional groups is substituted.

Recent combined dielectric and photon-correlation spectroscopy studies conducted on alcohols with attached phenyl groups suggested that the formation of supramolecular clusters promoted by hydrogen bonds is not suppressed in those compounds compared to their aliphatic counterparts, but their architecture varies from chain- to ringlike shapes as the phenyl ring moves closer to the hydroxyl group [12]. In turn, a series of our recent papers based on dielectric, infrared, and diffraction investigations present a rather different view on the association of molecules in phenyl alcohols. Namely, we suggested that the phenyl ring may excite the organization of molecules via $\text{OH} \cdots \pi$ interactions and, as a consequence of this, cause a diverse packing of molecules on the short- and medium-range scale [13]. Moreover, we demonstrated that the population of hydrogen bonds is more abundant in cyclic (aliphatic) than phenyl (aromatic) compounds [14]. Furthermore, using computer simulations, we revealed that despite the lack of the diffraction prepeak, which was proved to be a fingerprint of the organization of hydroxyl groups into associates, phenyl alcohols tend to create small H-bonded clusters [15].

In this paper we use molecular dynamics simulations supported by x-ray diffraction to fill the gap in understanding the intermolecular structure of phenyl and cyclic alcohols in the liquid state at ambient conditions. The very good compliance between the experimental and molecular dynamics data prompted us to analyze the optimized structural models in detail using computational methods. We also confirmed our findings in experimental results of infrared and dielectric spectroscopy. Investigations on the compounds were performed at room temperature, as these conditions are the most suitable to track differences in the degree of association and intermolecular arrangements between aromatic

*joanna.grelska@us.edu.pl

†karolina.jurkiewicz@us.edu.pl

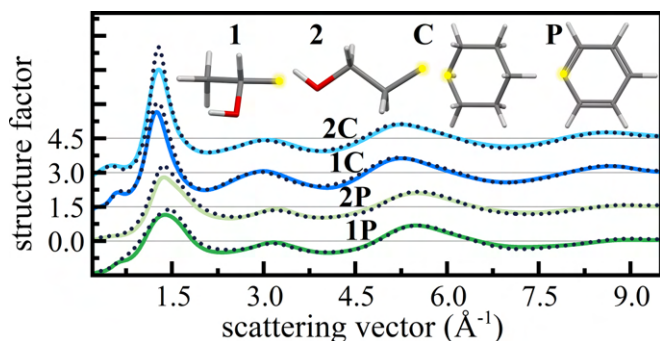


FIG. 1. Structure factors obtained from experiment (colored solid lines) and simulations (black dotted lines) for all investigated compounds. Models of their molecules are shown in upper part of graph as composed of two parts: alkyl chain (1 – or 2 –) and a hexagonal ring (C – cyclic, P – phenyl) with a connection linking both parts marked in yellow.

and nonaromatic H-bonded systems [10,11,13]. Namely, at room temperature, hydrogen bonds dominating in alcohols are weaker than at low temperatures and it is feasible to observe other interactions resulting from phenyl moiety.

II. METHODOLOGY

The investigated liquids are two isomers of phenyl alcohols: 1-phenylethanol (1P) and 2-phenylethanol (2P) with formula $C_8H_{10}O$, and their nonaromatic counterparts 1-cyclohexylethanol (1C) and 2-cyclohexylethanol (2C) with formula $C_8H_{16}O$, shown in the inset of Fig. 1. All compounds were purchased from Sigma-Aldrich. The difference between secondary (1) and primary (2) alcohols is in the positions of hydroxyl group relative to the carbon ring in the molecule. For simplicity, in the rest of the paper, the molecules with cyclic substituent will be called “cyclic” (C), while the aromatic ones will be alternatively called “phenyl” (P). The C and P alcohols in 1 and 2 configurations vary in the type of hexagonal carbon ring possessing very similar intramolecular architecture.

The experimental results were obtained at room temperature by wide-angle x-ray diffraction with Ag anode and normalized to the structure factor form (diffraction intensity per one atom). More details on the apparatus are contained in Ref. [15]. Molecular dynamics (MD) simulations were carried out using GROMACS package (version 2020) [16–18] at the NVT ensemble of 2000 molecules, at temperature 293.15 K. Topology files were created using the Antechamber module (AMBERTOOLS21) [19], and GAFF force field was used, which was developed for simulating organic compounds containing phenyl moieties [20]. Other parameters were analogous to those used in our previous paper [15]. Trajectories were collected after 2 ns of equilibration, from time of 2 ns. TRAVIS software [21–23] was used to calculate model-based structure factors, radial distribution functions, and combined functions of angular distribution versus radial distribution.

III. STRUCTURE PROPERTIES

The structure factors presented in Fig. 1 show very good compliance of the MD simulations with experimental re-

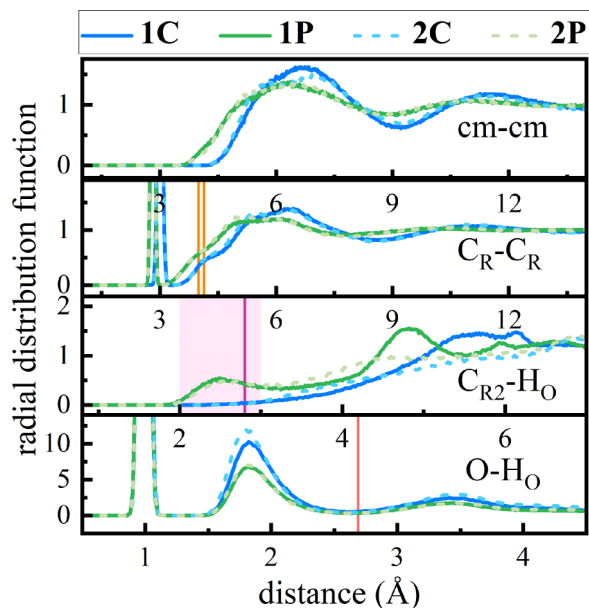


FIG. 2. Model-based radial distribution functions between centers of molecule masses, cm-cm, (top panel), as well as between first or fourth carbon atoms in rings, C_R-C_R ; fourth carbon atom in ring and hydrogen atom attached to oxygen, $C_{R2}-H_O$; oxygen and hydrogen attached to oxygen, $O-H_O$.

sults. Based on the data, one can see that the intermolecular structure of phenyl compounds 1P and 2P, manifested in low-scattering vectors up to $\sim 2.25 \text{ \AA}^{-1}$, differs significantly from that of cyclic counterparts 1C and 2C. The main diffraction peak of the aromatic systems is broader and has a clearly lower intensity in comparison to the aliphatic counterparts. That indicates a bigger disorder and heterogeneity of the nearest-neighbor intermolecular structure of phenyl alcohols. In turn, cyclic alcohols have clearly separated two values of the scattering vector in the range of intermolecular correlations: main-peak at $\sim 1.4 \text{ \AA}^{-1}$ and weaker prepeak at $\sim 0.7 \text{ \AA}^{-1}$. In real space, those translate to periodicities existing between nearest-neighbor molecules and groups of bonded molecules, respectively. What is interesting, the structure factor of phenyl compound 1P is also characterized by a weak prepeak at a similar position while for 2P the prepeak seems to be completely damped. On the molecular level, in 1P the distance between hydroxyl group and phenyl ring is 1 carbon atom while, for 2P, 2 carbon atoms separate the functional moieties. Therefore, one may expect a stronger steric hindrance on H bonding by the carbon ring in the case of 1P than 2P (and 1C than 2C). A detailed explanation of the prepeak feature is provided based on the simulated partial atom-atom structure factors in Supplemental Material [24].

Using the spatial organization of molecules optimized by the MD simulations, the radial distribution functions (rdfs) were calculated. Figure 2 shows the selected partial rdfs in the range of distances up to 4.5 \AA , where the intramolecular and short-contact intermolecular correlations give the main contribution. The intensity of the rdf peaks is proportional to the probability of finding two atoms (or groups of atoms) in

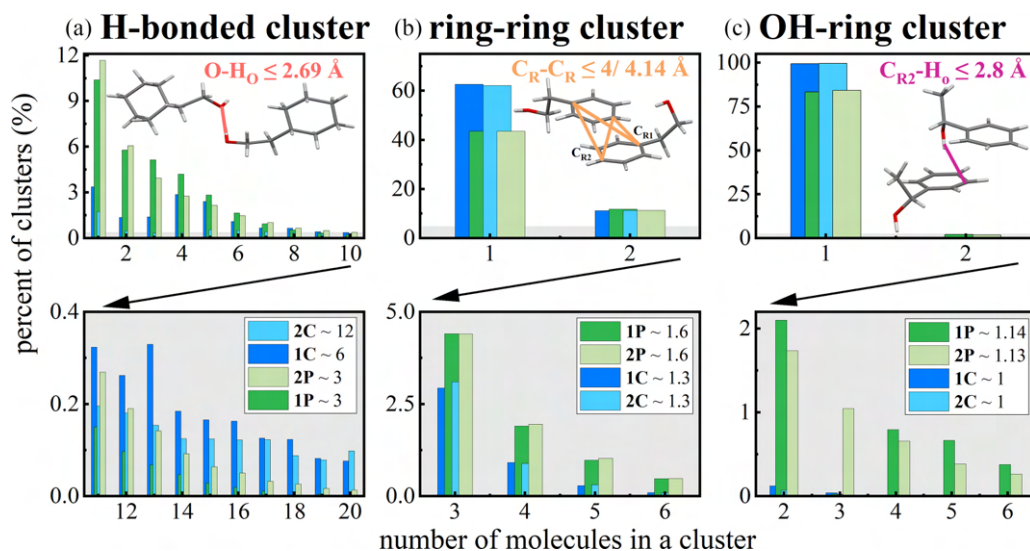


FIG. 3. Histograms of concentration of clusters obtained from optimized structural models as function of number of molecules associated in (a) H-bonded clusters, (b) ring clusters, and (c) OH-ring cluster. Average numbers of molecules in all types of clusters for all studied alcohols are depicted in legends on graphs. Distributions for higher values of molecules in a cluster are enclosed in separate graphs below. Criteria used for definition of all types of clusters are presented in insets.

the system at the given distance. A clear difference is visible again between the phenyl and cyclic alcohols. The former class is characterized by shorter distances between centers of molecular masses (cm-cm). This observation supports the fact that molecules in phenyl alcohols are more densely packed and have bigger molar density than their cyclic counterparts (see Supplemental Material [24] for density measurements). However, the differences in the packing of molecules between both types of alcohols can also originate from the distinct aggregation and stacking of phenyl and cyclic carbon rings.

In order to investigate this issue in more details, the C_{R-C_R} radial distribution function, which covers the correlations within and between the carbon rings, was calculated (Fig. 2). C_{R1} is the first carbon linking the ring with the tail of molecule and C_{R2} lies in the opposite position in the ring; see the scheme in Fig. 3. The C_{R-C_R} rdf follows a similar course above around 3 Å as the cm-cm function. The additional peak at the distance of around 2.8 Å, absent in the cm-cm function, originates from the intramolecular $C_{R1-C_{R2}}$ distances (ring diameter). It may be noticed that the diameter is slightly greater for more flexible cyclic molecules. The broad bump in the C_{R-C_R} function with maximum at around 6 Å, arising from the intermolecular correlations between carbon rings, is clearly shifted towards smaller distances for phenyl than cyclic alcohols. It raises the question about the arrangement of molecules at short distances, whether it is similar for phenyl and cyclic rings, or whether the effect of speculated $\pi\cdots\pi$ or $OH\cdots\pi$ interactions in the aromatic alcohols alters the structural organization.

The possible $OH\cdots\pi$ interactions would alter the arrangement of molecules in such a way that OH group of one molecule approaches the carbon ring of a neighboring molecule. Therefore, in order to detect such alignments we calculated the C_{R2-H_O} radial distribution function between the terminating carbon atom in the ring and hydrogen atom attached to oxygen. The average distance between the H_O

and C_{R2} atoms within the investigated molecules is bigger than 4 Å. Thus, the appearance of C_{R2-H_O} correlations at smaller distances would appear for an organization of C_{R2-H_O} atoms belonging to neighboring molecules. Indeed, a clear maximum at around 2.5 Å appears in the C_{R2-H_O} distribution function (marked in Fig. 2), but only for phenyl alcohols 1P and 2P. Thus, it confirms the spatial correlations of molecules where the $OH\cdots\pi$ interactions may occur. The distance is in the range of $OH\cdots\pi$ interaction reported in the literature (2.3–3 Å) [25,26].

Moreover, the $O-H_O$ radial distribution function, taking into account oxygen atoms and the hydrogen atoms attached to oxygens, is shown in the bottom panel of Fig. 2. It provides information about the spatial correlations of molecules connected by hydrogen bonds. The first peak of this function at a distance of around 1 Å results from the intramolecular $O-H_O$ connections. Further peaks can be assigned to the intermolecular distances. For all of the studied alcohols, the next maximum of the $O-H_O$ function appears around 1.8 Å and has a similar shape, suggesting that the pattern of H bonds and their strength does not differ significantly between the cyclic and phenyl alcohols. However, the intensity of this peak is clearly higher for cyclic compounds indicating a higher concentration of hydrogen bonds in those systems. The distance in which the intensity of $O-H_O$ peaks fades is around 2.69 Å for all samples. Therefore, that value can be taken as the maximum $O-H_O$ distance in the hydrogen-bonding pattern for all modeled systems.

All these results explain well some peculiarities observed in infrared spectroscopy studies on these compounds (see Fig. S2 in Supplemental Material [24]). In fact, Fourier transform infrared (FTIR) spectra of 1C and 2C contain a single broad OH stretching band which points to almost full association of OH groups [27]. Maximum of this band is shifted towards lower wave numbers for 2C, which (following previous reports) may indicate bigger H-bonded aggregates at

room temperature compared to the 1C isomer. Contrary to the cyclic alcohols, room-temperature FTIR spectra of the phenyl analogs, beside OH stretching band, contain less-intense band which, following previous reports [8,9,11], we attribute as a stretching mode of the OH groups involved in OH- π interactions. Hence, its occurrence in the case of phenyl alcohols indicates that they associate to some extent by OH- π forces and therefore their degree of intermolecular association via hydrogen bonds at room temperature is lower than for cyclic alcohols. Additionally, higher full width at half maximum of the OH stretching band of phenyl alcohols confirms more heterogeneous distribution of the H-bonded agglomerates.

IV. CLUSTER ANALYSIS

The presented structural correlations between atoms belonging to different molecules prove the supramolecular organization of the studied alcohols. However, the clustering pattern is significantly different between molecules with cyclic and phenyl rings. In order to deepen the analysis of the obtained models, the number of molecules in various supramolecular clusters was calculated using the `gmx_cluster` program in GROMACS package. Three types of clusters were considered.

The first type of clustering is prompted by the H bonding. The criterion for a molecule to be associated in the cluster linked by H bonds was taken as the distance between O and H_O atoms of neighboring molecules smaller than 2.69 Å, based on the cutoff of the O-H_O radial distribution function (ticked in Fig. 2). That distance also covers the usual H-bonding criteria, which are O-OH angle $\leq 30^\circ$ and O-O distance ≤ 3.5 Å, based on the triangle relation. As can be seen from the cluster distributions in Fig. 3(a), for 2P and 1P the number of molecules unassociated in H-bonded clusters (single molecules) is much higher ($\sim 10\%$) than for cyclic compounds ($\sim 2\%$). Thus, the proposed models exhibit a destructive effect of carbon-ring aromaticity on the H-bond connections. As can be retrieved from the average number of molecules in such clusters, the alcohol that creates the largest H-bonded clusters is cyclic 2C (12 molecules), then 1C (6 molecules), and the smaller clusters, composed of 3 molecules on average, form 2P and 1P. The determined average cluster size is strongly dominated by large clusters, occurring especially in the cyclic alcohols. Thus, the most probable cluster size, which is 5–6 and 4 molecules for 2C and 1C, respectively, provides a more realistic picture of these structures. Moreover, the effect of the steric hindrance induced by the location of the OH group in the short distance relative to the carbon ring is significant in the case of cyclic alcohols: 1C has more unassociated molecules and creates smaller clusters of H-bonded molecules, on average, than 2C. In turn, for phenyl alcohols, the position of the OH group has much smaller impact on the average size of H-bonded associates.

The second type of clusters analyzed in the optimized models concerned the organization of carbon rings—we will call them “ring clusters.” The above-presented cm-cm and C_R-C_R radial distribution functions demonstrated significant differences in the structuring of rings between the cyclic and phenyl compounds. As a criterion for the ring cluster, the maximum distance between C_{R1} or C_{R2} of all atoms in

molecules was taken as 4 Å for phenyl compounds and 4.14 Å for cyclic ones (ticked in Fig. 2). These values were chosen to be higher than ring diameter and at the lower limit of cm-cm distance. The value for cyclic alcohols was increased, taking into account the density proportion (~ 0.92 g/cm³ for cyclic and ~ 1 g/cm³ for phenyl compounds). It is worth noting that similar $\pi\cdots\pi$ interaction distance, around 3.8 Å, was found in the face-to-face alignment of phenyl-ring centroids [28]. The histograms of the ring clusters are shown in Fig. 3(b). Accordingly, 40% of all cyclic and 60% of all phenyl molecules are associated in ring clusters. Dimers are the most abundant type of ring associates—involving above 10% of phenyl molecules. In turn, the ring dimers in cyclic alcohols constitute below 10% of all molecules and the concentration of bigger ring clusters is negligible. The average number of molecules in the ring cluster (1.6 for phenyl and 1.3 for cyclic alcohols) supports the idea that phenyl alcohols exhibit a stronger tendency toward ring organization than cyclic alcohols, caused by their ability to form $\pi\cdots\pi$ interactions.

The third type of cluster is induced by OH $\cdots\pi$ arrangement and called “OH-ring cluster.” In order to calculate the distribution of this cluster we chose carbon atom C_{R2} and hydrogen next to oxygen H_O, the same as presented in the rdf function, with the limit value of 2.8 Å (ticked in Fig. 2). The obtained results in Fig. 3(c) show that this type of cluster does not occur in cyclic compounds, while in phenyl ones they are significant (constitute around 20%). A little bit higher probability of such OH-ring cluster exists for 1P than for 2P, which has more favorable location of OH group for this kind of cluster arrangement.

In order to illustrate the spatial organization of molecules in the investigated models, the selected plane cuts of the simulation boxes are presented in Fig. 4. For a clear presentation of the discussed H-bonded and ring clusters, molecular skeletons without H atoms are shown in the left column while in the right column neat OH groups were extracted. For 2C alcohol, one can see that OH groups link into long chains the size of a few nanometers. There are no visible free molecules. The structure of 1C consists of shorter OH chains and other small clusters. From the histogram [Fig. 3(a)] one can see that 1C has a tendency to group into four molecules, which is confirmed in the picture of the organization of molecules and H bonds in Fig. 4. In the case of phenyl compounds 1P and 2P, there are only short H-bonded chains of few molecules, and many molecules are not linked with each other.

A closer look at the models allows us to notice that the aggregation of carbon rings is a characteristic feature of phenyl compounds. There is a great diversity of the arrangements adopted by molecules in such ring-ring clusters: *T* type, parallel, offset parallel, and perpendicular shaped, which are marked in light orange in Fig. 4. Similar configurations were reported for benzene—the archetypal aromatic system exhibiting $\pi\cdots\pi$ interactions [29]. Besides the molecular layouts supporting the existence of $\pi\cdots\pi$ interactions in phenyl alcohols, the models also exhibit the arrangement of molecules where OH $\cdots\pi$ interaction may occur (see clusters marked in light pink in Fig. 4). On the other hand, such arrangements in the models of cyclic alcohols are rare and incidental.

These outcomes explain well the differences in dielectric response of alcohols with cyclic and phenyl rings. Namely,

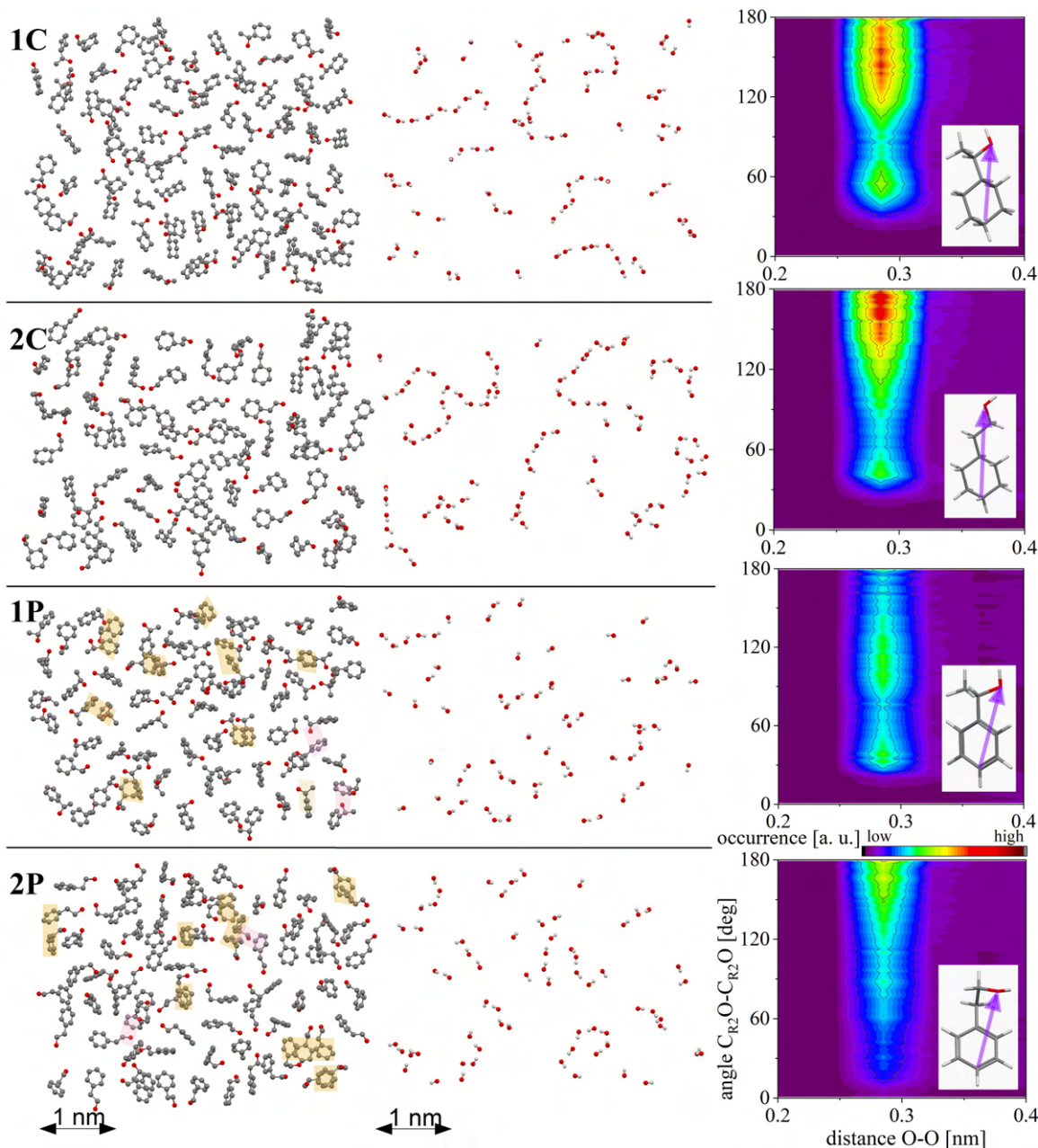


FIG. 4. Two-dimensional planes cut from the optimized structural models of cyclic and phenyl alcohols. (Left) Skeletons of molecules without hydrogen atoms are presented for clarity. In next column, only OH groups extracted from molecules are displayed. Centroids of molecular fragments fitting in planes are presented in each case. Therefore, these two representations differ in number of visible O and OH groups. For 1P and 2P possible $\pi \cdots \pi$ and $\text{OH} \cdots \pi$ related arrangements are marked in light orange and pink, respectively. (Right) Combined functions of angular distribution $\text{C}_{\text{R}_2\text{O}}\text{-C}_{\text{R}_2\text{O}}$ vs O-O radial distribution. Purple arrows mark molecules' chosen vectors in insets.

a characteristic feature of MD of alcohols is the Debye process, which reflects the mobility of the supramolecular nanostructures with a nonzero resultant dipole moment [27]. It was observed that a well-separated Debye peak of a high amplitude characterizes the dielectric spectra of alcohols with cyclohexyl ring (including 1C and 2C) [13,14]. In turn, dielectric spectra of aromatic alcohols such as 1P and 2P contain broadened Debye peaks of relatively low amplitude, additionally characterized by a small separation from the structural relaxation [10,13]. Our

studies show that these features are strictly connected with the small size of H-bonded clusters, as well as more heterogeneous supramolecular nanostructure due to $\pi \cdots \pi$ and $\text{OH} \cdots \pi$ arrangements.

Finally, we investigated the mutual alignment of molecules in their theoretical models derived from MD simulations. The intermolecular angular distributions of the selected vectors with reference to the intermolecular oxygen-oxygen distance were derived using TRAVIS software (Fig. 4). Vectors of molecules start from the terminating carbon atom C_{R_2} and

end in the most electronegative oxygen atom O (see inset of Fig. 4 for visualization of the vectors). From graphs presented in Fig. 4 one can clearly notice the highest intensity in distributions for cyclic compounds. That is in line with the fact that these compounds tend to associate strongly through hydrogen-bond interaction and therefore give the highest contribution to O-O rdf function. The difference is, however, visible in the angular distribution of intensity. The nearest molecules in 2C tend to align antiparallel, which confirms the chainlike type of H-bonded clusters. In 1C the dominating vectors' angle covers the range of 100° – 180° that is most likely the result of the formation of more branched systems of H bonds in clusters. The phenyl equivalents mimic the angular distributions of cyclic compounds. Most likely to create branchedlike cluster formations is 1P; 2P molecules with the highest intensity of 180° tend to stack in the antiparallel manner.

The above statements are in agreement with the behavior of Kirkwood-Fröhlich correlation factor g_k , which is the parameter providing information on cross correlation of dipole moments between adjacent molecules (see our results in Fig. S3 in Supplemental Material [24]). Value of $g_k > 1$ indicates parallel arrangement of dipole moments (chainlike structure) while $g_k < 1$ suggests negative cross correlation (circular structure). As presented in Fig. S3, there are clear differences in g_k between the studied alcohols at room temperature. Under these conditions, the nonaromatic 2C distinguishes itself by the highest value of g_k (which exceeds 2), suggesting the preferred chainlike organization of molecules within the aggregates. Alcohols 1C and 2P are characterized by lower value of g_k , indicating less occurrence of linear structures and more heterogeneous or branched ones. In turn, the sterically hindered aromatic 1P alcohol is characterized by the lowest g_k

value, close to 1, which suggests a heterogeneous alignment of adjacent dipole moment vectors.

V. SUMMARY

To sum up, we probed the structure of two isomers of simple cyclic alcohols and their phenyl counterparts to describe in details their supramolecular nanostructure. It was demonstrated that cyclic compounds tend to associate into long H-bonded chains. In phenyl alcohols, the association by H bonds is damped compared to cyclic compounds while additional phenyl ring aggregation, related to $\pi\cdots\pi$ and $\text{OH}\cdots\pi$ interactions, arises. The model of the structure of phenyl compounds consists mostly of dimeric and trimeric H-bonded clusters and dimers aggregated by the aromatic rings or by the ring and OH group. Our results explain at the molecular level some previous assumptions derived by infrared studies (formation of $\text{OH}\cdots\pi$ interactions) and dielectric spectroscopy (occurrence of the Debye process, the behavior of the Kirkwood-Fröhlich factor) for phenyl and cyclic compounds. We believe the provided pictures of the structure of such model compounds will be vitally useful to better understand the structural properties of complex systems where multiple weak interactions, such as hydrogen and π – π bonds, participate in the formation of the supramolecular nanostructure.

ACKNOWLEDGMENTS

J.G., K.J., and S.P. are thankful for the financial support from the National Science Centre, Poland within the OPUS Project No. UMO-2019/35/B/ST3/02670. The authors thank Prof. A. Burian for guidance in the treatment of experimental diffraction data.

-
- [1] V. Basavalingappa *et al.*, Mechanically rigid supramolecular assemblies formed from an Fmoc-Guanine conjugated peptide nucleic acid, *Nat. Commun.* **10**, 5256 (2019).
- [2] A. Arinstein, M. Burman, O. Gendelman, and E. Zussman, Effect of supramolecular structure on polymer nanofibre elasticity, *Nat. Nanotechnol.* **2**, 59 (2007).
- [3] B. J. G. E. Pieters, M. B. van Eldijk, R. J. M. Nolte, and J. Mecnović, Natural supramolecular protein assemblies, *Chem. Soc. Rev.* **45**, 24 (2016).
- [4] M. Diener, J. Adamcik, A. Sánchez-Ferrer, F. Jaedig, L. Schefer, and R. Mezzenga, Primary, secondary, tertiary and quaternary structure levels in linear polysaccharides: From random coil, to single helix to supramolecular assembly, *Biomacromolecules* **20**, 1731 (2019).
- [5] S. L. Higashi, N. Rozi, S. A. Hanifah, and M. Ikeda, Supramolecular architectures of nucleic acid/peptide hybrids, *Int. J. Mol. Sci.* **21**, 9458 (2020).
- [6] S. Cichosz and A. Masek, IR study on cellulose with the varied moisture contents: Insight into the supramolecular structure, *Materials* **13**, 4573 (2020).
- [7] J. Paturej, K. Koperwas, M. Tarnacka, K. Jurkiewicz, P. Maksym, J. Grelska, M. Paluch, and K. Kamiński, Supramolecular structures of self-assembled oligomers under confinement, *Soft Matter* **18**, 4930 (2022).
- [8] H. W. Roesky and M. Andruh, The Interplay of coordinative, hydrogen bonding and π – π stacking interactions in sustaining supramolecular solid-state architectures, *Coord. Chem. Rev.* **236**, 91 (2003).
- [9] W.-R. Zhuang, Y. Wang, P.-F. Cui, L. Xing, J. Lee, D. Kim, H.-L. Jiang, and Y.-K. Oh, Applications of π – π stacking interactions in the design of drug-delivery systems, *J. Controlled Release* **294**, 311 (2019).
- [10] A. Nowok, K. Jurkiewicz, M. Dulski, H. Hellwig, J. G. Małecki, K. Grzybowska, J. Grelska, and S. Pawlus, Influence of molecular geometry on the formation, architecture and dynamics of H-bonded supramolecular associates in 1-phenyl alcohols, *J. Mol. Liq.* **326**, 115349 (2021).
- [11] A. Nowok, M. Dulski, K. Jurkiewicz, J. Grelska, A. Z. Szeremeta, K. Grzybowska, and S. Pawlus, Molecular stiffness and aromatic ring position – crucial structural factors in the self-assembly processes of phenyl alcohols, *J. Mol. Liq.* **335**, 116426 (2021).
- [12] T. Böhmer, J. P. Gabriel, T. Richter, F. Pabst, and T. Blochowicz, Influence of molecular architecture on the dynamics of H-

- bonded supramolecular structures in phenyl-propanols, *J. Phys. Chem. B* **123**, 10959 (2019).
- [13] A. Nowok, M. Dulski, J. Grelska, A. Z. Szeremeta, K. Jurkiewicz, K. Grzybowska, M. Musiał, and S. Pawlus, Phenyl ring: A steric hindrance or a source of different hydrogen bonding patterns in self-organizing systems? *J. Phys. Chem. Lett.* **12**, 2142 (2021).
- [14] N. Soszka *et al.*, Aromaticity effect on supramolecular aggregation. aromatic vs. cyclic monohydroxy alcohols, *Spectrochim. Acta, Part A* **276**, 121235 (2022).
- [15] J. Grelska, K. Jurkiewicz, A. Burian, and S. Pawlus, Supramolecular structure of phenyl derivatives of butanol isomers, *J. Phys. Chem. B* **126**, 3563 (2022).
- [16] M. J. Abraham, T. Murtola, R. Schulz, S. Páll, J. C. Smith, B. Hess, and E. Lindahl, GROMACS: High performance molecular simulations through multi-level parallelism from laptops to supercomputers, *SoftwareX* **1–2**, 19 (2015).
- [17] S. Páll, M. J. Abraham, C. Kutzner, B. Hess, and E. Lindahl, Tackling exascale software challenges in molecular dynamics simulations with GROMACS, in *Solving Software Challenges for Exascale*, edited by S. Markidis and E. Laure (Springer International Publishing, Cham, 2015), Vol. 8759, pp. 3–27.
- [18] S. Pronk *et al.*, GROMACS 4.5: A high-throughput and highly parallel open source molecular simulation toolkit, *Bioinformatics* **29**, 845 (2013).
- [19] D. A. Case, H. M. Aktulga, K. Belfon, I. Y. Ben-Shalom, S. R. Brozell, D. S. Cerutti, T. E. Cheatham III, G. A. Cisneros, V. W. D. Cruzeiro, T. A. Darden, R. E. Duke, G. Giambasu, M. K. Gilson, H. Gohlke, A. W. Goetz, R. Harris, S. Izadi, S. A. Izmailov, C. Jin, K. Kasavajhala *et al.*, *Amber 2021, AmberTools21* (University of California, San Francisco, 2021).
- [20] J. Wang, R. M. Wolf, J. W. Caldwell, P. A. Kollman, and D. A. Case, Development and testing of a general amber force field, *J. Comput. Chem.* **25**, 1157 (2004).
- [21] M. Brehm and B. Kirchner, TRAVIS - A free analyzer and visualizer for Monte Carlo and molecular dynamics trajectories, *J. Chem. Inf. Model.* **51**, 2007 (2011).
- [22] O. Hollóczy, M. Macchiagodena, H. Weber, M. Thomas, M. Brehm, A. Stark, O. Russina, A. Triolo, and B. Kirchner, Triphasic ionic-liquid mixtures: Fluorinated and non-fluorinated aprotic ionic-liquid mixtures, *ChemPhysChem* **16**, 3325 (2015).
- [23] M. Brehm, M. Thomas, S. Gehrke, and B. Kirchner, TRAVIS—A free analyzer for trajectories from molecular simulation, *J. Chem. Phys.* **152**, 164105 (2020).
- [24] See Supplemental Material at <http://link.aps.org/supplemental/10.1103/PhysRevE.108.024603> for simulated partial atom-atom structure factors; density measurements; infrared spectroscopy measurements; and Kirkwood factors calculated based on dielectric spectroscopy measurements. Supplemental Material also contains Refs. [10,11,15].
- [25] K. Shin-ya, H. Sugeta, S. Shin, Y. Hamada, Y. Katsumoto, and K. Ohno, Absolute configuration and conformation analysis of 1-phenylethanol by matrix-isolation infrared and vibrational circular dichroism spectroscopy combined with density functional theory calculation, *J. Phys. Chem. A* **111**, 8598 (2007).
- [26] Q.-S. Du, Q.-Y. Wang, L.-Q. Du, D. Chen, and R.-B. Huang, Theoretical study on the polar hydrogen- π ($H\pi-\pi$) interactions between protein side chains, *Chem. Cent. J.* **7**, 92 (2013).
- [27] R. Böhmer, C. Gainaru, and R. Richert, Structure and dynamics of monohydroxy alcohols—milestones towards their microscopic understanding, 100 years after Debye, *Phys. Rep.* **545**, 125 (2014).
- [28] C. Janiak, A critical account on $\pi-\pi$ stacking in metal complexes with aromatic nitrogen-containing ligands, *J. Chem. Soc. Dalton Trans.* **21**, 3885 (2000).
- [29] T. F. Headen, Temperature dependent structural changes in liquid benzene studied using neutron diffraction, *Mol. Phys.* **117**, 3329 (2019).

Supplementary Information for

Computer simulations as an effective way to distinguish supramolecular nanostructure in cyclic and phenyl alcohols

Joanna Grelska^{1,*}, Karolina Jurkiewicz^{1,*}, Andrzej Nowok^{2,3}, Sebastian Pawlus¹

¹ A. Chełkowski Institute of Physics, University of Silesia in Katowice, ul. 75 Pułku Piechoty 1, 41-500 Chorzów, Poland

² Department of Experimental Physics, Wrocław University of Science and Technology, Wybrzeże Stanisława Wyspiańskiego 27, 50-370 Wrocław, Poland

³ Laboratoire National des Champs Magnétiques Intenses, UPR 3228, CNRS-UGA-UPS-INSA, Grenoble and Toulouse, France

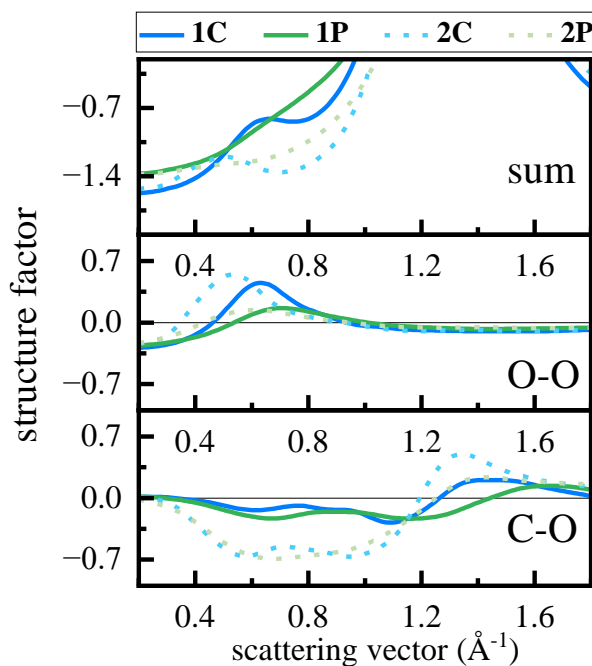
*Correspondence e-mails: joanna.grelska@us.edu.pl, karolina.jurkiewicz@us.edu.pl

1. DIFFRACTON PRE-PEAK FEATURE

The peculiar pre-peak feature was also observed in the diffraction data for some other phenyl alcohols in our previous articles. In [1] we showed that 1-phenyl-1-propanol and 1-phenyl-2-propyn-1-ol display a visible pre-peak unlike their isotopes 3-phenyl-1-propanol and 3-phenyl-2-propyn-1-ol (having three carbon atoms between ring and OH group) exhibiting only one broad diffraction maximum up to $\sim 2 \text{ \AA}^{-1}$. Moreover, various alcohols with the phenyl ring and OH group separated by one carbon atom (1-phenylethanol, 1-phenyl-1-propanol, 1-phenyl-1-butanol, 2-methyl-1-phenyl-1-propanol), considered in the paper [2], demonstrated the appearance of the diffraction pre-peak. In contrast, the X-ray scattering data for phenyl alcohols investigated in [3] with two (2-methyl-1-phenyl-2-propanol), three (2-methyl-3-phenyl-1-propanol, 4-phenyl-2-butanol), or four carbon atoms between hydroxyl group and carbon ring (4-phenyl-1-butanol) were reported with no evidence of a clear pre-peak feature.

Due to the fact that the entire pre-peak in the total structure factor is often the result of partially canceling contributions between the partial structure factors, the interpretation of the pre-peak intensity from the experimental total diffraction data is not trivial. The models obtained herein from computer simulations were used to calculate theoretical values of the partial atom-atom contributions to the total structure factors for the investigated alcohols. The O-O and C-O partial structure factors, depicted in Figure S1, give the highest contribution among all atom-atom functions to the total structure factor in the pre-peak region. Moreover, the O-O correlations, which are referred to the periodicity between H-bonded clusters in real space, are more intense for cyclic alcohols than for their phenyl counterparts. Looking at the C-O structure factor in the same range, an interesting dependence can be seen – it has local minima for 2C and 2P, while 1C and 1P have almost no oscillations in this region. Summing all partial contributions (O-O, C-O and remaining C-C, C-H, H-H and O-H), one can get the shape of the total structure factor with the resultant pre-peak or its lack. The compounds can be

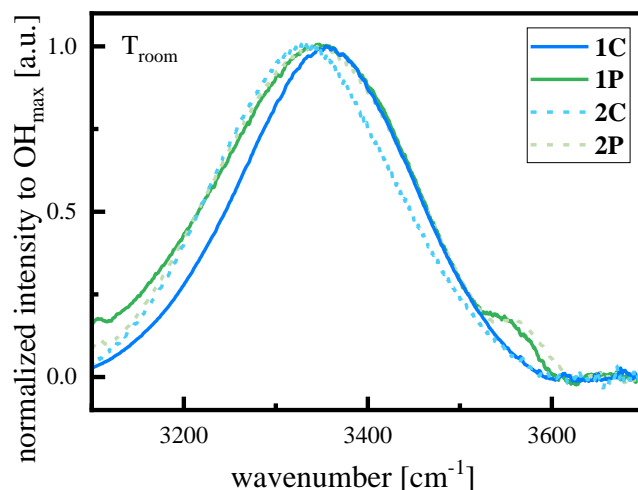
ordered by the falling intensity of the pre-peak in total structure factor: 1C (strong O-O maximum), 2C (strong O-O maximum but C-O minimum), 1P (weak O-O maximum) and 2P (weak O-O maximum and C-O minimum). In 2P, the contributed partial functions cancel each other in the region of the pre-peak and this feature cannot be observed in the total experimental data. A similar situation takes place in the previously investigated phenyl compounds where molecules are characterized by two or more carbon atoms placed between phenyl and OH groups - the negative C-O contribution cancels out the positive O-O bump. As a result, no pre-peak is observed in the experimental structure factor for these compounds.



S1. Total (sum) and selected partial (O-O, C-O) structure factors in the low scattering vector range, calculated based on alcohol's models obtained from molecular dynamics simulations.

2. EXPERIMENTAL INFRARED SPECTRA

FTIR measurements of alcohols 1C, 2C, 1P and 2P were performed at room temperature (298 K) by means of Thermo Scientific IS50 spectrometer equipped with a standard source. In order to maintain sample thickness, a small quantity of each alcohol was placed between CaF₂ glasses spaced 1 μm apart. The spectra were captured in absorbance mode within the range of 400 - 4000 cm^{-1} range. Each spectrum was generated from the accumulation of 16 scans with a spectral resolution of 4 cm^{-1} . Following data acquisition, the baseline was adjusted, and water and carbon dioxide corrections were applied during the post-processing. Data are presented in the Figure S2.



S2. Infrared spectra measured for all four alcohols. Single broad band in the 3100 – 3600 cm^{-1} spectral region is OH stretching band, less-intense band centered above 3550 cm^{-1} is a stretching mode of the OH groups involved in OH- π interactions.

3. EXPERIMENTAL KIRKWOOD FACTOR

In order to calculate the Kirkwood factor for the alcohols in question, we perform density, refractometry and broadband dielectric measurements as a function of temperature.

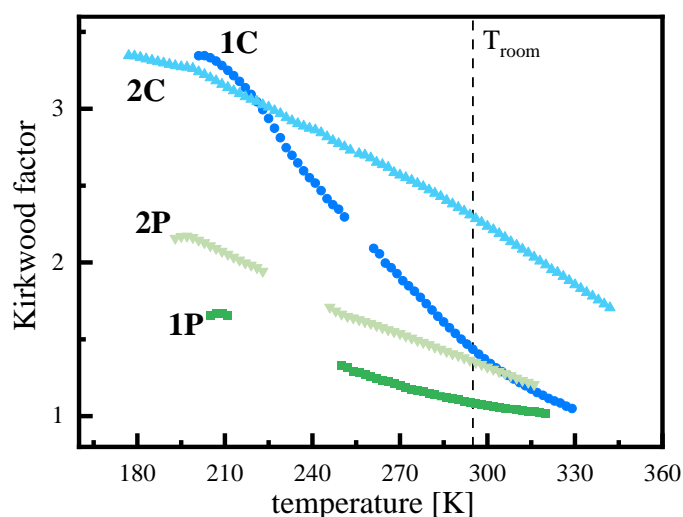
Dielectric studies of alcohols 1C, 2C, 1P and 2P were performed at various temperatures in the frequency range spanning 10^{-1} - 10^9 Hz. A Novocontrol BDS spectrometer equipped with an Alpha Impedance Analyzer was utilized for measurements between 10^{-1} and 10^6 Hz. The capacitor implemented in these measurements consisted of two parallel stainless-steel plates, each with a 10 mm diameter, spaced by two glass fibers of 100 μm thickness and sealed with a Teflon ring. In turn, capacitor featuring two gold-plated electrodes (5 mm in diameter) spaced by 0.06 mm was used for the high-frequency (10^6 - 10^9 Hz) dielectric measurements. In this frequency range, measurements were conducted by means of the Agilent 4291B impedance analyzer connected with the Novocontrol GMBH system. Quasi-static conditions were maintained throughout the studies, with temperature stabilized by nitrogen gas and controlled by Quatro Cryosystem with precision better than 0.2 K. using the Quatro Cryosystem. The temperature was stabilized using Quatro Cryosystem with a precision better than 0.2 K. Measurements of the aforementioned alcohols were conducted only above their glass transition temperature with a step of $\Delta T = 2\text{K}$.

Mettler Toledo refractometer RM40 with a Peltier thermostat was utilized for refractometric studies of 1C, 2C, 1P and 2P in their liquid state. Measurements were conducted between 293 and 353 K with a resolution of 0.0001. During them, temperature was controlled with precision better than 0.1 K. Refractive index n was measured for all samples.

A vibrating-tube densimeter DMA 4500 M (Anton Paar, Austria) was utilized to determine the density (d) of alcohols 1C, 2C and 2P at various temperature conditions. Before measurements, the apparatus was calibrated in accordance with the manufacturer's

recommendations, employing dry air and redistilled water. Furthermore, automatic correction for viscosity-related errors was applied throughout the full range, and this was tested with the oil N100 at 293.15 and 323.15 K. Temperature-dependent measurements of the alcohols mentioned before were conducted at intervals of 10 K in-between 283 - 363 K, with a minimum of two independent values recorded at each temperature. The standard uncertainties associated with ρ and T were $u(\rho) = 0.002 \cdot d$ and $u(T) = 0.01$ K, respectively. Densities at room temperatures were accordingly 0.92 (2C), 0.92 (1C), 1.02 (2P), 1.01 (1P) g/cm³.

Kirkwood factor was defined by the mathematical formula: $g_k = \frac{9k_B \epsilon_0 M T (\epsilon_s - \epsilon_\infty)(2\epsilon_s + \epsilon_\infty)}{N_A \rho \mu^2 \epsilon_s (\epsilon_\infty + 2)^2}$, where k_B is Boltzmann's constant, M - molar mass, ϵ_0 - vacuum permittivity, ϵ_s - static dielectric permittivity, ϵ_∞ - dielectric permittivity at infinite frequencies, N_A - Avogadro number, ρ - density, and μ is molecular dipole moment. For calculations, ϵ_s and ϵ_∞ were taken from dielectric and refractometry measurements ($\epsilon_\infty = n^2$), respectively. Data of calculated Kirkwood factor are shown in the Figure S3.



S3. Experimental Kirkwood factor calculated for all four alcohols with marked room temperature.

References

- [1] A. Nowok, M. Dulski, K. Jurkiewicz, J. Grelska, A. Z. Szeremeta, K. Grzybowska, and S. Pawlus, *Molecular Stiffness and Aromatic Ring Position – Crucial Structural Factors in the Self-Assembly Processes of Phenyl Alcohols*, *J. Mol. Liq.* **335**, 116426 (2021).
- [2] A. Nowok, K. Jurkiewicz, M. Dulski, H. Hellwig, J. G. Małcki, K. Grzybowska, J. Grelska, and S. Pawlus, *Influence of Molecular Geometry on the Formation, Architecture and Dynamics of H-Bonded Supramolecular Associates in 1-Phenyl Alcohols*, *J. Mol. Liq.* **326**, 115349 (2021).
- [3] J. Grelska, K. Jurkiewicz, A. Burian, and S. Pawlus, *Supramolecular Structure of Phenyl Derivatives of Butanol Isomers*, *J. Phys. Chem. B* **126**, 3563 (2022).

C. P3. Comment on “Universal features in the lifetime distribution of clusters in hydrogen-bonding liquids” by I. Jukić, M. Požar, B. Lovrinčević and A. Perera, *Phys. Chem. Chem. Phys.*, 2021, 23, 19537

Grelska, J. (2024). *Physical Chemistry Chemical Physics*, 26(6), 5713-5716.

DOI:10.1039/D3CP05269A

Punkty MNiSW (2024): 100

Impact Factor (2023): 3.3

Mój wkład w publikację polegał na wykonaniu symulacji dynamiki molekularnej, analizie wyników i przygotowaniu artykułu.

COMMENT



Cite this: *Phys. Chem. Chem. Phys.*,
2024, 26, 5713

Received 30th October 2023,
Accepted 18th January 2024

DOI: 10.1039/d3cp05269a

rsc.li/pccp

Comment on “Universal features in the lifetime distribution of clusters in hydrogen-bonding liquids” by I. Jukić, M. Požar, B. Lovrinčević and A. Perera, *Phys. Chem. Chem. Phys.*, 2021, 23, 19537

Joanna Grelska 

In the article published by Jukić *et al.* [I. Jukić *et al.*, *Phys. Chem. Chem. Phys.*, 2021, **23**, 19537], the authors discovered a specific lifetime distribution of hydrogen bonds in some pure hydrogen-bonding liquids. The distribution derived by computer simulations in the range of 0–0.15 ps consists of three characteristic peaks. They call the first maximum the ‘dimer peak’, the second the ‘cluster peak’, and the third the ‘topology peak’. In the article in question, mostly linear- and circular-cluster-forming mono-ols were simulated to show that the third peak is universal in these H-bonding substances. Moreover, the topology of the clusters, which was wrongly assumed to be detected in the tertiary lifetime peak, is instead seen in the distribution of the first maximum.

The hydrogen bonding mechanism is found in many essential substances that compose living organisms. Hence, it is of primary importance to characterize all the features of the hydrogen-bonding process in detail. In ref. 1, the authors presented a previously unknown feature of the lifetime distribution of hydrogen bonds in the picosecond range calculated *via* computer simulations. The specific distribution was assigned to molecular H-bonded dimers located both within and outside the clusters. The authors examined various hydrogen-bonded systems, namely, monohydroxy alcohols and water, and obtained universal hydrogen-bond lifetime maxima, which are summarized in Fig. 1.

The presented distribution plot (Fig. 1) was obtained with a fixed angle restriction ($\text{O-H-O} < 30^\circ$) and changing hydrogen-bonding distances. The authors in ref. 1 described the first maximum seen at the H-bond distance cutoff of 2.5 Å as the ‘dimer peak’. The ‘dimer peak’ at short distances reflects short-lived, tightly hydrogen-bonded dimers with a high probability of occurrence, and at larger cutoff distances (3.5 Å), it shows dimers that live longer but are less probable.

However, at a cutoff of around 2.9 Å, the authors of ref. 1 note the appearance of two additional peaks, which have stable positions up to the cutoff distance of 3.5 Å. They called the second peak at 0.02 ps the ‘cluster peak’ originating from dimers involved in clusters (larger hydrogen-bonded structures), and the third peak at 0.05 ps the ‘topology peak’ originating from the topology of these clusters.

The conclusions of the discussed article are also employed in another article by the same authors² concerning water–alcohol mixtures. There, the authors also indicate that the tertiary peak corresponds to the topology of clusters, whether these are chain, loop or lasso clusters found in mono-ols.

The present work aims to verify the origin of the tertiary peak through investigation of mono-ols that form either mainly linear (chain-like) or circular (loop) clusters. First, in order to verify the accuracy of the methodology, the lifetime distribution of 1-propanol was calculated and compared with the authors’ result in ref. 1. Similarly, computer simulations were carried

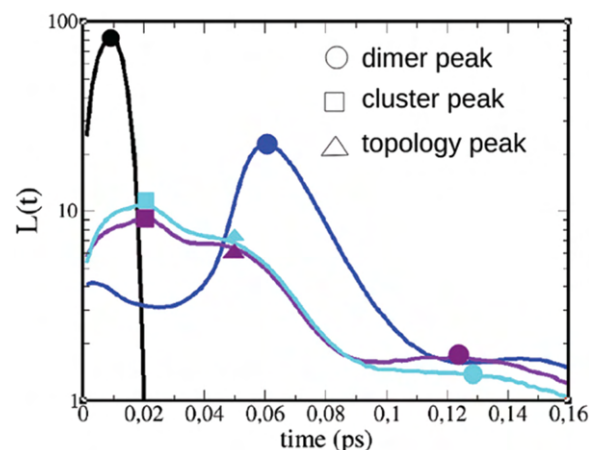


Fig. 1 Reproduced from ref. 1 with permission from the PCCP Owner Societies. Illustration summarizing the correspondence between H-bond lifetime characteristic peaks.

A. Chelkowski Institute of Physics, University of Silesia in Katowice, 75 Pulku
Piechoty 1, 41-500 Chorzów, Poland. E-mail: joanna.grelska@us.edu.pl

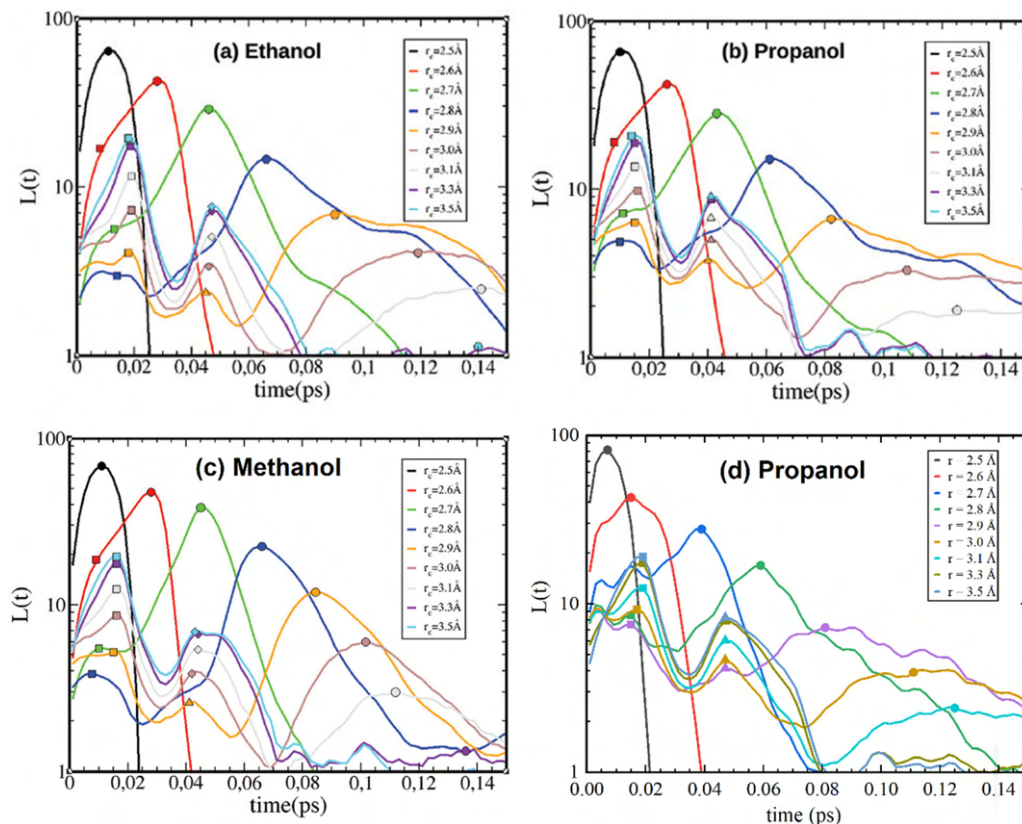


Fig. 2 Reproduced from ref. 1 with permission from the PCCP Owner Societies. H-bond lifetime distribution for OPLS ethanol (a), propanol (b), and methanol (c), with reference to H-bonding distances. Lifetime distribution of GAFF propanol calculated in this paper (d).

out in the GROMACS package^{3–5} with a time step 0.002 ps of a production run of 300 ps. The systems were simulated in NVT ensembles with a known density at room conditions, and a production run of 2 ns was used. Topology files were created using the Antechamber module (AmberTool21),⁶ and the GAFF force field was applied.⁷ The program *gmxhbond* with the *-life* option (within the GROMACS package) was used for the calculation of H-bond lifetime distributions. The obtained results (Fig. 2d) were satisfyingly consistent with the results for propanol (Fig. 2b) from ref. 1.

Therefore, the described methodology was used for the investigation of linear- and globular-cluster-forming mono-ols. Namely, *n*-butanol, which was previously reported to have mainly linear clusters, and its isomer, *tert*-butanol, with predominantly circular-like clusters,⁸ are presented in Fig. 3c and a. Additionally, 2-ethyl-1-hexanol, which forms mostly linear clusters, and 2-methyl-3-hexanol,⁹ which forms mostly globular clusters, were calculated (Fig. 3d and b). At first glance, one can notice that the positions and shapes of the secondary and tertiary peaks are the same as those reported for mono-ols in ref. 1 and do not change within different cluster-forming substances. However, presenting data over a wider range, up to 0.2 ps, helps one to notice another relationship. One can see that small peaks (oscillations) appear in the range 0.08–0.2 ps, but they were not further discussed, as the authors of ref. 1 assigned them to the impact of alkyl tails surrounding the OH

groups, which do not significantly vary among the various probed mono-ols.

What is worth noting is that the first peak with increasing distance cutoff (around 3 Å) moves toward the shorter time distribution for *n*-butanol and 2-ethyl-1-hexanol compared to *tert*-butanol and 2-methyl-3-hexanol. *tert*-Butanol and 2-methyl-3-hexanol, which have predominantly circular clusters in the systems, exhibit longer time distributions for the first lifetime maximum. This leads to a simple conclusion: dimers in circular clusters live longer than in linear ones, and this feature is seen in the first ‘dimer peak’.

Moreover, this relation can also be noticed in ref. 1. Although it was reported that molecular aggregates in liquid methanol, ethanol, and propanol can take different shapes, from cyclic to branched structures,¹⁰ in the Supporting Information of ref. 1, one can see the cluster size distribution and the indication that ethanol is more likely than methanol to create cyclic clusters that consist of around five molecules. That observation results in the mentioned position of the first peak – at a cutoff distance 3 Å, it moves toward longer lifetimes for ethanol in comparison to methanol (see Fig. 2a and c).

To sum up, it was simply shown that the tertiary peak, called the ‘topology peak’ in the H-bond lifetime distribution in ref. 1, does not depend on the type of clusters formed in the mono-ols. On the contrary, it is universal in mono-ols, but the other feature related to the first maximum, the ‘dimer peak’ in ref. 1,

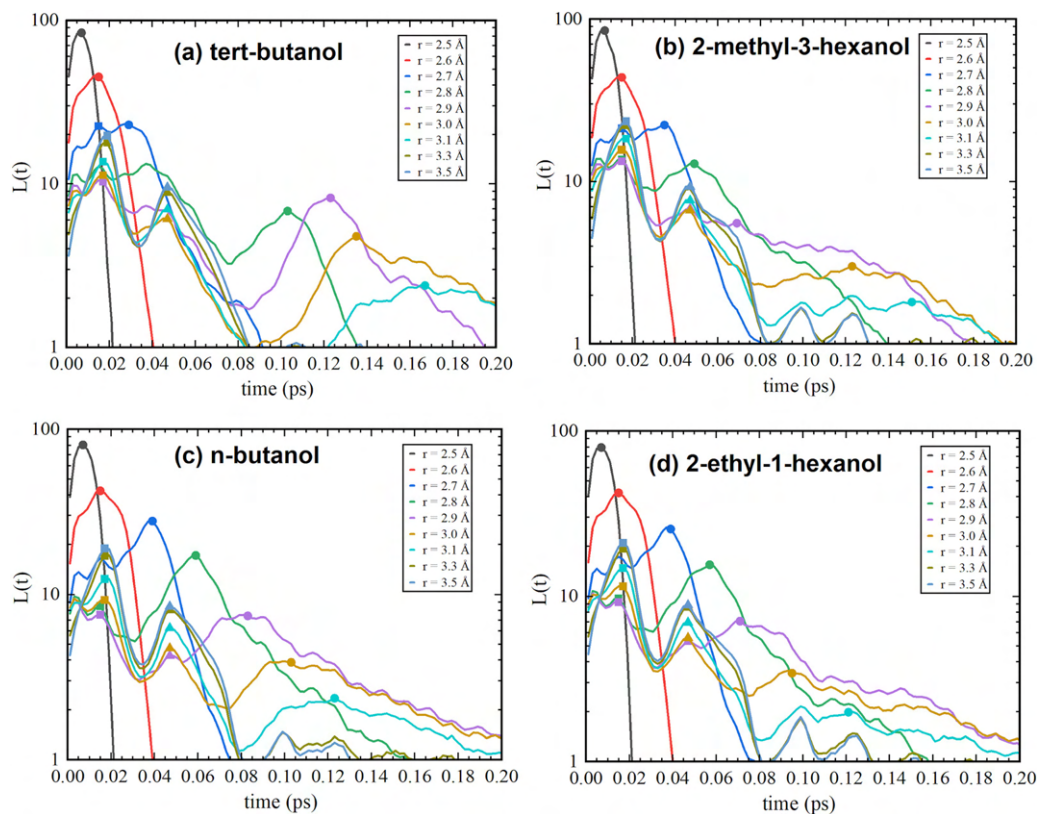


Fig. 3 H-bond lifetime distributions determined in the present work of *tert*-butanol (a), 2-methyl-3-hexanol (b), *n*-butanol (c), and 2-ethyl-1-hexanol (d).

was noted to depend on the cluster shape – dimers in the circular-cluster-forming substances tend to live longer than in linear ones. Therefore, there is doubt as to whether the description of the lifetime distribution peaks used in ref. 1 is correct.

Conflicts of interest

There are no conflicts to declare.

Acknowledgements

The author acknowledges the support from the National Science Center, Poland (grant no. UMO-2019/35/B/ST3/02670) and computational time at PL-Grid, Poland (grant no. PLG/2022/015982).

References

- I. Jukić, M. Požar, B. Lovrinčević and A. Perera, Universal Features in the Lifetime Distribution of Clusters in Hydrogen-Bonding Liquids, *Phys. Chem. Chem. Phys.*, 2021, **23**, 19537.
- I. Jukić, M. Požar, B. Lovrinčević and A. Perera, Lifetime Distribution of Clusters in Binary Mixtures Involving Hydrogen Bonding Liquids, *Sci. Rep.*, 2022, **12**, 9120.
- M. J. Abraham, T. Murtola, R. Schulz, S. Páll, J. C. Smith, B. Hess and E. Lindahl, GROMACS: High Performance Molecular Simulations through Multi-Level Parallelism from Laptops to Supercomputers, *SoftwareX*, 2015, **1–2**, 19.
- S. Páll, M. J. Abraham, C. Kutzner, B. Hess and E. Lindahl, Tackling Exascale Software Challenges in Molecular Dynamics Simulations with GROMACS, in *Solving Software Challenges for Exascale*, ed. S. Markidis and E. Laure, Springer International Publishing, Cham, 2015, vol. 8759, pp. 3–27.
- S. Pronk, *et al.*, GROMACS 4.5: A High-Throughput and Highly Parallel Open Source Molecular Simulation Toolkit, *Bioinformatics*, 2013, **29**, 845.
- D. A. Case, H. M. Aktulga, K. Belfon, I. Y. Ben-Shalom, S. R. Brozell, D. S. Cerutti, T. E. Cheatham III, G. A. Cisneros, V. W. D. Cruzeiro, T. A. Darden, R. E. Duke, G. Giambasu, M. K. Gilson, H. Gohlke, A. W. Goetz, R. Harris, S. Izadi, S. A. Izmailov, C. Jin, K. Kasavajhala, M. C. Kaymak, E. King, A. Kovalenko, T. Kurtzman, T. S. Lee, S. LeGrand, P. Li, C. Lin, J. Liu, T. Luchko, R. Luo, M. Machado, V. Man, M. Manathunga, K. M. Merz, Y. Miao, O. Mikhailovskii, G. Monard, H. Nguyen, K. A. O'Hearn, A. Onufriev, F. Pan, S. Pantano, R. Qi, A. Rahnamoun, D. R. Roe, A. Roitberg, C. Sagui, S. Schott-Verdugo, J. Shen, C. L. Simmerling, N. R. Skrynnikov, J. Smith, J. Swails, R. C. Walker, J. Wang, H. Wei, R. M. Wolf, X. Wu, Y. Xue, D. M. York, S. Zhao and P. A. Kollman, *Amber 2021, AmberTools21*, University of California, San Francisco, 2021.
- J. Wang, R. M. Wolf, J. W. Caldwell, P. A. Kollman and D. A. Case, Development and Testing of a General Amber Force Field, *J. Comput. Chem.*, 2004, **25**, 1157.

- 8 J. Grelska, K. Jurkiewicz, A. Burian and S. Pawlus, Supramolecular Structure of Phenyl Derivatives of Butanol Isomers, *J. Phys. Chem. B*, 2022, **126**, 3563.
- 9 M. Wikarek, S. Pawlus, S. N. Tripathy, A. Szulc and M. Paluch, How Different Molecular Architectures Influence the Dynamics of H-Bonded Structures in Glass-Forming Monohydroxy Alcohols, *J. Phys. Chem. B*, 2016, **120**, 5744.
- 10 A. Vrhovšek, O. Gereben, A. Jamnik and L. Pusztai, Hydrogen Bonding and Molecular Aggregates in Liquid Methanol, Ethanol, and 1-Propanol, *J. Phys. Chem. B*, 2011, **115**, 13473.

D. P4. High-Pressure and Temperature Effects on the Clustering Ability of Monohydroxy Alcohols

Grelska, J., Temleitner, L., Park, C., Jurkiewicz, K., & Pawlus, S. (2024). *The Journal of Physical Chemistry Letters*, 15, 3118-3126. DOI:10.1021/acs.jpcllett.4c00085

Punkty MNiSW (2024): 200

Impact Factor (2023): 5.7

Mój wkład w publikację polegał na wykonaniu pomiarów dyfrakcji rentgenowskiej w warunkach zmiennej temperatury, oraz pod ciśnieniem, wykonaniu symulacji dynamiki molekularnej, współpracy przy tworzeniu programu komputerowego, analizie wyników i ich dyskusji oraz przygotowaniu artykułu.

High-Pressure and Temperature Effects on the Clustering Ability of Monohydroxy Alcohols

Joanna Grelska,* Łászló Temleitner, Changyong Park, Karolina Jurkiewicz,* and Sebastian Pawlus

 Cite This: *J. Phys. Chem. Lett.* 2024, 15, 3118–3126

 Read Online

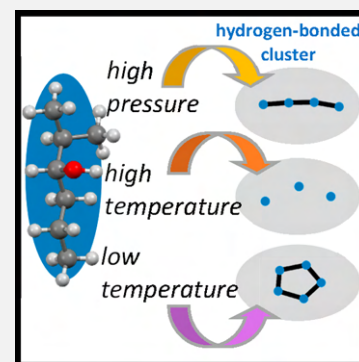
ACCESS |

 Metrics & More

 Article Recommendations

 Supporting Information

ABSTRACT: This study examined the clustering behavior of monohydroxy alcohols, where hydrogen-bonded clusters of up to a hundred molecules on the nanoscale can form. By performing X-ray diffraction experiments at different temperatures and under high pressure, we investigated how these conditions affect the ability of alcohols to form clusters. The pioneering high-pressure experiment performed on liquid alcohols contributes to the emerging knowledge in this field. Implementation of molecular dynamics simulations yielded excellent agreement with the experimental results, enabling the analysis of theoretical models. Here we show that at the same global density achieved either by alteration of pressure or temperature, the local aggregation of molecules at the nanoscale may significantly differ. Surprisingly, high pressure not only promotes the formation of hydrogen-bonded clusters but also induces the serious reorganization of molecules. This research represents a milestone in understanding association under extreme thermodynamic conditions in other hydrogen bonding systems such as water.



Monohydroxy alcohols gained a lot of interest in recent years as these simple chemical compounds are a benchmark for studying the most important substance for humans—water. Alcohols, unlike water, usually do not crystallize but vitrify when supercooled and can exist in the liquid state over a wide range of thermodynamic conditions, making them perfect candidates for investigating the behaviors of hydrogen bonds. They can create supramolecular clusters in size starting of a few to even a hundred molecules linked together.^{1,2} The variation of temperature and pressure influence on the alcohol's clustering constitutes an analogy for the behavior of water inside and on the Earth.^{3,4} However, the thermodynamic stability of such superstructures has yet to be uncovered.

High-pressure diffraction experiments have been a challenge which along with the development of synchrotron facilities and pressure compression systems became possible to realize for solid^{5–9} and liquid samples.^{10–14} Yet, the high-pressure X-ray diffraction measurements of weakly scattering liquids such as alcohols still remain difficult. On the other hand, the advance of molecular dynamics simulations enables to complement experimental data and also provides additional structural properties unachievable from experiments.^{4,15–17} The combination of both simulation and experimental methods is the most effective to reveal new information about the structure of the liquid phase of various hydrogen-bonded systems. Nevertheless, the behavior of molecular clusters in liquid systems under high pressure has not been studied so far. It is unknown whether high pressure favors the formation of H-bonded clusters or causes their breaking. It is also questioned whether pressure-induced changes in the structure resemble to

some extent temperature-involved alteration. These questions still need to be addressed.

Herein, we probed the evolution of the supramolecular structure at the nanoscale of two model alcohols in the pressure range of 0.1–3 GPa and temperature range of 163–413 K. The studied 2-ethyl-1-hexanol (2E1H) with the chemical formula $C_8H_{18}O$ and 2-methyl-3-hexanol (2M3H) with the formula $C_7H_{16}O$ are simple monohydroxy alcohols (see Figure 1). In previous studies,¹⁸ it was suggested that 2E1H having the OH group located at the terminal position is more likely to create chain-like clusters of H-bonds. In contrast, 2M3H with the nonterminal position of the OH group tends to cluster also in ring-like aggregates¹⁹ (see Figure 1 for cluster type visualization). In this Letter, we aim to examine how changes of thermodynamic conditions modulate the supramolecular self-assembly of 2E1H and 2M3H. We present good-quality high-pressure diffraction results and compare them with outcomes of the molecular dynamics simulations (see details in the Supporting Information). The results reveal so far an unknown picture of the H bond organization at extreme conditions.

The structural factors calculated from the diffraction data for 2E1H and 2M3H are presented in Figure 2. The results show two universal features: the less intense prepeak at the scattering

Received: January 9, 2024

Revised: February 20, 2024

Accepted: February 22, 2024

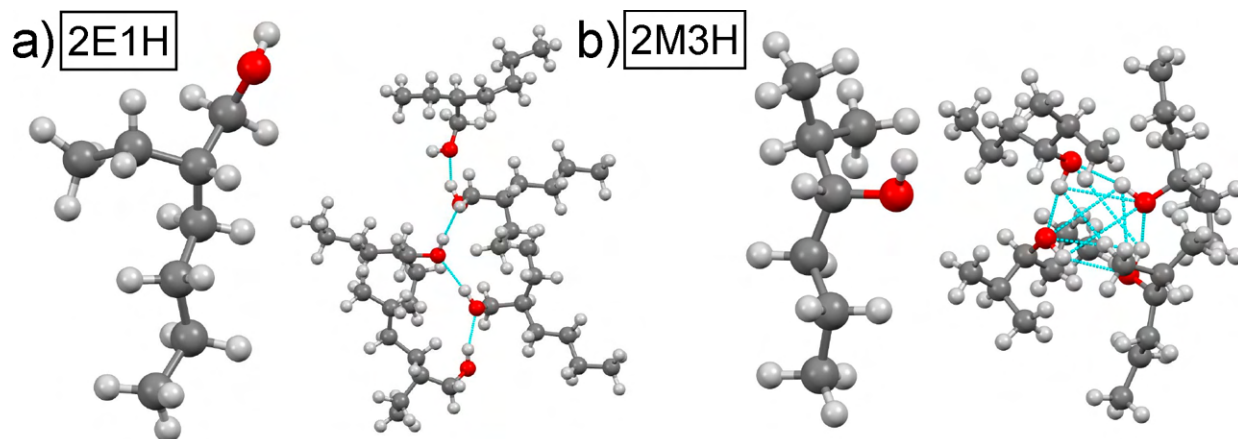


Figure 1. Structure of investigated molecules and typical supramolecular clusters formed in the systems (a) 2-ethyl-1-hexanol and linear cluster and (b) 2-methyl-3-hexanol and ring cluster. The clusters with hydrogen bonds marked in cyan were derived from models optimized by molecular dynamics simulations.

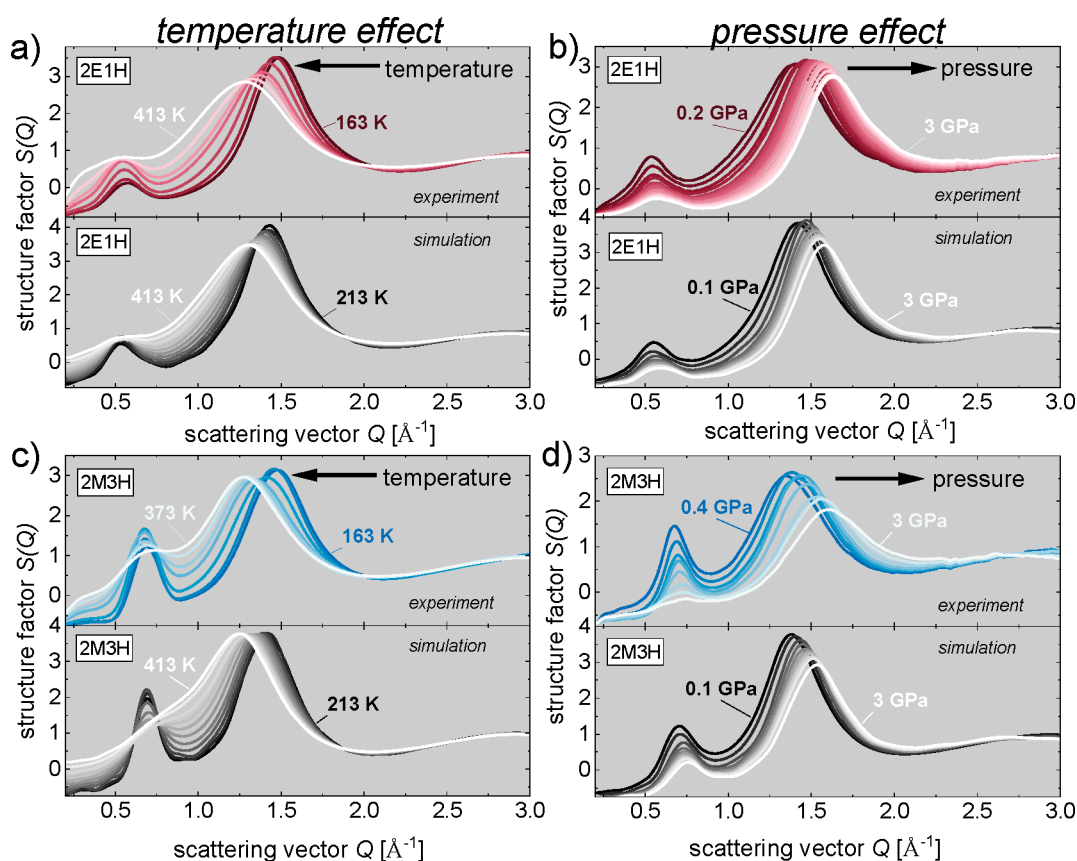


Figure 2. Structure factors calculated from experimental and simulation results obtained at ambient pressure and changing temperature for (a) 2E1H and (c) 2M3H and at ambient temperature and changing pressure for (b) 2E1H and (d) 2M3H.

vector position around 0.5 \AA^{-1} and the main peak at around 1.5 \AA^{-1} . Fourier transform of these positions to the real space gives the average correlation distance of 12.5 and 4.2 Å between the H-bonded clusters and the nearest-neighboring molecules, respectively.^{20,21} The prepeak is a consequence of scattering on the centers of OH groups separated by the carbon parts of molecules. The strong hydrogen-bonding interaction allows the OH groups to organize in ordered structures. Interestingly, in water, the OH network is isotropic, and no prepeak feature is visible.²² One can notice that temperature and pressure changes have a big impact on the

position of the main peak, but the prepeak position practically remains stable. This is because the average repeating distance between OH groups associated in clusters is more or less preserved despite the possible changes in the size and architecture of clusters with the temperature and pressure. In turn, the neighboring molecules come closer to each other due to mobile alkyl tails with both high pressure and low temperature, which is the expected density effect.

However, taking into consideration the intensities and widths of diffraction peaks, we recognize distinct effects of pressure and temperature. Namely, lowering temperature

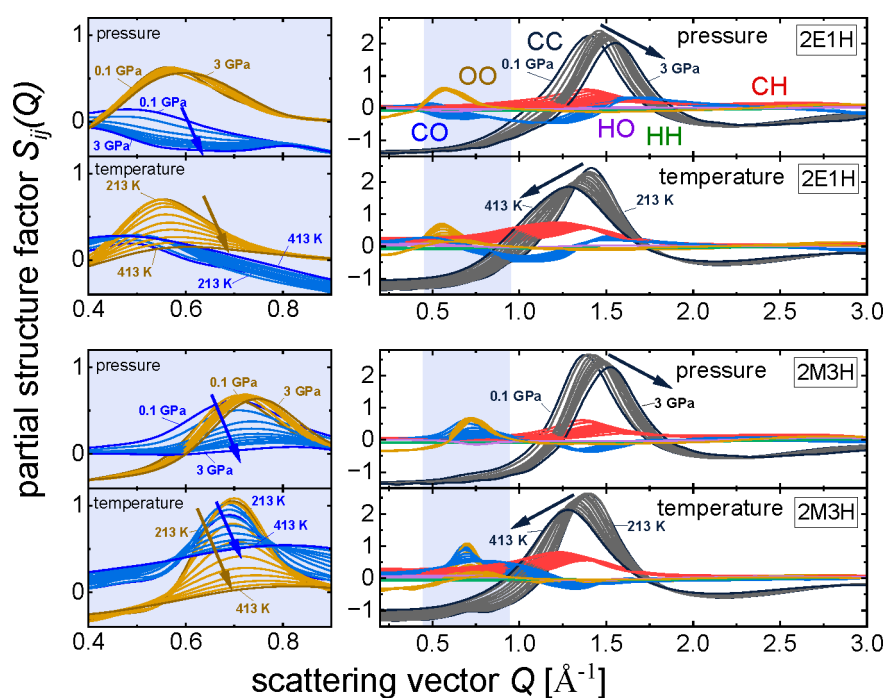


Figure 3. Partial structure factors of investigated alcohols (2E1H: upper panel; 2M3H: lower panel) as functions of pressure and temperature obtained by molecular dynamics simulations. Individual functions are marked with symbol of the same color. The arrows indicate the direction of the shifts of selected partial functions along with pressure or temperature increase. Pressure results are presented for 0.1 GPa, the range 0.25–2 GPa (with a 0.25 GPa step), and 3 GPa; temperature results are presented in the range 213–413 K (with a 20 K step).

causes clear sharpening and an increase in amplitude of both peaks, whereas under high temperature they are seriously broadened and damped. The effect of the increasing background with growing temperature at the low scattering vector range, giving an impression of an apparent increase in the prepeak's intensity, has already been observed²³ and explained by changes in the compressibility.²⁴ With increasing pressure, the diffraction peaks gradually decrease and become wider. In real space, the lower and broader diffraction peak can be interpreted as damping of the intermolecular order. Although, based on this, one may intuitively hypothesize that high pressure induces a destructive effect on the intermolecular structure, such a straightforward interpretation may be incorrect. Recent molecular dynamics simulations have shown that a simplified analysis of only the total diffraction intensities obtained in experiments may lead to wrong conclusions.^{22,23,25} In fact, the total structure factor consists of partial atomic functions, which describe the correlations between specific atom types and can be easily derived from a theoretical molecular model. Therefore, given the very good compliance between the experimental and simulation results presented in Figure 2, we further analyze the partial functions derived from optimized theoretical models.

Partial structure factors obtained from the molecular dynamics simulations for 2E1H and 2M3H are listed in Figure 3. They contain structural correlations of all atom cross and like pairs; for example, HH is a like function of all hydrogen atoms in the systems, and CO is a cross-function of oxygens and carbons. The sum of all six partial functions gives the total structure factors shown in Figure 2. One can see that the major contribution to the total structure factor comes from the CC function as carbon has the highest concentration and scattering power in the systems. The prepeak region in Figure 3 is highlighted in light purple. It can be seen that the major

contribution to the prepeak is provided by the OO correlations that are additionally enclosed in the inset on the left. At first glance the prominent temperature effect can be seen; rising temperature dramatically dampens the OO partial structure factor that explains the prepeak's suppression in the total structure factor. Because the OO correlations arise as a result of structuring of O atoms in clusters by H bonds, such damping of the OO peak naturally indicates destroying of this structure. Additionally, due to rise of temperature, the OO peak position slightly shifts toward higher scattering vectors (smaller intercluster distances), which is opposite to the expected thermal expansion effect. The explanation of this observation can be better spatial packing of the formed smaller clusters. One of the most intriguing observations is that increasing pressure has almost no effect on the magnitude of the OO peak. Thus, the evident suppression of the prepeak's amplitude at higher pressure in the total structure factors of both alcohols (Figure 2) cannot be explained based on the changes in the structuring of O atoms in H-bonded clusters. This distinguishes the effect of the pressure on the H-bonded clustering of monohydroxy alcohols from that of the temperature.

The next strong contribution to the prepeak region comes from the CO function. It has a noticeably higher amplitude for 2M3H which was thought to create mostly circular type clusters. It is in line with our previous studies^{1,26} where we concluded that high intensity of CO partial function in prepeak region is connected with creating such a ring-like structure in the system. What we notice from Figure 3 is a drop in the CO function along with rising pressure for both alcohols. That behavior explains the damping of the prepeak's intensity in total structure factor with rising pressure presented in Figure 2. A substantial change of the CO function can be noticed also with rising temperature for 2M3H. Summarizing the effects

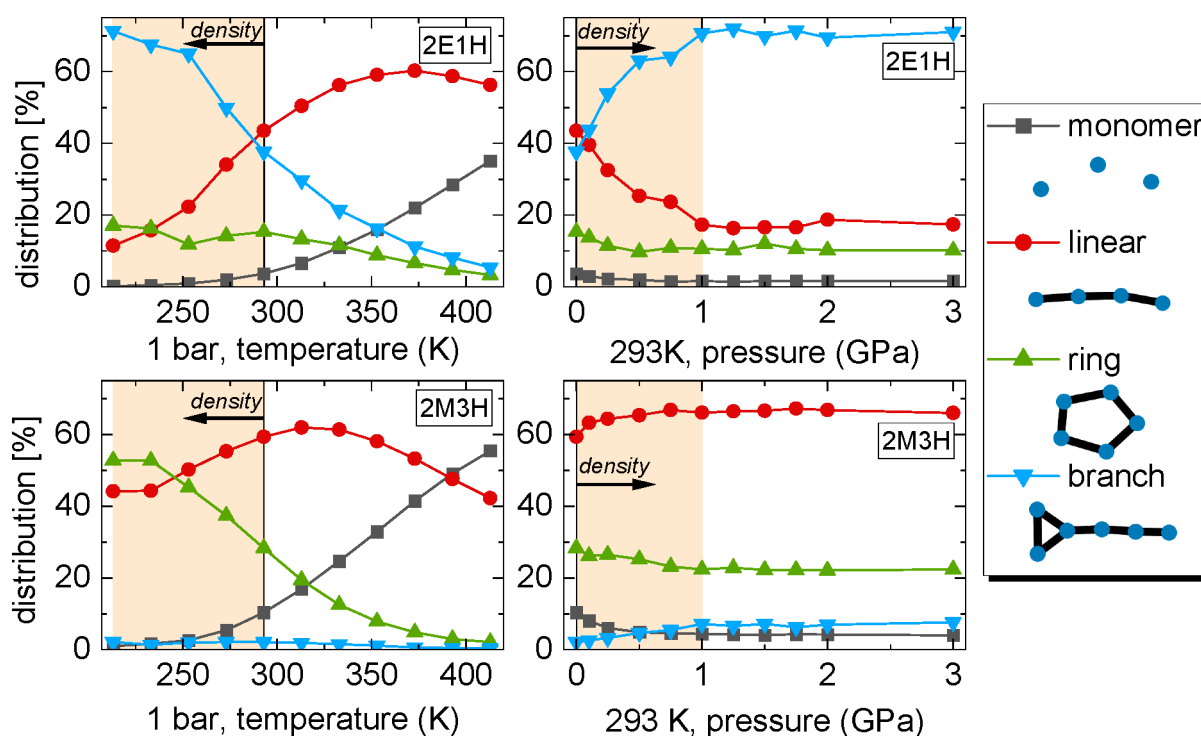


Figure 4. Distributions of monomers and H-bonded clusters as functions of temperature and pressure for the investigated systems derived from simulations. The common areas of density are marked in the same light orange color. The same state at ambient conditions is marked with vertical black line. The direction of the density increase is illustrated with arrow. The legend on the right presents schemes of the studied cluster types.

temperature and pressure on the longer-range atomic correlations resulting in the prepeak feature, we can state that the biggest changes with temperature occur in the organization between OO atoms, while with pressure, between CO atoms.

Another important representation of the molecular order obtained from simulations was partial radial distribution functions (see the section Partial Radial Distribution Functions and Figure S1 in the Supporting Information). From these functions we observed the effect of strengthening H bonds with higher pressure or lower temperature and weakening of H bonds with higher temperature. That conclusion was also drawn by experimental methods probing hydrogen bonds.

In the next approach, we tested how the density factor influences the molecular clustering. The macroscopic density of the alcohols at various thermodynamic conditions was estimated based on experimental main peak positions and also calculated from molecular dynamics simulations (see the section Density Approximation in the Supporting Information). From Figure S2, one can see some common density states for each alcohol, which can be achieved by both temperature and pressure changes but also low-density states that can be achieved only at high-temperature and high-density states achievable only by strong compression. Additionally, we reported a lower density of 2E1H glass probed at the T_g (for $p = 1$ bar) than at the p_g (for $T = 298, 323, 348,$ and 373 K): ~ 1.07 and ~ 1.37 g/cm³, respectively. From the structural models presented later in the paper, it will be clear that it is possible to obtain countless numbers of glasses with different frozen H-bonded structures by controlling thermodynamic conditions.

In order to obtain a whole picture of the self-association of molecules in 2E1H and 2M3H alcohols under the entire range of pressure and temperature conditions, we analyzed the H-

bonded clusters based on the optimized simulation models. The clusters that we define are averaged over the simulation ensemble and simulation time of 10–50 ns, which is much longer than the lifetime of hydrogen bonds, around 0.02–0.15 ps.²⁷ Thus, the determined sizes and architectures represent statistically time-averaged stable H-bonded clusters. The average models from the molecular dynamics simulations remained close to their respective reference structures probed by the diffraction experiment at certain thermodynamic conditions. A distinction for three considered cluster types (linear, ring, and branch) is described in detail in the Supporting Information. An example of each cluster type is depicted in the legend in the right panel of Figure 4. The left panels of Figure 4 show the distributions of the different cluster types under various thermodynamic conditions. The numbers of molecules bonded into all cluster types along with monomers sum to 100%. These distributions present interesting properties which are summarized in a few points below.

- (1) The monomer's number greatly increases for both alcohols with temperature rise at ambient pressure. In contrast, as the pressure increases up to around 0.5 GPa at room temperature, the numbers of monomers drop almost to zero. For both temperature and pressure changes, starting from the same point at ambient conditions, the number of monomers decreases as the density increases.
- (2) Branch structures are abundant in 2E1H and become more dominant with density increase and less probable at higher temperature. It means that strong thermal vibrations at high temperatures significantly reduce the chances for double H bonds per molecule. For 2M3H, on the other hand, branched structures are almost

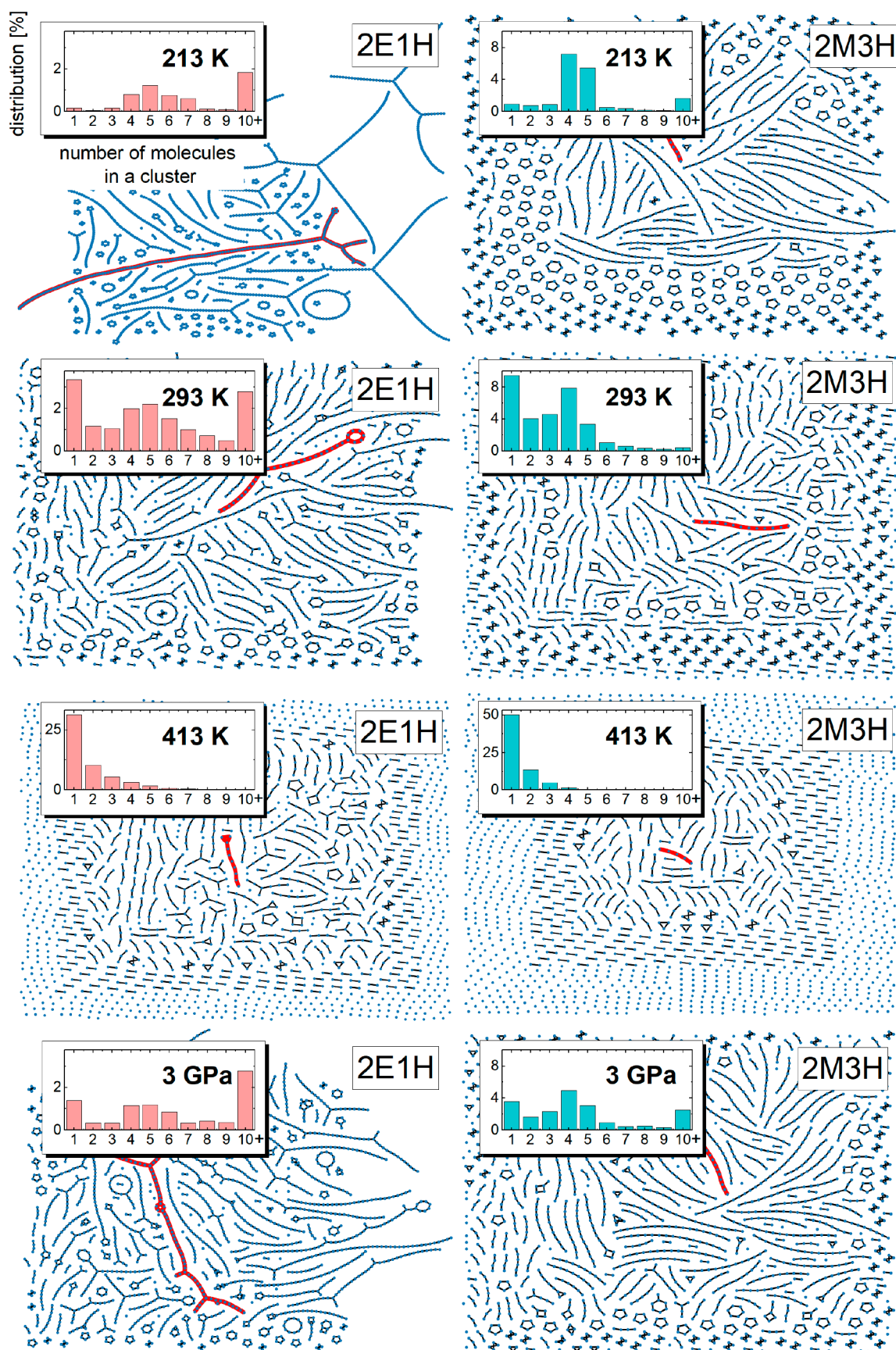


Figure 5. Visualization of lone and bonded hydroxyl groups derived from one configuration of simulation trajectory for 2E1H and 2M3H. The spatial organization of these is arbitrary and presents only cluster architecture at chosen conditions. The cluster colored in red is the largest one in the configuration. The insets show the histograms of the number of molecules in a cluster. For clarity, the 10+ in histograms indicate the added values for percentages from 10 to the highest values.

nonexistent. The OH group in the nonterminal position in the 2M3H molecule apparently hinders the formation of branched double H bonds.

- (3) Ring clusters constitute about half of the 2M3H system at low temperatures approaching the T_g at ambient pressure. They become less abundant with rise of both temperature and pressure. A similar situation is observed for 2E1H, but the ring clusters do not constitute a large percentage there. Indeed, the nonterminal position of the OH group in the 2M3H molecule clearly favors the creation of ring clusters by H bonds, as was reported previously.
- (4) Linear chain clusters are found in large percentages in both alcohol systems. The temperature dependence of the number of linear clusters has a maximum of 60% at about 370 K for 2E1H and 320 K for 2M3H at ambient pressure. Linear clusters are the most resistant to high temperature. At higher pressure, the number of linear clusters decreases for 2E1H at the expense of branch clusters that start to dominate. On the other hand, the linear structures increase for 2M3H at the expense of monomers, and ring population.

Generally, the characteristics of supramolecular clustering are different between 2E1H and 2M3H in the regions of the same density marked in light orange in Figure 4. In the case of 2E1H the increase of density either with low temperature or high pressure seems to have a similar effect on the distribution of the most abundant types of clusters: the number of linear clusters decreases while branch clusters increases with both lowering temperature and increasing pressure. In turn, for 2M3H, one can observe another behavior: the number of ring clusters increases with lowering temperature but decreases with pressure rise. Furthermore, the number of linear associates changes nonmonotonically with lowering temperature: it first increases down to ~ 300 K and then decreases, whereas it monotonically increases with higher pressure.

Particularly interesting is the effect of high pressure on ring clusters, when they clearly reorganize in favor of branched or linear structures because the number of monomers is almost zero at such conditions. It is worth noting that dielectric studies conducted under high pressure derived similar conclusions. The motion of hydrogen-bonded structures in monohydroxy alcohols is manifested by an exponential relaxation process in the dielectric spectra—commonly termed the Debye relaxation, which is slower than the structural relaxation (α) process associated with the collective rearrangement of molecules. A good description of the origin of the Debye relaxation is the transient chain model.^{28,29} Adopting this model, generally observed weaker temperature and pressure dependencies of the Debye relaxation time compared to the α -relaxation time near T_g of monohydroxy alcohols were explained.³⁰ Interestingly, here we found a similar behavior of the position of the diffraction prepeak—weaker response to the temperature and pressure—and the main peak, which experiences much stronger shifts. Therefore, it can be stated that a correlation between the two relaxation processes and two diffraction maxima occurs. The amplitude of the Debye relaxation process, which is known to rise with the proportion of chain-like clusters, was observed to increase with higher pressure for 2M3H and to decrease for 2E1H.^{18,19,31} Therefore, based on the above, one can simply deduce that in 2M3H some ring clusters break and become linear clusters,

while in 2E1H the linear cluster's numbers decrease in favor of branched clusters. Moreover, the destruction of ring clusters in favor of linear ones for monohydroxy alcohols was suggested by dielectric spectroscopy studies also under other external conditions such as electric field^{32,33} or mechanical shearing.³⁴ This effect was more prominent in alcohols with the nonterminal position of the OH group, and so for the alcohols with an advantage of ring clusters over other architectures, it is in line with the results presented here. We can therefore conclude that nondirect information about the H-bonded clustering derived from dielectric spectroscopy is in great agreement with direct insight into the structure by molecular dynamics simulations.

Another peculiarity worthy of attention can be noticed in the temperature dependence of the cluster distributions in Figure 4. One can recognize an anomaly point in the distributions of the cluster types at about 250 K for 2E1H and 230 K for 2M3H along the 1 bar isobar. Actually, the 250 K anomaly in the hydrogen bond equilibrium has also been found for 2E1H and other monohydroxy alcohols.^{35,36} In more detail, the combined dielectric, near-infrared, and nuclear magnetic resonance study showed that this peculiar point is a transition from more stable hydrogen bonded structures at lower temperatures into less durable structures at higher temperatures. That is the exact observation that we can deduce from Figure 4, from which it stems that above the temperature of around 250 K, the linear cluster distribution grows rapidly for both alcohols, whereas the amount of branch/ring clusters drops rapidly for 2E1H/2M3H, respectively. Thus, our studies demonstrate that the suggested disturbance of H bond equilibrium leads to the nonmonotonical structural transition where the reformation of the cluster's architecture occurs.

Moreover, the temperature dependencies of the linear H bond structures in Figure 4 show a characteristic maximum of around 60% at about 370 K for 2E1H and 320 K for 2M3H at ambient pressure. This effect is the result of an initial increase in the number of linear clusters as the ring and branch clusters disintegrate into linear ones and then the dissociation of the linear clusters into monomers. In turn, based on the pressure dependencies of the monomer and cluster distributions, it is possible to explain the interesting behavior of the main diffraction peak's intensity with rising pressure—the intensity initially increases and then decreases with higher pressure (Figure 2). This behavior is associated with an increase in the nearest-neighbor correlations in both alcohols up to a pressure of around 0.5 GPa, followed by a decrease in these correlations with higher pressures. The physics behind this is simply linking of monomers to the H-bonded clusters up to pressures around 0.5 GPa. From Figure 4 one can see that around 0.5 GPa the number of monomers drops down to almost 0%. As a result of the bonding of molecules, an increase in the short-range order is observed. For higher pressures, the intensity decreases because the number of more complex branched structures increases, and the pressure causes suppression of the short-range organization of molecules, where flexible and mobile alkyl tails easily rearrange under pressure and improve the packing density.

Finally, pictures of the self-association of molecules by H bonds, in different thermodynamic conditions, are presented in Figure 5. Each image represents one configuration from the trajectories collected from simulations at different temperature and pressure states. As a supplement, the inset histograms in Figure 5 show the distributions of the number of molecules in

any cluster, regardless of the architecture type, calculated from the whole trajectory. First, the impact of cluster type on the number of molecules in a cluster is noticeable. Ring clusters consist of a maximum of 6 molecules for 2M3H and around 15 molecules for 2E1H while linear and branched structures achieve sizes of even 100 molecules. That indicates a specific attribute of the ring cluster, i.e., small size is geometrically favorable. The advantage of ring clusters in 2M3H in 213 K impacts the average number of molecules joined in clusters, which is around 4–5 in that condition. That number is similar at room temperature; however, a higher number of monomers emerges with the rise of temperature. At 413 K both 2E1H and 2M3H show no preference for the number of molecules in clusters and are composed of a considerably large percent of free molecules.

One of the very few studies conducted under high temperature or at high pressure up to around 1 GPa on alcohols²³ is consistent with our results. Increasing the temperature was reported to decrease the sizes of H-bonded aggregates in diols, while the prepeak position remained stable in the temperature-dependent diffraction patterns. Another study¹⁷ demonstrated destruction of the medium-range order of linear alcohols at high pressure, resulting in vanishing of the diffraction prepeak intensity. Here, we can clarify the issue of changes in the medium-range order at the nanoscale. Our results clearly show that the medium-range order of oxygen atoms connected in H bonds is not destroyed; only the CO correlations are damped under the influence of high pressure. It means that the disorder refers to the unbounded tails of molecules. Nevertheless, with changes in temperature, both components of the medium-range order, OO and CO correlations, are affected. It is also worth referring to the study conducted on water–alcohol mixtures¹⁶ that revealed the effect of the decrease in the number of ring clusters in response to high pressure as well. However, it was more evident for lower methanol concentrations (note the lack of preference for creating a ring cluster for pure methanol). Finally, our latest paper based on infrared spectroscopy, X-ray diffraction, and molecular dynamics simulations with another force field also demonstrated intensified molecular clustering via H bonds in 2E1H under high pressure.³⁷ This nice agreement with other studies reflects the validity of the proposed structural models of the studied alcohols at the very wide range of thermodynamic conditions.

The results obtained here give us an important insight into the clustering ability of monohydroxy alcohols at wide pressure and temperature ranges. We revealed that despite the same bulk density at some thermodynamic conditions, the cluster architecture at the nanoscale may significantly differ; it is possible to create liquid systems of the same global density but distinct structural properties. Especially, increasing temperature has a destructive effect on H bond stability, resulting in an abundance of monomers. Also, branch structure is not preferred at high temperature, as simultaneous creation of two H bonds by a single molecule is too demanding during strong thermal vibrations. On the other hand, branched clusters may not form in the first place because of unfavorable internal molecular structure with nonterminal position of OH group seen for 2M3H. Linear aggregates are the most lasting with higher temperature. Importantly, in this study, we clarify the issue that compression favors the H bonds creation in monohydroxy alcohols, and changes of diffraction prepeak visible in structure factor are connected to supramolecular

reorganization. Some percent of ring clusters, probably not bonded strongly enough, is destroyed with higher pressure, and they become linear or branched clusters. The analysis of H bonds provided herein is universal and can be used in analogy to other H-bonded substances like water. In water, various, but mostly ring and branched, H-bonded structures are created,³⁸ thus, the results of presented H-bonded systems are very useful. Certainly, further parametrization of the clustering ability under thermodynamic conditions in the field of dynamics or entropy would be beneficial.

■ ASSOCIATED CONTENT

SI Supporting Information

The Supporting Information is available free of charge at <https://pubs.acs.org/doi/10.1021/acs.jpcllett.4c00085>.

Description of the methodology applied: ambient pressure X-ray diffraction experiment, high-pressure X-ray diffraction experiment, molecular dynamics simulations, and analysis of H-bonded clusters; additional figures and descriptions of partial radial distribution functions and density approximation (PDF)

Transparent Peer Review report available (PDF)

■ AUTHOR INFORMATION

Corresponding Authors

Joanna Greliska – A. Chełkowski Institute of Physics,
University of Silesia in Katowice, 41-500 Chorzów, Poland;
orcid.org/0000-0002-7001-4083;
Email: joanna.greliska@us.edu.pl

Karolina Jurkiewicz – A. Chełkowski Institute of Physics,
University of Silesia in Katowice, 41-500 Chorzów, Poland;
orcid.org/0000-0002-4289-7827;
Email: karolina.jurkiewicz@us.edu.pl

Authors

László Temleitner – HUN-REN Wigner Research Centre for
Physics, H-1121 Budapest, Hungary

Changyong Park – High Pressure Collaborative Access Team
(HPCAT), X-ray Science Division, Argonne National
Laboratory, Lemont, Illinois 60439, United States;
orcid.org/0000-0002-3363-5788

Sebastian Pawlus – A. Chełkowski Institute of Physics,
University of Silesia in Katowice, 41-500 Chorzów, Poland;
orcid.org/0000-0001-9209-4056

Complete contact information is available at:
<https://pubs.acs.org/doi/10.1021/acs.jpcllett.4c00085>

Author Contributions

S.P. provided the funding and research idea. J.G. and K.J. performed the temperature X-ray diffraction experiment. J.G., K.J., and C.P. conducted the high-pressure X-ray diffraction experiment, J.G. prepared samples, and C.P. designed and operated the experimental setup. J.G. and L.T. performed molecular dynamics simulations. L.T. created H bond analysis programs, and J.G. analyzed the results. J.G., S.P., and K.J. interpreted the results, J.G. and K.J. wrote the manuscript with contributions of all authors.

Notes

The authors declare no competing financial interest.

ACKNOWLEDGMENTS

J.G., K.J., and S.P. acknowledge the support from the National Science Center, Poland, Grant UMO-2019/35/B/ST3/02670. J.G. acknowledges computational time at PL-Grid, Poland, Grant PLG/2022/015982. The authors appreciate the computational time and calculation help from Liquid Structure Research Group, Wigner Research Centre for Physics, Hungary. The National Research, Development, and Innovation Office (NKFIH) under Grant K142429 and from Eötvös Loránd Research Network (ELKH, Hungary) via their special fund, Grant SA-89/2021, are acknowledged by L.T. Portions of this work were performed at HPCAT (Sector 16), Advanced Photon Source (APS), Argonne National Laboratory. HPCAT operations are supported by DOE-NNSA's Office of Experimental Sciences. The Advanced Photon Source is a U.S. Department of Energy (DOE) Office of Science User Facility operated for the DOE Office of Science by Argonne National Laboratory under Contract DE-AC02-06CH11357. J.G. is thankful for the support during graduate internship at High Pressure Collaborative Access Team at Argonne Photon Source, USA.

REFERENCES

- (1) Grelska, J.; Jurkiewicz, K.; Burian, A.; Pawlus, S. Supramolecular Structure of Phenyl Derivatives of Butanol Isomers. *J. Phys. Chem. B* **2022**, *126* (19), 3563–3571.
- (2) Pothoczki, S.; Pusztai, L.; Bakó, I. Variations of the Hydrogen Bonding and Hydrogen-Bonded Network in Ethanol–Water Mixtures on Cooling. *J. Phys. Chem. B* **2018**, *122* (26), 6790–6800.
- (3) Drewitt, J. W. E. Liquid Structure under Extreme Conditions: High-Pressure x-Ray Diffraction Studies. *J. Phys.: Condens. Matter* **2021**, *33* (50), 503004.
- (4) Katayama, Y.; Hattori, T.; Saitoh, H.; Ikeda, T.; Aoki, K.; Fukui, H.; Funakoshi, K. Structure of Liquid Water under High Pressure up to 17 GPa. *Phys. Rev. B* **2010**, *81* (1), 014109.
- (5) Dmowski, W.; Yoo, G. H.; Gierlotka, S.; Wang, H.; Yokoyama, Y.; Park, E. S.; Stelmakh, S.; Egami, T. High Pressure Quenched Glasses: Unique Structures and Properties. *Sci. Rep.* **2020**, *10* (1), 9497.
- (6) Bykova, E.; Dubrovinsky, L.; Dubrovinskaya, N.; Bykov, M.; McCammon, C.; Ovsyannikov, S. V.; Liermann, H.-P.; Kuppenko, I.; Chumakov, A. I.; Rüffer, R.; Hanfland, M.; Prakapenka, V. Structural Complexity of Simple Fe₂O₃ at High Pressures and Temperatures. *Nat. Commun.* **2016**, *7* (1), 10661.
- (7) Neumann, M. A.; Van De Streek, J.; Fabbiani, F. P. A.; Hidber, P.; Grassmann, O. Combined Crystal Structure Prediction and High-Pressure Crystallization in Rational Pharmaceutical Polymorph Screening. *Nat. Commun.* **2015**, *6* (1), 7793.
- (8) Xie, X.; Ding, J.; Wu, B.; Zheng, H.; Li, S.; Wang, C.-T.; He, J.; Liu, Z.; Wang, J.-T.; Liu, Y. Pressure-Induced Dynamic Tuning of Interlayer Coupling in Twisted WSe₂/WSe₂ Homobilayers. *Nano Lett.* **2023**, *23* (19), 8833–8841.
- (9) Bian, K.; Singh, A. K.; Hennig, R. G.; Wang, Z.; Hanrath, T. The Nanocrystal Superlattice Pressure Cell: A Novel Approach To Study Molecular Bundles under Uniaxial Compression. *Nano Lett.* **2014**, *14* (8), 4763–4766.
- (10) Morard, G.; Hernandez, J.-A.; Guarguaglini, M.; Bolis, R.; Benuzzi-Mounaix, A.; Vinci, T.; Fiquet, G.; Baron, M. A.; Shim, S. H.; Ko, B.; Gleason, A. E.; Mao, W. L.; Alonso-Mori, R.; Lee, H. J.; Nagler, B.; Galtier, E.; Sokaras, D.; Glenzer, S. H.; Andraud, D.; Garbarino, G.; Mezouar, M.; Schuster, A. K.; Ravasio, A. In Situ X-Ray Diffraction of Silicate Liquids and Glasses under Dynamic and Static Compression to Megabar Pressures. *Proc. Natl. Acad. Sci. U. S. A.* **2020**, *117* (22), 11981–11986.
- (11) Briggs, R.; Gorman, M. G.; Zhang, S.; McGonegle, D.; Coleman, A. L.; Coppari, F.; Morales-Silva, M. A.; Smith, R. F.; Wicks, J. K.; Bolme, C. A.; Gleason, A. E.; Cunningham, E.; Lee, H. J.; Nagler, B.; McMahon, M. I.; Eggert, J. H.; Fratanduono, D. E. Coordination Changes in Liquid Tin under Shock Compression Determined Using *In Situ* Femtosecond x-Ray Diffraction. *Appl. Phys. Lett.* **2019**, *115* (26), 264101.
- (12) Dias, R. P.; Silvera, I. F. Observation of the Wigner-Huntington Transition to Metallic Hydrogen. *Science* **2017**, *355* (6326), 715–718.
- (13) Funamori, N.; Tsuji, K. Pressure-Induced Structural Change of Liquid Silicon. *Phys. Rev. Lett.* **2002**, *88* (25), 255508.
- (14) Funamori, N.; Tsuji, K. Structural Transformation of Liquid Tellurium at High Pressures and Temperatures. *Phys. Rev. B* **2001**, *65* (1), 014105.
- (15) Henry, L.; Mezouar, M.; Garbarino, G.; Sifré, D.; Weck, G.; Datchi, F. Liquid–Liquid Transition and Critical Point in Sulfur. *Nature* **2020**, *584* (7821), 382–386.
- (16) Temleitner, L.; Hattori, T.; Abe, J.; Nakajima, Y.; Pusztai, L. Pressure-Dependent Structure of Methanol–Water Mixtures up to 1.2 GPa: Neutron Diffraction Experiments and Molecular Dynamics Simulations. *Molecules* **2021**, *26* (5), 1218.
- (17) Mariani, A.; Ballirano, P.; Angiolari, F.; Caminiti, R.; Gontrani, L. Does High Pressure Induce Structural Reorganization in Linear Alcohols? A Computational Answer. *ChemPhysChem* **2016**, *17* (19), 3023–3029.
- (18) Wikarek, M.; Pawlus, S.; Tripathy, S. N.; Szulc, A.; Paluch, M. How Different Molecular Architectures Influence the Dynamics of H-Bonded Structures in Glass-Forming Monohydroxy Alcohols. *J. Phys. Chem. B* **2016**, *120* (25), 5744–5752.
- (19) Pawlus, S.; Wikarek, M.; Gainaru, C.; Paluch, M.; Böhmer, R. How Do High Pressures Change the Debye Process of 4-Methyl-3-Heptanol? *J. Chem. Phys.* **2013**, *139* (6), 064501.
- (20) Požar, M.; Bolle, J.; Sternemann, C.; Perera, A. On the X-Ray Scattering Pre-Peak of Linear Mono-Ols and the Related Microstructure from Computer Simulations. *J. Phys. Chem. B* **2020**, *124* (38), 8358–8371.
- (21) Ghoufi, A. Molecular Origin of the Prepeak in the Structure Factor of Alcohols. *J. Phys. Chem. B* **2020**, *124* (50), 11501–11509.
- (22) Perera, A. Charge Ordering and Scattering Pre-Peaks in Ionic Liquids and Alcohols. *Phys. Chem. Chem. Phys.* **2017**, *19* (2), 1062–1073.
- (23) Tomšič, M.; Cerar, J.; Jamnik, A. Supramolecular Structure vs. Rheological Properties: 1,4-Butanediol at Room and Elevated Temperatures. *J. Colloid Interface Sci.* **2019**, *557*, 328–335.
- (24) Parola, A.; Reatto, L. Liquid State Theories and Critical Phenomena. *Adv. Phys.* **1995**, *44* (3), 211–298.
- (25) Požar, M.; Perera, A. On the Micro-Heterogeneous Structure of Neat and Aqueous Propylamine Mixtures: A Computer Simulation Study. *J. Mol. Liq.* **2017**, *227*, 210–217.
- (26) Grelska, J.; Jurkiewicz, K.; Nowok, A.; Pawlus, S. Computer Simulations as an Effective Way to Distinguish Supramolecular Nanostructure in Cyclic and Phenyl Alcohols. *Phys. Rev. E* **2023**, *108* (2), 024603.
- (27) Jukić, I.; Požar, M.; Lovrinčević, B.; Perera, A. Universal Features in the Lifetime Distribution of Clusters in Hydrogen-Bonding Liquids. *Phys. Chem. Chem. Phys.* **2021**, *23* (35), 19537–19546.
- (28) Böhmer, R.; Gainaru, C.; Richert, R. Structure and Dynamics of Monohydroxy Alcohols—Milestones towards Their Microscopic Understanding, 100 Years after Debye. *Phys. Rep.* **2014**, *545* (4), 125–195.
- (29) Gainaru, C.; Meier, R.; Schildmann, S.; Lederle, C.; Hiller, W.; Rössler, E. A.; Böhmer, R. Nuclear-Magnetic-Resonance Measurements Reveal the Origin of the Debye Process in Monohydroxy Alcohols. *Phys. Rev. Lett.* **2010**, *105* (25), 258303.
- (30) Ngai, K. L.; Pawlus, S.; Paluch, M. Explanation of the Difference in Temperature and Pressure Dependences of the Debye Relaxation and the Structural α -Relaxation near T of Monohydroxy Alcohols. *Chem. Phys.* **2020**, *530*, 110617.
- (31) Gainaru, C.; Wikarek, M.; Pawlus, S.; Paluch, M.; Figuli, R.; Wilhelm, M.; Hecksher, T.; Jakobsen, B.; Dyre, J. C.; Böhmer, R.

Oscillatory Shear and High-Pressure Dielectric Study of 5-Methyl-3-Heptanol. *Colloid Polym. Sci.* **2014**, *292* (8), 1913–1921.

(32) Young-Gonzales, A. R.; Richert, R. Field Induced Changes in the Ring/Chain Equilibrium of Hydrogen Bonded Structures: 5-Methyl-3-Heptanol. *J. Chem. Phys.* **2016**, *145* (7), 074503.

(33) Singh, L. P.; Richert, R. Watching Hydrogen-Bonded Structures in an Alcohol Convert from Rings to Chains. *Phys. Rev. Lett.* **2012**, *109* (16), 167802.

(34) Patil, S.; Sun, R.; Cheng, S.; Cheng, S. Molecular Mechanism of the Debye Relaxation in Monohydroxy Alcohols Revealed from Rheo-Dielectric Spectroscopy. *Phys. Rev. Lett.* **2023**, *130* (9), 098201.

(35) Bauer, S.; Burlafinger, K.; Gainaru, C.; Lunkenheimer, P.; Hiller, W.; Loidl, A.; Böhmer, R. Debye Relaxation and 250 K Anomaly in Glass Forming Monohydroxy Alcohols. *J. Chem. Phys.* **2013**, *138* (9), 094505.

(36) Gainaru, C.; Kastner, S.; Mayr, F.; Lunkenheimer, P.; Schildmann, S.; Weber, H. J.; Hiller, W.; Loidl, A.; Böhmer, R. Hydrogen-Bond Equilibria and Lifetimes in a Monohydroxy Alcohol. *Phys. Rev. Lett.* **2011**, *107* (11), 118304.

(37) Hachuła, B.; Włodarczyk, P.; Jurkiewicz, K.; Grelska, J.; Scelta, D.; Fanetti, S.; Paluch, M.; Pawlus, S.; Kamiński, K. Pressure-Induced Aggregation of Associating Liquids as a Driving Force Enhancing Hydrogen Bond Cooperativity. *J. Phys. Chem. Lett.* **2024**, *15* (1), 127–135.

(38) Ludwig, R. Water: From Clusters to the Bulk. *Angew. Chem., Int. Ed.* **2001**, *40* (10), 1808–1827.

Supporting Information for

High-Pressure and Temperature Effects on the Clustering Ability of Monohydroxy Alcohols

Joanna Grelska^{1,}, László Temleitner², Changyong Park³, Karolina Jurkiewicz^{1,*},
Sebastian Pawlus¹*

¹ A. Chełkowski Institute of Physics, University of Silesia in Katowice, 75 Pułku Piechoty 1, 41-500 Chorzów, Poland

² HUN-REN Wigner Research Centre for Physics, Konkoly Thege út 29-33, H-1121 Budapest, Hungary

³ High Pressure Collaborative Access Team (HPCAT), X-Ray Science Division, Argonne National Laboratory, Lemont, IL, 60439, USA

*Correspondence e-mails: joanna.grelska@us.edu.pl, karolina.jurkiewicz@us.edu.pl

1. Methods

Ambient pressure X-ray diffraction experiment

The investigated 2-ethyl-1-hexanol and 2-methyl-3-hexanol were purchased from Sigma Aldrich. The experimental measurements at ambient pressure were performed on a Rigaku-Denki S/MAX RAPID II-R diffractometer equipped with two-dimensional image plate detector and Ag rotating anode. Incident beam was monochromatized with graphite (002) and the wavelength 0.5608 Å was used. Temperature was controlled by Oxford Cryostream Plus and Compact Cooler. Samples were measured from the lowest achievable temperature of 163 K up to the highest temperature for which the sample did not evaporate (2E1H – 413K, 2M3H – 373 K). Two dimensional images were collected and converted into one-dimensional patterns of the scattering intensity versus scattering angle. The patterns measured for background (empty capillary) were subtracted. After correcting the data for the Compton scattering, absorption and polarization, the structure factors were calculated according to the procedure described in¹.

High-pressure X-ray diffraction experiment

The high-pressure diffraction measurements were performed at 16-BM-D beamline, Advanced Photon Source, Argonne National Laboratory, USA, equipped with micro-focused beam. The energy of the incident beam was 20 keV (it corresponds to the wavelength of 0.619 Å).

Liquid samples were packed and measured in diamond anvil cells. Pressure was controlled by a gas membrane, ruby fluorescence method was used to measure the actual pressure on the sample. Measurements were taken at ambient temperature and pressure starting from around 0.1 GPa up to around 3 GPa. For 2E1H, pressure measurements were additionally carried out at temperatures of 50°C, 75°C and 100°C using the temperature chamber and pressure up to around 5 GPa. Empty diamond anvil cell was measured as the background reference, and subtracted from the two-dimensional diffractograms of the measured samples in Dioptas² software. Masking of artifacts coming from diamond reflections was performed in the same software. The diffractograms converted from the two- to one-dimensional patterns of the scattering intensity as the function of the scattering vector were then transformed into the structure factor representations using Amorpheus³ program. Results have been slightly smoothed without changing the shape of the functions.

Molecular dynamics simulations

Molecular dynamics simulations were conducted in GROMACS 2022 and 2023⁴⁻⁶ package. NPT ensemble was used with Nose-Hoover temperature coupling (time constant 0.1 ps) and MTTK pressure coupling (time constant 1 ps). Simulations run in two regimes, decreasing temperature and increasing pressure. Starting configurations in both cases was run at 413 K with a simulation box containing 2000 randomly distributed molecules and the box size set assuming the room temperature density of the compounds (0.8344 g/cm³ for 2E1H and 0.821 g/cm³ for 2M3H). The topology files were created in the Antechamber module⁷ and GAFF⁸ force field was used, since it gave satisfactory results in our previous works^{1,9}. Time step was 0.001 ps, while integration velocity Verlet algorithm was implemented along with 2 nm cut-off for van der Waals interactions and 2 nm distance for PME electrostatic interactions. Simulations time for all pressure steps in the range of 0.1–3 GPa and temperatures in the range of 213–273 K was 50 ns, and for temperatures in the range of 293–413 K was 10 ns (regarding faster relaxation of molecules). The last 101 and 96 trajectories respectively to the simulation times 50 and 10 ns were used for further analysis. Structure factors, partial structure factors and partial radial distribution functions were calculated using TRAVIS software¹⁰⁻¹² according to formulas described in¹.

Analysis of H-bond clusters

Developed in-house software¹³ was used for the analysis and visualization of the H-bonded clusters. Only H-bonds between hydroxyl parts of molecules were considered for H-bonds analysis. The condition for the formation of hydrogen bonding was implemented as follows: intermolecular distance O-O < 4 Å, intermolecular distance O-H_O < 2.7 Å, H-bond angle OH_O-O < 40° (where H_O is the hydrogen atom covalently linked into O atom). Those criteria were found to cover all H-bonds at various temperature and pressure steps. Especially such O-H_O distance was found invariant in various temperature conditions. Then, architectures of the H-bond connections in the formed clusters were analyzed. The H-bonded cluster was defined as linear – when neat chain with free hydroxyl group in the chain ends was created; as ring - when closed chain with no free hydroxyl groups was formed; and branched – when at least one molecule in chain was connected to two hydroxyl groups. Visualization of such defined H-bonded structures was built with in-house software using Python. Moreover, the general distributions of the number of molecules in the H-bonded clusters, aside from their architectures, were calculated from the collected trajectories using GROMACS gmx clustsize program, providing only the condition for the distance O-O < 3.5 Å (found to be the best suitable without the angle condition).

2. Supplementary Figures

Partial radial distribution functions

Partial radial distribution functions are presented in Figure S1. These are the functions of intensity proportional to the probability of finding any inter-atomic distances in the system. The position of the first maximum of OO radial distribution function is 2.8 Å, which is the typical distance between oxygen atoms in hydrogen bonds formed in alcohols. The first HO peak around 1 Å is due to intramolecular bonds between oxygen and hydrogen in hydroxyl groups. Interestingly, the HO covalent bonds with both rising pressure and lowering temperature are elongating in favor of shortening OO bond distance. This effect of strengthening H-bond with higher pressure (and opposite effect of high temperature) was also observed in nuclear magnetic resonance^{14,15} and Fourier transform infrared¹⁶ spectroscopy studies. The observations described in the literature demonstrated similar effects of increasing pressure and decreasing temperature on H-bonds strength. However, our results reveal that the probability of finding the H-bonds (their amount) decreases rapidly with rising temperature, remaining invariant for pressure changes (the

OO functions in Figure S1). The similar effect that was deduced from partial structure factors results (Figure 3).

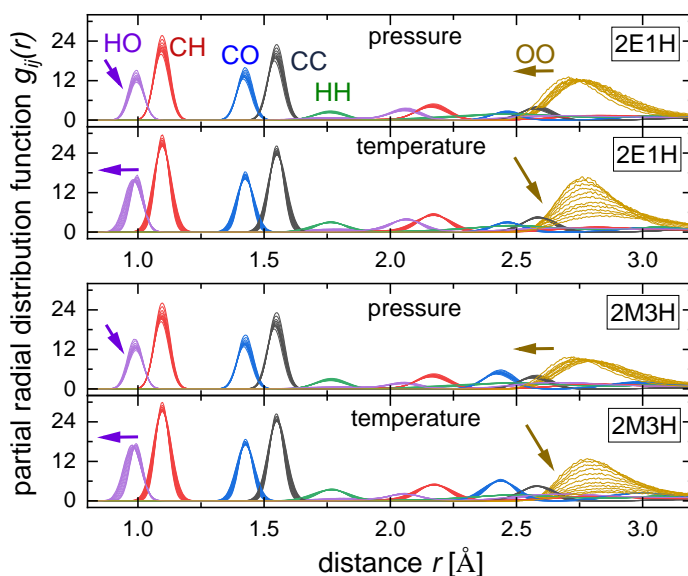


Figure S1. Partial radial distribution functions of investigated compounds obtained by molecular dynamics simulations. Individual functions are marked with symbol of the same color. The arrows indicate the direction of shifts of selected partial functions along with pressure or temperature increase.

Density approximation

A global factor that influences molecular and supramolecular aggregation is density. The bulk density is possible to be obtained from molecular dynamics simulations. Based on experimental diffraction data, it is possible to estimate changes in density - the main diffraction peak position to the third power is expected to be proportional to density of a simple liquid¹⁷. However, also for associating ionic liquids, it was recently found that position of main diffraction peak arising due to nearest-neighbour structure follows the density scaling¹⁸. Thus, we adopted such approximation for studied alcohols. Knowing the density of the alcohols at room temperature and ambient pressure (see the Methods part), densities at other thermodynamics conditions were calculated based on the main peak positions and compared with the values obtained from simulations – Figures S2a and b. In the graphs one can see some common areas marked in light orange. These are states of density that can be achieved experimentally either by lowering temperature down to 163 K or by pressurization up to 1 GPa. On the other hand, from the course

of these dependencies, one can see that there are ranges of very low or very high density that can be achieved only by very high temperature and high pressure, respectively. Comparison of experimental and simulation based values of density shows good agreement for high temperature and low pressure ranges, but then some discrepancies appear for low temperature and high pressure. This is a result of slowdown of molecular dynamics under these conditions and the greater inaccuracy of the models. However, the overall course of experimental and simulation-based functions is consistent.

The ability of measurements at high pressures and temperatures up to 100°C has prompted us to observe the density behavior of 2E1H at different pressure/temperature states. The diffraction data for these isotherms are not shown in the article, but the main peak positions were obtained to estimate the density and depicted in Figure S2c. For 2E1H, the values of glass transition temperature and pressure are known: $T_g = 143$ K (in 1 bar) and $p_g = 2.58$ GPa (in 25°C)¹⁶, so the density dependences on temperature and pressure can be estimated in reference to the glass transition points – see Figure S2c. From the graph one can see that different measurements under high pressure and various temperature lay on the same curve. At low pressure the high temperature isotherms are shifted a little bit to the smaller density which is typical temperature effect. But increasing the pressure seems to have a uniform impact on density regardless the temperature of the sample. Although the range of investigated temperatures is not very significant compared to the pressure range, it is evident that pressure change has bigger control of density in the case of 2E1H.

Furthermore, when temperature and pressure dependence is compared in respect to the glass transition points, one will see that at two glass states lying in the T/T_g and $p/p_g = 1$ (marked in Figure S2) the density of 2E1H is very different. The density of glass achieved by pressurization in 25°C is higher than that of glass predicted to be achieved by lowering temperature in 1 bar. Such high and low density glassy states triggered by thermodynamic conditions were already reported for amorphous ice¹⁹. Certainly, there is a factor that strongly influences the density of hydrogen-bonded substances at various thermodynamic conditions. Moreover, previous studies stated that self-association of molecules in alcohols strongly affects the glass transition temperature and other properties. For such self-associating systems, T_g was observed to be higher than for simple glass

formers of similar molecular mass^{20,21}. Thus, clustering of molecules seems to have a significant impact on global properties of the system.

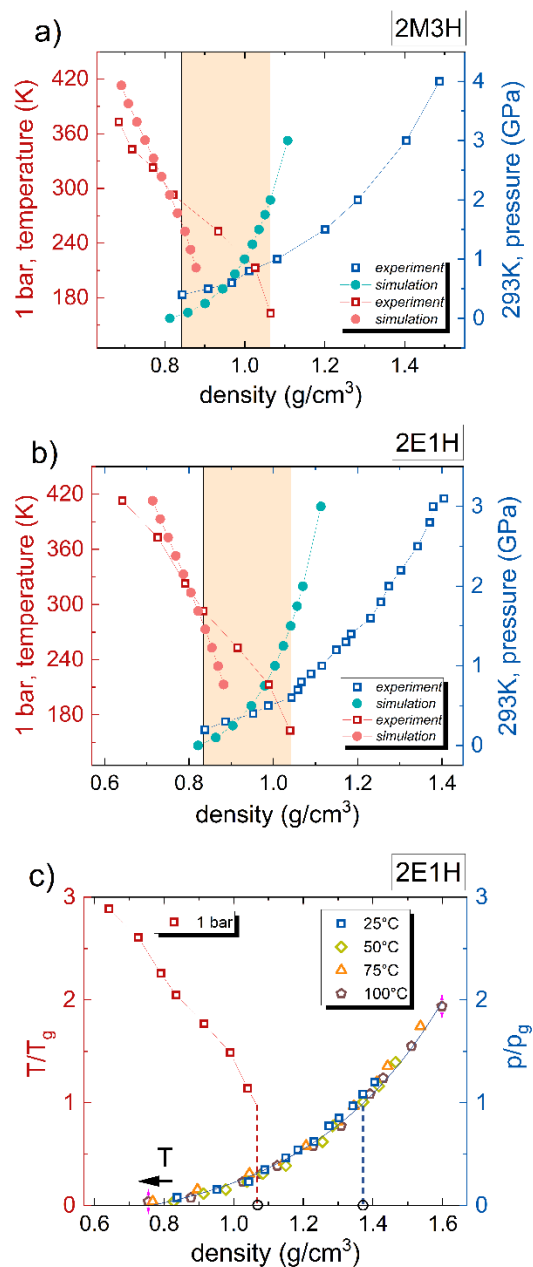


Figure S2. The temperature and pressure dependence on density obtained from experiment and simulations for a) 2M3H and b) 2E1H. Temperature and pressure dependences on density measured for one isobar and four isotherms for c) 2E1H presented in the scale of glass transition points T/T_g and p/p_g . The common areas of density are marked in the same light orange. The same state at ambient conditions is marked with vertical black line.

References

- (1) Grelska, J.; Jurkiewicz, K.; Burian, A.; Pawlus, S. Supramolecular Structure of Phenyl Derivatives of Butanol Isomers. *J. Phys. Chem. B* **2022**, *126* (19), 3563–3571. <https://doi.org/10.1021/acs.jpcc.2c01269>.
- (2) Prescher, C.; Prakapenka, V. B. *DIOPTAS*: A Program for Reduction of Two-Dimensional X-Ray Diffraction Data and Data Exploration. *High Pressure Research* **2015**, *35* (3), 223–230. <https://doi.org/10.1080/08957959.2015.1059835>.
- (3) Boccato, S.; Garino, Y.; Morard, G.; Zhao, B.; Xu, F.; Sanloup, C.; King, A.; Guignot, N.; Clark, A.; Garbarino, G.; Morand, M.; Antonangeli, D. Amorpheus: A Python-Based Software for the Treatment of X-Ray Scattering Data of Amorphous and Liquid Systems. *High Pressure Research* **2022**, *42* (1), 69–93. <https://doi.org/10.1080/08957959.2022.2032032>.
- (4) Abraham, M. J.; Murtola, T.; Schulz, R.; Páll, S.; Smith, J. C.; Hess, B.; Lindahl, E. GROMACS: High Performance Molecular Simulations through Multi-Level Parallelism from Laptops to Supercomputers. *SoftwareX* **2015**, *1–2*, 19–25. <https://doi.org/10.1016/j.softx.2015.06.001>.
- (5) Páll, S.; Abraham, M. J.; Kutzner, C.; Hess, B.; Lindahl, E. Tackling Exascale Software Challenges in Molecular Dynamics Simulations with GROMACS. In *Solving Software Challenges for Exascale*; Markidis, S., Laure, E., Eds.; Lecture Notes in Computer Science; Springer International Publishing: Cham, 2015; Vol. 8759, pp 3–27. https://doi.org/10.1007/978-3-319-15976-8_1.
- (6) Pronk, S.; Páll, S.; Schulz, R.; Larsson, P.; Bjelkmar, P.; Apostolov, R.; Shirts, M. R.; Smith, J. C.; Kasson, P. M.; van der Spoel, D.; Hess, B.; Lindahl, E. GROMACS 4.5: A High-Throughput and Highly Parallel Open Source Molecular Simulation Toolkit. *Bioinformatics* **2013**, *29* (7), 845–854. <https://doi.org/10.1093/bioinformatics/btt055>.
- (7) Case, D. A.; Aktulga, H. M.; Belfon, K.; Ben-Shalom, I. Y.; Brozell, S. R.; Cerutti, D. S.; Cheatham, T. E., III; Cisneros, G. A.; Cruzeiro, V. W. D.; Darden, T. A.; Duke, R. E.; Giambasu, G.; Gilson, M. K.; Gohlke, H.; Goetz, A. W.; Harris, R.; Izadi, S.; Izmailov, S. A.; Jin, C.; Kasavajhala, K.; Kaymak, M. C.; King, E.; Kovalenko, A.; Kurtzman, T.; Lee, T. S.; LeGrand, S.; Li, P.; Lin, C.; Liu, J.; Luchko, T.; Luo, R.; Machado, M.; Man, V.; Manathunga, M.; Merz, K. M.; Miao, Y.; Mikhailovskii, O.; Monard, G.; Nguyen, H.; O’Hearn, K. A.; Onufriev, A.; Pan, F.; Pantano, S.; Qi, R.; Rahnamoun, A.; Roe, D. R.; Roitberg, A.; Sagui, C.; Schott-Verdugo, S.; Shen, J.; Simmerling, C. L.; Skrynnikov, N. R.; Smith, J.; Swails, J.; Walker, R. C.; Wang, J.; Wei, H.; Wolf, R. M.; Wu, X.; Xue, Y.; York, D. M.; Zhao, S.; Kollman, P. A. *Amber 2021, AmberTools21; University of California: San Francisco, 2021*.
- (8) Wang, J.; Wolf, R. M.; Caldwell, J. W.; Kollman, P. A.; Case, D. A. Development and Testing of a General Amber Force Field. *J. Comput. Chem.* **2004**, *25* (9), 1157–1174. <https://doi.org/10.1002/jcc.20035>.
- (9) Grelska, J.; Jurkiewicz, K.; Nowok, A.; Pawlus, S. Computer Simulations as an Effective Way to Distinguish Supramolecular Nanostructure in Cyclic and Phenyl Alcohols. *Phys. Rev. E* **2023**, *108* (2), 024603. <https://doi.org/10.1103/PhysRevE.108.024603>.
- (10) Brehm, M.; Thomas, M.; Gehrke, S.; Kirchner, B. TRAVIS—A Free Analyzer for Trajectories from Molecular Simulation. *J. Chem. Phys.* **2020**, *152* (16), 164105. <https://doi.org/10.1063/5.0005078>.
- (11) Brehm, M.; Kirchner, B. TRAVIS - A Free Analyzer and Visualizer for Monte Carlo and Molecular Dynamics Trajectories. *J. Chem. Inf. Model.* **2011**, *51* (8), 2007–2023. <https://doi.org/10.1021/ci200217w>.
- (12) Hollóczki, O.; Macchiagodena, M.; Weber, H.; Thomas, M.; Brehm, M.; Stark, A.; Russina, O.; Triolo, A.; Kirchner, B. Triphasic Ionic-Liquid Mixtures: Fluorinated and Non-Fluorinated Aprotic Ionic-Liquid Mixtures. *ChemPhysChem* **2015**, *16* (15), 3325–3333. <https://doi.org/10.1002/cphc.201500473>.
- (13) Temleitner, L. Hydrogen Bond Analysis Software Package, 2023. <https://doi.org/10.5281/ZENODO.8360239>.

- (14) Ohtaki, H. Effects of Temperature and Pressure on Hydrogen Bonds in Water and in Formamide. *Journal of Molecular Liquids* **2003**, *103–104*, 3–13. [https://doi.org/10.1016/S0167-7322\(02\)00124-1](https://doi.org/10.1016/S0167-7322(02)00124-1).
- (15) Czeslik, C.; Jonas, J. Pressure and Temperature Dependence of Hydrogen-Bond Strength in Methanol Clusters. *Chemical Physics Letters* **1999**, *302* (5–6), 633–638. [https://doi.org/10.1016/S0009-2614\(99\)00170-0](https://doi.org/10.1016/S0009-2614(99)00170-0).
- (16) Hachuła, B.; Kamińska, E.; Koperwas, K.; Wrzalik, R.; Jurkiewicz, K.; Tarnacka, M.; Scelta, D.; Fanetti, S.; Pawlus, S.; Paluch, M.; Kamiński, K. A Study of O H...O Hydrogen Bonds along Various Isolines in 2-Ethyl-1-Hexanol. Temperature or Pressure - Which Parameter Controls Their Behavior? *Spectrochimica Acta Part A: Molecular and Biomolecular Spectroscopy* **2022**, *283*, 121726. <https://doi.org/10.1016/j.saa.2022.121726>.
- (17) Weck, G.; Datchi, F.; Garbarino, G.; Ninet, S.; Queyroux, J.-A.; Plisson, T.; Mezouar, M.; Loubeyre, P. Melting Curve and Liquid Structure of Nitrogen Probed by X-Ray Diffraction to 120 GPa. *Phys. Rev. Lett.* **2017**, *119* (23), 235701. <https://doi.org/10.1103/PhysRevLett.119.235701>.
- (18) Hansen, H. W.; Lundin, F.; Adrjanowicz, K.; Frick, B.; Matic, A.; Niss, K. Density Scaling of Structure and Dynamics of an Ionic Liquid. *Phys. Chem. Chem. Phys.* **2020**, *22* (25), 14169–14176. <https://doi.org/10.1039/D0CP01258K>.
- (19) Mariedahl, D.; Perakis, F.; Späh, A.; Pathak, H.; Kim, K. H.; Benmore, C.; Nilsson, A.; Amann-Winkel, K. X-Ray Studies of the Transformation from High- to Low-Density Amorphous Water. *Phil. Trans. R. Soc. A* **2019**, *377* (2146), 20180164. <https://doi.org/10.1098/rsta.2018.0164>.
- (20) Nakanishi, M.; Nozaki, R. Systematic Study of the Glass Transition in Polyhydric Alcohols. *Phys. Rev. E* **2011**, *83* (5), 051503. <https://doi.org/10.1103/PhysRevE.83.051503>.
- (21) Qin, Q.; McKenna, G. B. Correlation between Dynamic Fragility and Glass Transition Temperature for Different Classes of Glass Forming Liquids. *Journal of Non-Crystalline Solids* **2006**, *352* (28–29), 2977–2985. <https://doi.org/10.1016/j.jnoncrysol.2006.04.014>.

E. Oświadczenia współautorów

Chorzów, 12.03.2024

Prof. dr hab. Andrzej Burian
Instytut Fizyki im. A. Chełkowskiego
Wydział Nauk Ścisłych i Technicznych
Uniwersytet Śląski w Katowicach
ul. 75 Pułku Piechoty 1, 41-500 Chorzów

OŚWIADCZENIE

Oświadczam, że w pracy:

P1. Grelska, J., Jurkiewicz, K., Burian, A., & Pawlus, S. (2022). Supramolecular Structure of Phenyl Derivatives of Butanol Isomers. *The Journal of Physical Chemistry B*, 126(19), 3563

Mój wkład polegał na współpracy przy analizie wyników dyfrakcji rentgenowskiej, dyskusji otrzymanych wyników oraz korekcie manuskryptu.

ABurian

Tuluza, 12.03.2024

Dr Andrzej Nowok

Katedra Fizyki Doświadczalnej

Wydział Podstawowych Problemów Techniki

Politechnika Wrocławska

Wybrzeże Stanisława Wyspiańskiego 27, 50-370 Wrocław

Laboratoire National des Champs Magnétiques Intenses (LNCMI), UPR3228

143 avenue de Ranguel, 31400 Tuluza, Francja

OŚWIADCZENIE

Oświadczam, że w pracy:

P2. Grelska, J., Jurkiewicz, K., Nowok, A., & Pawlus, S. (2023). Computer simulations as an effective way to distinguish supramolecular nanostructure in cyclic and phenyl alcohols.

Physical Review E, 108(2), 024603

Mój wkład polegał na pomiarach oraz analizie wyników ze spektroskopii w podczerwieni oraz szerokopasmowej spektroskopii dielektrycznej, dyskusji otrzymanych wyników oraz korekcji manuskryptu.

Nowok Andrzej

Budapest, 13.03.2024

László Temleitner, Ph.D.

HUN-REN Wigner Research Centre for Physics

Konkoly Thege út 29-33

H-1121 Budapest, Hungary

STATEMENT

I hereby state that in the work:

P4. Grelska, J., Temleitner, L., Park, C., Jurkiewicz, K., & Pawlus, S. (2024). High-Pressure and Temperature Effects on the Clustering Ability of Monohydroxy Alcohols. *The Journal of Physical Chemistry Letters*, 15, 3118

My contribution was collaboration on performing molecular dynamics simulations, writing analysis software, discussion of results and editing the manuscript.



Lemont, 13.03.2024

Changyong Park, Ph.D.

High Pressure Collaborative Access Team (HPCAT)

X-Ray Science Division

Argonne National Laboratory

Lemont, IL, 60439, USA

STATEMENT

I hereby state that in the work:

P4. Grelka, J., Temleitner, L., Park, C., Jurkiewicz, K., & Pawlus, S. (2024). High-Pressure and Temperature Effects on the Clustering Ability of Monohydroxy Alcohols. *The Journal of Physical Chemistry Letters*, 15, 3118

My contribution was collaboration on high-pressure diffraction experiment and editing the manuscript.

3/13/2024 Park, Changyong

Chorzów, 14.03.2024

Dr inż. Karolina Jurkiewicz
Instytut Fizyki im. A. Chełkowskiego
Wydział Nauk Ścisłych i Technicznych
Uniwersytet Śląski w Katowicach
ul. 75 Pułku Piechoty 1, 41-500 Chorzów

OŚWIADCZENIE

Oświadczam, że w następujących pracach:

P1. Grelska, J., Jurkiewicz, K., Burian, A., & Pawlus, S. (2022). Supramolecular Structure of Phenyl Derivatives of Butanol Isomers. *The Journal of Physical Chemistry B*, 126(19), 3563

Mój wkład polegał na nadzorowaniu przeprowadzanego eksperymentu, współpracy przy analizie wyników, dyskusji otrzymanych wyników oraz współtworzeniu manuskryptu.

P2. Grelska, J., Jurkiewicz, K., Nowok, A., & Pawlus, S. (2023). Computer simulations as an effective way to distinguish supramolecular nanostructure in cyclic and phenyl alcohols. *Physical Review E*, 108(2), 024603

Mój wkład polegał na nadzorowaniu przeprowadzanego eksperymentu, współpracy przy analizie wyników, dyskusji otrzymanych wyników oraz współtworzeniu manuskryptu.

P4. Grelska, J., Temleitner, L., Park, C., Jurkiewicz, K., & Pawlus, S. (2024). High-Pressure and Temperature Effects on the Clustering Ability of Monohydroxy Alcohols. *The Journal of Physical Chemistry Letters*, 15, 3118

Mój wkład polegał na nadzorowaniu przeprowadzanego eksperymentu, współpracy przy pomiarach dyfrakcji rentgenowskiej pod ciśnieniem i analizie wyników, dyskusji otrzymanych wyników oraz współtworzeniu manuskryptu.



Chorzów, 14.03.2024

Prof. dr hab. Sebastian Pawlus
Instytut Fizyki im. A. Chełkowskiego
Wydział Nauk Ścisłych i Technicznych
Uniwersytet Śląski w Katowicach
ul. 75 Pułku Piechoty 1, 41-500 Chorzów

OŚWIADCZENIE

Oświadczam, że w następujących pracach:

P1. Grelska, J., Jurkiewicz, K., Burian, A., & Pawlus, S. (2022). Supramolecular Structure of Phenyl Derivatives of Butanol Isomers. *The Journal of Physical Chemistry B*, 126(19), 3563

Mój wkład polegał na nadzorowaniu przeprowadzanych analiz, dyskusji otrzymanych wyników oraz korekcji manuskryptu.

P2. Grelska, J., Jurkiewicz, K., Nowok, A., & Pawlus, S. (2023). Computer simulations as an effective way to distinguish supramolecular nanostructure in cyclic and phenyl alcohols. *Physical Review E*, 108(2), 024603

Mój wkład polegał na nadzorowaniu przeprowadzanych analiz, dyskusji otrzymanych wyników oraz korekcji manuskryptu.

P4. Grelska, J., Temleitner, L., Park, C., Jurkiewicz, K., & Pawlus, S. (2024). High-Pressure and Temperature Effects on the Clustering Ability of Monohydroxy Alcohols. *The Journal of Physical Chemistry Letters*, 15, 3118

Mój wkład polegał na nadzorowaniu przeprowadzanych analiz, dyskusji otrzymanych wyników oraz korekcji manuskryptu.



Aktywność naukowa

Wystąpiłam z prezentacją ustną na konferencjach krajowych o tematyce dyfrakcji rentgenowskiej:

- *Szkoły i warsztaty XRD, XRF, OES, GDOES, LIBS*, Węgierska Górka (16-19.10.2023), Temperaturowe badania dyfrakcyjne ciekłych alkoholi
- *Szkoły i warsztaty XRD, XRF, ICP-OES*, Ustroń (18-21.10.2021), Badania cieczy asocjujących za pomocą metody dyfrakcji rentgenowskiej – jakich informacji dostarcza analiza w zakresie nisko- i szerokokątowym?

Ponadto, jestem współautorką publikacji niepowiązanych z tematyką pracy doktorskiej:

S1. Goraus, J., **Grelska, J.**, Kubacki, J., Czerniewski, J., Barylski, A., Zajac, M., Sawicki, B., & Prusik, K. (2023). Which crystal structure is present on the surface of Ti₂CrAl compound—a deduction from electronic structure measurements and calculations. *Surface Science*, 733, 122288

S2. Heczko, D., **Grelska, J.**, Jurkiewicz, K., Spsychalska, P., Kasprzycka, A., Kaminski, K., Paluch, M., & Kaminska, E. (2021). Anomalous narrowing of the shape of the structural process in derivatives of trehalose at high pressure. The role of the internal structure. *Journal of Molecular Liquids*, 336, 116321

S3. Nowok, A., Cieslik, W., **Grelska, J.**, Jurkiewicz, K., Makieieva, N., Kupka, T., Aleman, J., Musiol, R., & Pawlus, S. (2022). Simple Rules for Complex Near-Glass-Transition Phenomena in Medium-Sized Schiff Bases. *International Journal of Molecular Sciences*, 23(9), 5185

S4. Goraus, J., Witas, P., **Grelska, J.**, Calvayrac, F., Czerniewski, J., & Balin, K. (2022). Magnetic properties of Gd₃Cu₃Sb₄. *Journal of Magnetism and Magnetic Materials*, 550, 169075

S5. Heczko, D., Jurkiewicz, K., **Grelska, J.**, Kaminski, K., Paluch, M., & Kaminska, E. (2020). Influence of High Pressure on the Local Order and Dynamical Properties of the Selected Azole Antifungals. *The Journal of Physical Chemistry B*, 124(52), 11949

S6. Tarnacka, M., Geppert-Rybczynska, M., Dulski, M., **Grelska, J.**, Jurkiewicz, K., Grzybowska, K., Kaminski, K., & Paluch, M. (2021). Local structure and molecular dynamics of highly polar propylene carbonate derivative infiltrated within alumina and silica porous templates. *The Journal of Chemical Physics*, 154(6), 064701

- S7. Heczko, D., Jurkiewicz, K., Tarnacka, M., **Grelska, J.**, Wrzalik, R., Kaminski, K., Paluch, M., & Kaminska, E. (2020). The impact of chemical structure on the formation of the medium-range order and dynamical properties of selected antifungal APIs. *Physical Chemistry Chemical Physics*, 22(48), 28202
- S8. Nowok, A., Cieslik, W., Dulski, M., Jurkiewicz, K., **Grelska, J.**, Aleman, J., Musiol, R., Szeremeta, A. Z., & Pawlus, S. (2022). Glass-forming Schiff bases: Peculiar self-organizing systems with bifurcated hydrogen bonds. *Journal of Molecular Liquids*, 348, 118052
- S9. Heczko, D., Jesionek, P., Hachula, B., Jurkiewicz, K., **Grelska, J.**, Tarnacka, M., Kaminski, K., Paluch, M., & Kaminska, E. (2022). Variation in the local ordering, H-bonding pattern and molecular dynamics in the pressure densified ritonavir. *Journal of Molecular Liquids*, 351, 118666
- S10. Talik, A., Tarnacka, M., Minecka, A., Hachula, B., **Grelska, J.**, Jurkiewicz, K., Kaminski, K., Paluch, M., & Kaminska, E. (2021). Anormal Thermal History Effect on the Structural Dynamics of Probucol Infiltrated into Porous Alumina. *The Journal of Physical Chemistry C*, 125(7), 3901
- S11. Paturej, J., Koperwas, K., Tarnacka, M., Jurkiewicz, K., Maksym, P., **Grelska, J.**, Paluch, M., & Kaminski, K. (2022). Supramolecular structures of self-assembled oligomers under confinement. *Soft Matter*, 18(26), 4930
- S12. Bielas, R., Maksym, P., Tarnacka, M., Minecka, A., Jurkiewicz, K., Talik, A., Geppert-Rybczynska, M., **Grelska, J.**, Mielanczyk, L., Bernat, R., Kaminski, K., Paluch, M., & Kaminska, E. (2021). Synthetic strategy matters: The study of a different kind of PVP as micellar vehicles of metronidazole. *Journal of Molecular Liquids*, 332, 115789
- S13. Tranova, T., Pyteraf, J., Kurek, M., Jamroz, W., Brniak, W., Spalovska, D., Loskot, J., Jurkiewicz, K., **Grelska, J.**, Kramarczyk, D., Muzikova, J., Paluch, M., & Jachowicz, R. (2022). Fused Deposition Modeling as a Possible Approach for the Preparation of Orodispersible Tablets. *Pharmaceuticals*, 15(1), 69

Referencje

- [1] V. Basavalingappa et al., *Mechanically Rigid Supramolecular Assemblies Formed from an Fmoc-Guanine Conjugated Peptide Nucleic Acid*, *Nat Commun* **10**, 5256 (2019).
- [2] M. Diener, J. Adamcik, A. Sánchez-Ferrer, F. Jaedig, L. Schefer, and R. Mezzenga, *Primary, Secondary, Tertiary and Quaternary Structure Levels in Linear Polysaccharides: From Random Coil, to Single Helix to Supramolecular Assembly*, *Biomacromolecules* **20**, 1731 (2019).
- [3] B. J. G. E. Pieters, M. B. van Eldijk, R. J. M. Nolte, and J. Mecnović, *Natural Supramolecular Protein Assemblies*, *Chem. Soc. Rev.* **45**, 24 (2016).
- [4] S. L. Higashi, N. Rozi, S. A. Hanifah, and M. Ikeda, *Supramolecular Architectures of Nucleic Acid/Peptide Hybrids*, *IJMS* **21**, 9458 (2020).
- [5] J. W. E. Drewitt, *Liquid Structure under Extreme Conditions: High-Pressure x-Ray Diffraction Studies*, *J. Phys.: Condens. Matter* **33**, 503004 (2021).
- [6] Y. Katayama, T. Hattori, H. Saitoh, T. Ikeda, K. Aoki, H. Fukui, and K. Funakoshi, *Structure of Liquid Water under High Pressure up to 17 GPa*, *Phys. Rev. B* **81**, 014109 (2010).
- [7] J. Jączyń and J. Świergiel, *Mesoscopic Clustering in Butanol Isomers*, *Journal of Molecular Liquids* **314**, 113652 (2020).
- [8] M. Požar, J. Bolle, C. Sternemann, and A. Perera, *On the X-Ray Scattering Pre-Peak of Linear Mono-Ols and the Related Microstructure from Computer Simulations*, *J. Phys. Chem. B* **124**, 8358 (2020).
- [9] S. Choi, S. Parameswaran, and J.-H. Choi, *Effects of Molecular Shape on Alcohol Aggregation and Water Hydrogen Bond Network Behavior in Butanol Isomer Solutions*, *Phys. Chem. Chem. Phys.* **23**, 12976 (2021).
- [10] O. Gereben and L. Pusztai, *Hydrogen Bond Connectivities in Water–Ethanol Mixtures: On the Influence of the H-Bond Definition*, *Journal of Molecular Liquids* **220**, 836 (2016).
- [11] P. A. Guńka, A. Olejniczak, S. Fanetti, R. Bini, I. E. Collings, V. Svitlyk, and K. F. Dziubek, *Crystal Structure and Non-Hydrostatic Stress-Induced Phase Transition of Urotropine Under High Pressure*, *Chemistry A European J* **27**, 1094 (2021).
- [12] N. Funamori and K. Tsuji, *Pressure-Induced Structural Change of Liquid Silicon*, *Phys. Rev. Lett.* **88**, 255508 (2002).
- [13] W. Dmowski, G. H. Yoo, S. Gierlotka, H. Wang, Y. Yokoyama, E. S. Park, S. Stelmakh, and T. Egami, *High Pressure Quenched Glasses: Unique Structures and Properties*, *Sci Rep* **10**, 9497 (2020).
- [14] R. Böhmer, C. Gainaru, and R. Richert, *Structure and Dynamics of Monohydroxy Alcohols—Milestones towards Their Microscopic Understanding, 100 Years after Debye*, *Physics Reports* **545**, 125 (2014).
- [15] C. Gainaru, R. Meier, S. Schildmann, C. Lederle, W. Hiller, E. A. Rössler, and R. Böhmer, *Nuclear-Magnetic-Resonance Measurements Reveal the Origin of the Debye Process in Monohydroxy Alcohols*, *Phys. Rev. Lett.* **105**, 258303 (2010).
- [16] S. Lotze, C. C. M. Groot, C. Vennehaug, and H. J. Bakker, *Femtosecond Mid-Infrared Study of the Dynamics of Water Molecules in Water–Acetone and Water–Dimethyl Sulfoxide Mixtures*, *J. Phys. Chem. B* **119**, 5228 (2015).

- [17] K. M. Murdoch, T. D. Ferris, J. C. Wright, and T. C. Farrar, *Infrared Spectroscopy of Ethanol Clusters in Ethanol–Hexane Binary Solutions*, *The Journal of Chemical Physics* **116**, 5717 (2002).
- [18] C. Gainaru, M. Wikarek, S. Pawlus, M. Paluch, R. Figuli, M. Wilhelm, T. Hecksher, B. Jakobsen, J. C. Dyre, and R. Böhmer, *Oscillatory Shear and High-Pressure Dielectric Study of 5-Methyl-3-Heptanol*, *Colloid Polym Sci* **292**, 1913 (2014).
- [19] T. Böhmer, J. P. Gabriel, T. Richter, F. Pabst, and T. Blochowicz, *Influence of Molecular Architecture on the Dynamics of H-Bonded Supramolecular Structures in Phenyl-Propanols*, *J. Phys. Chem. B* **123**, 10959 (2019).
- [20] S. Kołodziej, J. Knapik-Kowalczyk, K. Grzybowska, A. Nowok, and S. Pawlus, *Essential Meaning of High Pressure Measurements in Discerning the Properties of Monohydroxy Alcohols with a Single Phenyl Group*, *Journal of Molecular Liquids* **305**, 112863 (2020).
- [21] M. Wikarek, S. Pawlus, S. N. Tripathy, A. Szulc, and M. Paluch, *How Different Molecular Architectures Influence the Dynamics of H-Bonded Structures in Glass-Forming Monohydroxy Alcohols*, *J. Phys. Chem. B* **120**, 5744 (2016).
- [22] K. L. Ngai, S. Pawlus, and M. Paluch, *Explanation of the Difference in Temperature and Pressure Dependences of the Debye Relaxation and the Structural α -Relaxation near T of Monohydroxy Alcohols*, *Chemical Physics* **530**, 110617 (2020).
- [23] P. Debye, *Zerstreuung von Röntgenstrahlen*, *Annalen Der Physik* **351**, 809 (1915).
- [24] S. Boccatto et al., *Amorpheus: A Python-Based Software for the Treatment of X-Ray Scattering Data of Amorphous and Liquid Systems*, *High Pressure Research* **42**, 69 (2022).
- [25] M. J. Abraham, T. Murtola, R. Schulz, S. Páll, J. C. Smith, B. Hess, and E. Lindahl, *GROMACS: High Performance Molecular Simulations through Multi-Level Parallelism from Laptops to Supercomputers*, *SoftwareX* **1–2**, 19 (2015).
- [26] S. Pronk et al., *GROMACS 4.5: A High-Throughput and Highly Parallel Open Source Molecular Simulation Toolkit*, *Bioinformatics* **29**, 845 (2013).
- [27] S. Páll, M. J. Abraham, C. Kutzner, B. Hess, and E. Lindahl, *Tackling Exascale Software Challenges in Molecular Dynamics Simulations with GROMACS*, in *Solving Software Challenges for Exascale*, edited by S. Markidis and E. Laure, Vol. 8759 (Springer International Publishing, Cham, 2015), pp. 3–27.
- [28] J. Wang, R. M. Wolf, J. W. Caldwell, P. A. Kollman, and D. A. Case, *Development and Testing of a General Amber Force Field*, *J. Comput. Chem.* **25**, 1157 (2004).
- [29] M. Brehm, M. Thomas, S. Gehrke, and B. Kirchner, *TRAVIS—A Free Analyzer for Trajectories from Molecular Simulation*, *J. Chem. Phys.* **152**, 164105 (2020).
- [30] M. Brehm and B. Kirchner, *TRAVIS - A Free Analyzer and Visualizer for Monte Carlo and Molecular Dynamics Trajectories*, *J. Chem. Inf. Model.* **51**, 2007 (2011).
- [31] O. Hollóczki, M. Macchiagodena, H. Weber, M. Thomas, M. Brehm, A. Stark, O. Russina, A. Triolo, and B. Kirchner, *Triphasic Ionic-Liquid Mixtures: Fluorinated and Non-Fluorinated Aprotic Ionic-Liquid Mixtures*, *ChemPhysChem* **16**, 3325 (2015).
- [32] L. Temleitner, *Hydrogen Bond Analysis Software Package*, (2023).
- [33] I. Jukić, M. Požar, B. Lovrinčević, and A. Perera, *Universal Features in the Lifetime Distribution of Clusters in Hydrogen-Bonding Liquids*, *Phys. Chem. Chem. Phys.* **23**, 19537 (2021).